CHALMERS
UNIVERSITY OF TECHNOLOGY

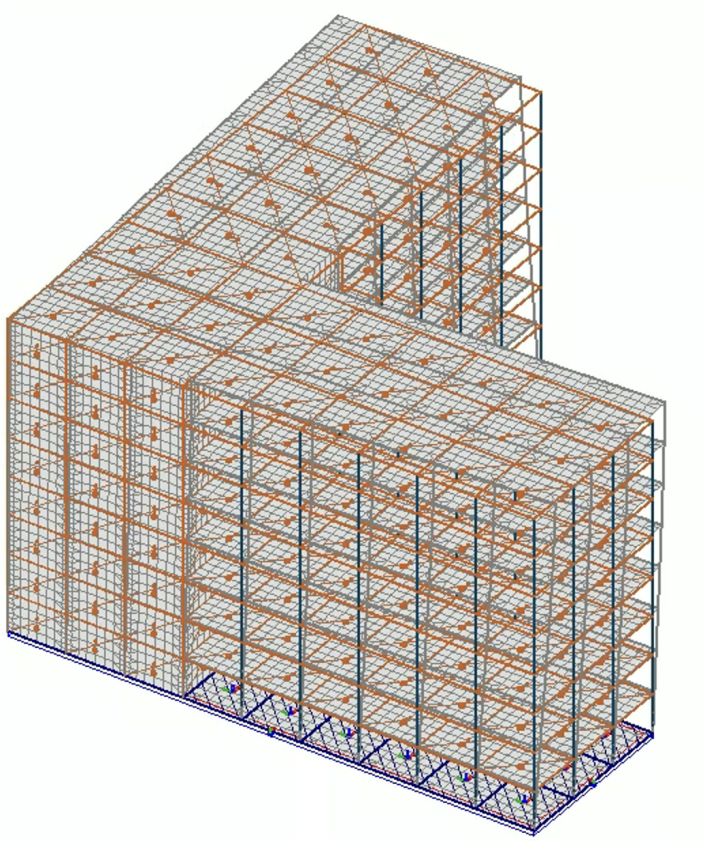

Torsional Wind Response in Asymmetrical Timber Buildings

A Parametric Study of Plan Irregularity in Mid-Rise Structures

Master's thesis in Structural Engineering and Building Technology

REBECKA DAHLGREN

DEPARTMENT OF ARCHITECTURE AND CIVIL ENGINEERING
CHALMERS UNIVERSITY OF TECHNOLOGY
Gothenburg, Sweden 2026
www.chalmers.se

Master's thesis 2026

Torsional Wind Response in Asymmetrical Timber Buildings

A Parametric Study of Plan Irregularity in Mid-Rise Structures

REBECKA DAHLGREN

CHALMERS
UNIVERSITY OF TECHNOLOGY

Department of Architecture and Civil Engineering
Division of Strcutural Engineering and Building Technology
Chalmers University of Technology
Gothenburg, Sweden 2026

Torsional Wind Response in Asymmetrical Timber Buildings
A Parametric Study of Plan Irregularity in Mid-Rise Structures
REBECKA DAHLGREN

Supervisor: John Hessel, Looström
Supervisor: Frida Tjernberg, Looström
Supervisor: Zhengyao Li, Department of Architecture and Civil Engineering
Examiner: Mahbube Subhani, Department of Architecture and Civil Engineering

Master's Thesis 2026
Department of Architecture and Civil Engineering
Division of Structural Engineering and Building Technology
Chalmers University of Technology
SE-412 96 Gothenburg
Telephone +46 31 772 1000

Cover: Analytical FEM model of an L-shaped mid-rise timber building used in the modal study, illustrating torsion in the fundamental mode. The parametric geometry and structural layout were created in Grasshopper and exported to FEM-Design via the FEM-Design API.

Typeset in LaTeX
Printed by Chalmers Reproservice
Gothenburg, Sweden 2026

Torsional Wind Response in Asymmetrical Timber Buildings
A Parametric Study of Plan Irregularity in Mid-Rise Structures
REBECKA DAHLGREN
Department of Architecture and Civil Engineering
Chalmers University of Technology

Abstract

Wind loading often governs the lateral response of mid-rise timber buildings and can be critical for torsion, since the structure may rotate in addition to swaying. This thesis applies a parametric modal study of rectangular and L-shaped timber floor plans to identify when torsion governs the fundamental mode, and which stabilizer layouts most effectively reduce torsional sensitivity. The study is limited to the chosen investigated plan sizes and the structural configuration is based on a 6×6 m column grid with constant span lengths, rigid diaphragm action, and stabilizing systems modelled using CLT shear walls and (where applicable) a core, whose lengths, and positions are varied parametrically. Effects such as openings/discontinuities, height/vertical irregularities, connection flexibility, additional bracing systems, and explicit wind-response/comfort checks are outside the scope.

Across both geometries, torsion is governed by the combined effect of (i) eccentricity, e, between the center of mass (CM) and the center of rigidity/rotation (CR), expressed as the normalized measure e/D, where D is the plan diagonal, and (ii) the torsional resistance provided by stabilizer lever arms, represented by the normalized torsional stiffness $R = \sqrt{K_\theta/(K_x + Ky)}$. Here, K_θ is the torsional stiffness about CR, while (K_x and (K_y are the total lateral bending stiffnesses resisting sway in the global x- and y-directions. For rectangular plans, torsion becomes consistently likely once eccentricity is high. In the compiled results, configurations with a normalized eccentricity over the diagonal of the building plan (D), $e/D \geq 0.16$ fall in the torsion-dominated region, while configurations with sufficiently high normalized torsional stiffness (R) (about $R \geq 13.5$ m) remain translation-dominated. The most efficient torsion-reducing measures in the rectangular study were therefore avoiding stabilizer asymmetry that shifts CR (especially off-centre core placement) and increasing lever arms by placing stabilizers toward façades/corners.

For L-shaped plans, torsion sensitivity is generally higher because geometric effects make low eccentricity harder to achieve in practice, so robustness relies more strongly on torsional resistance. In the combined L-shape summary, the key stiffness thresholds are $R_{crit,1}$=10.0 m and $R_{crit,2}$=28.11 m, with corresponding boundary ratios (R/(e/D)) of roughly 128 and 184. Practically, configurations below the lower stiffness level are consistently torsion-prone, whereas for moderate eccentricities, maintaining R above the upper level is associated with translational behaviour. The most effective measures in the L-shape study were moving stabilizers toward the plan corners and avoiding pronounced directional stiffness imbalance, which was shown to broaden the range of torsion-dominated configurations.

Overall, the analyses indicate that the most efficient design takes are (1) controlling eccentricity by limiting CR shifts (dominant for rectangles), and (2) maximizing stabilizer lever arms/torsional resistance (dominant for L-shapes). Configurations combining high eccentricity with low torsional resistance are the most torsion-sensitive and should be prioritized for detailed wind-serviceability verification.

Keywords: fundamental mode shape, torsion, translation, center of mass (CM), center of rigidity (CR), eccentricity, torsional stiffness, asymmetry, rectangle, L-shape

Acknowledgements

I would like to express my sincere gratitude to my supervisors at Looström, John Hessel and Frida Tjenberg, and to my examiner and supervisors at Chalmers University of Technology, Mahbube Subhanai and Zhengyao Li, for your guidance, feedback, and support throughout this work. I also thank Marco Pellegrino for his help with the FEM-Design API, and Alex Ek at Chalmers IT for assisting with the virtual desktop setup. Finally, I am deeply grateful to my family and friends for your constant encouragement and patience during this thesis and my time at Chalmers. I truly could not have done it without you.

Rebecka Dahlgren, Gothenburg, January 2026

List of Acronyms

Below is the list of acronyms that have been used throughout this thesis listed in alphabetical order:

API	Application Programming Interface (FEM-Design API)
BC	Boundary Condition
CLT	Cross-Laminated Timber
CM	Center of Mass
CR	Center of Rigidity/Center of Rotation
EC	Eurocode
EMM	Effective Modal Mass
FEA	Finite Element Analysis
FEM	Finite Element Method
FR	Frequency Ratio
GC	Geometrical Center
SLS	Serviceability Limit State
SW	Shear Wall
ULS	Ultimate Limit State

Terms and Definitions

Below are some terms and definitions that have been used throughout this thesis, in alphabetic order:

Amplification	Increase in structural response, typically associated with dynamic effects (e.g., resonance) and influenced by damping.
Aspect Ratio	Ratio between characteristic plan dimensions, e.g. length-to-width for rectangles or leg-length ratio for L-shaped plans.
Azimuth	Direction angle in plan, e.g. the wind direction measured relative to a reference axis.
Center of Mass (CM)	Point in the plan where the resultant floor mass can be considered to act; defined by mass-weighted coordinates.
Center of Rigidity (CR)	Point in the plan about which the floor tends to rotate under lateral loading; defined by stiffness-weighted coordinates.
Eccentricity	Offset between CM and CR, commonly measured as the distance between these points in plan.
Eigenfrequency	Natural frequency of the structure associated with a specific vibration mode.
Eigenmode	A vibration mode corresponding to an eigenfrequency, defined by an eigenfrequency and its associated mode shape.
Frequency Ratio (FR)	Ratio used to classify the fundamental response by comparing the first-mode frequency to the lowest translational frequency.
Fundamental Frequency	The lowest eigenfrequency of the structure (first natural frequency).
Fundamental Mode	The eigenmode associated with the fundamental frequency (Mode 1).
Mid-rise Building	A building of intermediate height, commonly in the range of approximately 4-10 storeys.

Mode	A distinct vibration pattern of a structure characterised by an eigenfrequency and a corresponding mode shape (e.g., translational or torsional).
Mode Shape	Spatial deformation pattern of a mode, describing the relative displacements of points in the structure during vibration.
Resonance	Condition where excitation contains significant energy close to an eigenfrequency, which may result in amplified response.
Sway	Global lateral drift of the building under horizontal loading; often used interchangeably with lateral translation.
Torsion	Rotational motion about the vertical axis in plan.
Torsional Stiffness	Resistance to rotation about the vertical axis, governed by the stiffness distribution and lever arms of the stabilising system.
Translation	Predominantly lateral motion of the floor plate without significant rotation.

Contents

List of Figures

List of Tables

1
Introduction

In recent years, the use of timber as a structural material has increased significantly in Sweden, driven both by sustainability ambitions, and by advances in timber technology. A key turning point came in 1994, when European design standards were revised to permit timber buildings taller than two storeys [4]. Since then, timber buildings have become increasingly more common in mid-rise formats (up to ten floors) as they provide a balance between urban density and climate goals. Today, Sweden regards timber construction as a central strategy for reducing the carbon footprint of the building sector, with several large-scale projects demonstrating its potential for mainstream urban development.

This development, however, brings new engineering challenges, particularly regarding wind-induced dynamics. One of the most critical effects is torsion, which arises when asymmetric floor plans or stiffness/mass irregularities offset the center of mass (CM) and the center of rigidity (CR), causing lateral wind loads to induce and amplify twisting motion [5][6]. All buildings have a set of eigenmodes, with corresponding natural frequencies and modes shapes, that depend on the mass and stiffness of the building. Turbulent wind acting on an eccentric building can produce torsional moments that couple sway and rotation. This torsional moment projects onto the torsional mode, and if the wind energy overlaps the natural frequency of the building, the twist is dynamically amplified into vibration, causing higher edge accelerations and uneven floor motion.

Wind-induced vibrations are even more pronounced in light weight, mid-rise timber buildings, where the lower mass and stiffness shift the natural frequencies into the range of human sensitivity, and reduce damping which makes resonance more likely to occur. Torsional motion can therefore affect both structural safety and serviceability even at low wind speeds, as occupants are particularly sensitive to rotational accelerations. [7][8]. Consequences include occupant discomfort as well as fatigue in connections, cracking of finishes, and long-term degradation of non-structural components [9][10]. Within the Eurocode (EC) framework, such effects are treated as part of the serviceability limit state (SLS), where horizontal displacements and vibrations must remain within limits to ensure both occupant comfort and structural reliability [11][12]. Early design choices, such as plan geometry, core placement, and global stiffness distribution, therefore play a decisive role in whether torsional or translational motion dominate the response of the fundamental mode (the first mode) and whether serviceability can be met without costly modifications.

If wind-induced torsion is not accounted for at an early stage, eccentric load paths can elevate the stresses in edge columns and connections, accelerating damage [9]. Since geometry, stiffness distribution, and diaphragm continuity are largely fixed during the conceptual design stage, overlooking torsion early can cause unfavorable dynamic characteristics that are expensive or even impossible to correct later. Despite its importance, wind-induced torsion in timber buildings remains relatively underexplored compared to studies on concrete and steel structures, highlighting the need for further research [13].

The results of this thesis are expected to improve the understanding of torsional response in mid-rise timber buildings. Since torsional effects can become critical and may be amplified under wind excitation, the study aims to identify plan configurations that are prone to torsion and clarifies how eccentricity, stiffness distribution, and plan irregularity influence whether the fundamental mode becomes torsional or predominantly translational. This deeper knowledge contributes academically by clarifying causes of torsional behavior in timber structures and narrowing current research gaps. From a practical perspective, the findings can support early design assessments and reduce uncertainty in the preliminary stages. More broadly, the study adds to the growing body of knowledge on timber construction, reinforcing the foundation for sustainable and resilient urban development.

1.1 Aim

The aim of this project is to investigate how mid-rise timber buildings respond to torsional effects caused by plan and structural asymmetry. Rectangular and L-shaped plan geometries are studied because they are among the most common layouts in mid-rise buildings. The rectangular configurations are used both as a baseline to isolate and explain the key mechanisms that trigger torsional behaviour, and to explore how much eccentricity can be introduced through stabilizer layout before torsion governs the fundamental mode. These insights are then transferred to the L-shaped cases, where the specific objective is to evaluate whether torsional sensitivity can be reduced using one unified stabilizing system, rather than treating the plan as two separate rectangular sub-buildings.

The study focuses on parameters that are both influential in the literature and controllable in early design, namely stiffness distribution in the stabilizing system, the resulting position of the center of rotation (CR), and plan aspect ratio. All configurations are stabilized using shear walls together with evenly distributed columns, allowing the influence of stabilizer placement and directional stiffness to be compared consistently across plan types.

The study will be structured around three main objectives:

- Identify the key factors that cause torsion to govern the fundamental mode in mid-rise timber buildings.
- Develop and apply simulation models to assess how these factors influence the torsional response.
- Establish relationships between these factors and the occurence of torsion in the fundamental vibration mode.

The intended outcome is to increase understanding of torsional wind response in asymmetrical mid-rise timber buildings by clarifying the geometric conditions under which torsion is likely to dominate the fundamental mode. This knowledge contributes academically by addressing a gap in current research on timber dynamics, while in practice it can support early design assessments and reduce uncertainty in preliminary stages.

1.2 Limitations

This study is limited to theoretical eight-storey mid-rise timber buildings and does not investigate a specific real-world project. The plan configurations are restricted to rectangular and L-shaped layouts, two common plan types in Sweden, and each geometry is studied using fixed baseline dimensions, with variations evaluated relative to these reference models. Rather than varying all possible design parameters, a selected set of influential parameters is examined through representative configurations, chosen based on findings in the literature and refined through the iterative modelling process as the most response-sensitive variables became evident.

The investigation is limited to modal properties (natural frequencies and mode-shape characteristics) and does not evaluate deflections, accelerations, or other serviceability (SLS), or ultimate limit state (ULS) responses. For each configuration, only the first three modes are extracted, since the first governing torsional mode typically appears within this range, and is most relevant for assessing whether torsion dominates the fundamental response.

All structural components are modelled in FEM-Design using relevant material properties. Connection design is outside the scope, and structural stiffness is therefore not reduced to account for connection flexibility. The modal analyses include self-weight and a portion of imposed loads through the mass definition, but wind loading is not applied as an external action in the eigenvalue analyses.

Wind is considered only in the interpretive sense, where the identified mode shapes describe deformation patterns that may be excited by wind in practice, but no dynamic wind-response, resonance checks, or aerodynamic effects are analyzed.

Finally, the study does not compare different design standards or building codes and is framed within the Eurocode context, which is the primary basis for timber building design in Sweden.

1.3 Literature Review

Wind-induced torsion has become a central concern in the design of mid-rise timber buildings because it affects both the overall structural safety and occupant comfort. The human body is particularly sensitive to rotational motion, which makes torsional accelerations and vibrations an important serviceability criterion as much as a structural one [5]. Despite this importance, research on wind-driven torsion remains relatively sparse compared to other aspects of wind engineering [6][13]. For timber buildings specifically, only a limited number of studies explicitly address wind-induced torsion, and even fewer consider the mid-rise scale, leaving a clear knowledge gap compared with concrete or steel constructions. In low-seismic regions such as Sweden, where wind governs horizontal stability, the lack of consistent design guidance underscores the need for studies that clarify the mechanisms behind torsional behaviour in timber structures [7]. Given the limited research on wind-induced torsion in mid-rise timber buildings, findings from concrete, steel, and tall building studies are considered relevant as reference points. Torsional effects may be even more critical in timber systems due to their lighter weight and lower inherent damping, which increase susceptibility to wind-induced accelerations.

1.3.1 Governing Factors of Torsional Response

Torsional response is governed by several interacting factors. In the following sections, key influences are outlined, including structural configuration (e.g., stiffness distribution, plan layout irregularities, and eccentricity), aerodynamic effects, and the building's dynamic response characteristics. In this study, the emphasis is placed on structural configuration, focusing on how plan geometry and the distribution and placement of stabilizing elements influence the torsional behaviour.

1.3.1.1 Structural Configuration

According to literature, the primary driver of torsional response is eccentricity. When the resultant wind load does not align with the center of mass (CM) and the center of rotation (CR) of the building, lateral shear induces a twisting moment about the vertical axis [14][5][13]. This is especially common in buildings with irregular plans compared to regular geometric forms [15], but may also result from off-center cores, uneven wall layouts, or mass irregularities, and diaphragm rigidity. Most of the studies presented in this section refer to concrete, steel, or generic building types rather than timber. Since timber systems generally have lower torsional stiffness, similar structural configurations may experience amplified torsional response when constructed in timber.

Firstly, plan geometry clearly interacts with eccentricity to shape torsional behaviour. In general, the more symmetrical the building, the less torsion. Studies on reinforced-concrete prototypes show that compact, regular polygons such as squares and octagons generate lower torsional demand than elongated or concave shapes, while re-entrant corners in L-, T-, or Z-forms are particularly prone to large drifts

and angular accelerations [16][17].

Wind-tunnel work on L-shaped low-rise buildings confirms that irregular footprints produce highly eccentric pressure fields, with torsional moments much greater than those in rectangular benchmarks. These effects are most severe when the wind approaches an internal corner, highlighting how plan shape and wind direction combine to govern torsional demand [18]. Prior studies comparing T- and L-shaped plans at 15, 25, and 30 storeys found T-shaped buildings consistently more wind-sensitive, showing larger displacements, storey drifts, and torsional moments. Responses in the T-shaped plan rose markedly for winds across the flange [19], and is close to zero when the wind aligns with the symmetry axis of T [20]. L-shaped plans, on the other hand, showed little directional variation when its two legs were of similar length [19], and larger torsional effects when the legs are of different lengths. As a result of the re-entrant corner and unequal leg lengths creating unbalanced pressures and a resultant that misses the CM and CR [21]. It was shown that torsion for L-shaped plans tend to peak when the wind runs broadly along one leg, rather than along a symmetry line. As the ratio between the legs grew, the torsional response became larger, while overall slenderness of the building had little effect in these tests [21].

However, even seemingly symmetric plan layouts can cause torsional rotation. Rectangular plans are directionally dependent, with weak-axis responses being substantially larger than strong-axis responses. Also, geometric features such as setbacks, chamfers, and projecting wings increase lever arms and torsional rotation [14]. Across a large wind-tunnel dataset, rectangles showed higher mean torsional offsets than squares (about 11.4% versus 8.3%), with circles lowest and triangles highest. Indicating that rectangular footprints are usually more prone to torsion [22]. Moreover, square plans do not guarantee a torsion proof solution, small eccentricities and geometric modifiers can redistribute along-wind, across-wind, and torsional responses in complex ways [23].

Secondly, core placement is a key driver to wind-induced torsion. Although most research on core location targets high-rise buildings where the effect is especially critical [24], the same mechanisms remain relevant at mid-rise scales. While the torsional response can be expected to be smaller, the position of a single core still governs the distribution of stiffness and mass. Consequently, affecting the eccentricity between CM and CR. A centrally positioned core generally minimizes this eccentricity, enhancing structural robustness, and load distributions [24][25].

Placing the core off-center, often done in asymmetrical plans to satisfy layout constraints, increases the CM-CR eccentricity and thus torsional susceptibility. Prior reviews and case studies note that, although such core placement can unlock plan freedom, it departs from the structurally efficient, torsion-resistant central arrangement [25][24].

Surveys of completed and ongoing timber high-rise projects indicate that central

cores are generally the most efficient, while peripheral or offset cores are used less often because of layout and stability considerations. [25]. Since core position interacts with plan irregularity, it should be treated as a primary design parameter rather than a secondary adjustment.

Lastly, the choice of structural system plays a decisive role in how buildings resist torsional effects. Wall-based systems suppress rotation by providing high stiffness, whereas frame or mixed systems distribute stiffness across the plan, aiding asymmetric layouts. Consistent with this, literature on multi-storey/tall timber buildings show widespread use of shear-wall and dual systems, often combining perimeter stiffening with an interior core to increase the torsional stiffness of the building [25]. In timber, cross-laminated timber (CLT) floor diaphragms and their collectors/chords control how lateral forces and accidental eccentricities are shared between vertical elements. Flexible or semi-rigid diaphragms increase the risk of torsional effects, while in-plane stiffness reduces torsion–translation coupling[26][27][28]. For mid-rise projects, asymmetrical floor plans can achieve adequate torsional stability without relying on concrete cores if stiffness is strategically distributed across the plan. At greater heights, however, studies show that replacing a CLT core with a concrete core markedly increases global lateral stiffness (68% for frame variants, 45% for wall variants, 23% for diagrid variants), illustrating why stiffer cores are often introduced to control wind drift and rotation [29][25].

Although some of the research was developed in a seismic context, the same principles (CM-CR eccentricity, stiffness distribution and diaphragm rigidity) govern wind-induced torsion [30][5][13]. Mechanistically, the goal is to minimize the CM–CR distance at each floor, reducing the overall torsion under wind actions. A principle consistently recommended in analytical and applied studies [31][32].

1.3.1.2 Aerodynamics

Wind acting on a building produces façade pressures that vary with height and around the perimeter due to boundary-layer turbulence, separation at edges and corners, and local shielding. The integrated pressure field often yields a lateral resultant whose line of action misses the CM and CR, creating eccentricities and torsional moments [7]. Studies on re-entrant corners and plus-/cross-shaped floor plans show that these reorganize the incoming boundary-layer flow, producing separation, channeling, and corner vortices that create highly non-uniform façade pressures and large eccentric resultants. Computational fluid dynamic studies on cross/plus-shaped towers further show that both corner depth and building height control these asymmetries, with deeper re-entrant wings generating larger suction peaks and greater torsional moments even when the mass layout is nominally symmetric [33]. Furthermore, wind-tunnel work on L-shaped buildings confirms that torsional loads can exceed those of rectangular shapes and tend to peak at oblique wind angles, reinforcing that irregular plan geometry strongly amplifies torsional demand [18].

Perimeter pressures vary with azimuth and over height, meaning that the total wind load naturally acquires a twisting component. This becomes stronger when the wind approaches at an oblique angle rather than along a principal symmetry line, which is why even a rectangular plan can exhibit clear torsional actions [5]. Corners and edges experience sharp pressure gradients, and vertical variation in pressure adds another layer of imbalance. Taken together, the flow field and its direction are key controls. Hence, it is not sufficient to only check winds aligned with the principal axes [5]. Since wind rarely approaches façades at right angles, and the perimeter pressures are seldom uniform, such misalignments are common even in apparently symmetric plans [7].

Previous studies also show that torsion develops simultaneously with significant lateral shear, underscoring that torsional demand is a primary aspect of wind response rather than a secondary effect [6]. In this thesis, aerodynamic effects are not considered, since wind actions are outside the scope of the analysis.

1.3.1.3 Dynamic Responses

Wind-induced vibrations arise from the unsteady nature of atmospheric flow and the modal characteristics of the building. The wind load can be decomposed into a mean, quasi-steady component and a fluctuating component caused by turbulence and flow separation. Turbulence produces broadband pressure fluctuations. If one of these peaks align with a natural frequency of the building, resonance increases the response and the affected mode becomes dominant [14]. In most buildings the fundamental modes are lateral sways in the principal directions, but asymmetry in the distribution of mass and stiffness can shift the first mode toward torsion or a coupled lateral–torsional form, increasing edge accelerations and differential floor motion [2][32].

Wind-induced motion is commonly decomposed into along-wind buffeting and across-wind/torsional excitation. Along-wind response comes from turbulence carried past the building and primarily excites translational sway. Across-wind and torsional effects arise from organized flow features (vortex shedding, separation/reattachment at sharp edges, corner vortices, and channeling at re-entrant corners), and often peak for oblique approach winds, especially in sharp-edged or irregular plans [13][32]. Since the façade pressures are inherently non-uniform around the perimeter and over the height of the building, the integrated lateral resultant typically includes torsion coupling into the global response, dominating serviceability [14].

These vibrations matter for two main reasons, serviceability and functionality, and occupant comfort. Amplified sway and torsion increases interstorey drift and differential slab motions, stressing non-structural elements and complicating diaphragm force paths. When torsion acts in a dominant mode, displacements and accelerations tend to concentrate at plan edges and corners [32][14]. For occupant comfort, numerous studies show that human perception and tolerance are frequency dependent and have a stronger correlation with acceleration than with displacement. People often

find torsional components particularly disturbing because different points move in different directions at the same time. For example, a person standing near a corner may feel larger lateral acceleration and a small sense of rotation, while someone near the core feels much less. That spatially uneven and rotational motion confuses what the eyes see and what the inner ear senses, making the body read the structure as unstable. The result is discomfort and sometimes nausea at lower acceleration levels than with simple side to side sway [34].

Serviceability is verified using frequency-dependent comfort criteria for whole-building motion , rather than by prescribing an avoidance frequency. Human-factors studies indicate a maximum nauseogenicity near 0.2 Hz. [35][36]. For mid-rise timber buildings, ambient-vibration measurements place fundamental modes broadly in the order of 1–3 Hz, so wind response is governed by the upper tail of the same spectrum rather than its deepest sub-0.1 Hz peak.

As a result, wind often governs design through acceleration limits, even where drift is acceptable, prompting the use of mitigation measures such as tuned mass dampers and architectural or aerodynamic modifications to reduce torsion [3].

In timber systems, these issues can be more pronounced because lower mass and stiffness yield lower natural frequencies and inherent damping, which can increase resonant accelerations under the same wind climate. Coupled torsional modes may therefore appear at comparatively low excitation levels in asymmetrical plans [32]. This elevates the importance to control the response by keeping the CM and CR close through careful plan geometry and core placement, ensuring sufficient stiffness, and by adding damping or redistributing stiffness where necessary [14][3].

1.3.2 Modelling Approaches and Assumptions in Asymmetrical Buildings

This section summarizes the common modelling approaches and assumptions used in the literature for asymmetrical buildings. It highlights parametric strategies and the key FEM and modal analysis choices that influence torsional response and mode identification.

1.3.2.1 Parametric Modelling

The literature shows consistent use of parametric strategies to study how geometric variation influences wind response. Experiments indicate that plan configuration can alter load distribution and flow patterns, and systematic variation reveals trends that single cases may miss [37]. Computational workflows similarly test families of geometries against wind data, supporting both architectural form-finding and structural optimization [38], and earlier probabilistic work with simplified models also demonstrated the value of controlled parameter sweeps in wind–structure interaction [39]. These strands support a parametric evaluation of torsional tendencies in

mid-rise buildings through controlled changes of plan irregularity.

1.3.2.2 Modelling Assumptions and Documentation

Reviews of timber dynamics report that assumptions about boundary conditions (BCs), diaphragm behaviour, and local stiffness from walls, joints, and secondary frames can shift natural frequencies and change the ordering of translational and torsional modes [10]. Studies therefore present eigenfrequencies together with the modelling choices that produced them so that results can be interpreted and compared [40].

1.3.2.3 Modal Analysis Practice in the Literature

Across FEM based studies, authors note that the setup of the mass model and the extraction of a sufficient set of modes influence the reported dynamics more than the brand of software. Many analyses include self-weight and a portion of imposed loads to avoid overestimating frequencies [41]. A common target is that the cumulative effective modal mass (EMM) in each principal direction approaches about 90% which is also reflected in software documentation [42]. Mode identification is often based on visual inspection of shapes together with participation factors in x-, y- and z-direction in order to distinguish coupled torsional modes from pure sway [43]. Case material shows that modal checks are used as the first diagnostic step before serviceability or wind response evaluation [44].

1.3.2.4 Boundary Conditions

Across studies that analyze wind response in timber and hybrid timber buildings, the reference model most often assumes a rigid foundation. Authors justify this choice when the foundation system is designed to be stiff, and then add sensitivity cases with elastic base springs only when foundation flexibility is expected to influence modal ordering or serviceability [10]. Floor diaphragms are frequently taken as rigid in baseline models, yet a parallel strand of work represents CLT diaphragms as semi rigid with orthotropic panel properties and measured connection slip in order to capture force sharing and the onset of torsion–translation coupling [26][27][10]. For frames, beam to column joints are often modelled with finite rotational stiffness based on tests or manufacturer data rather than as perfectly fixed, since joint stiffness has a measurable effect on natural frequencies and on the participation of torsional modes [10]. For shear walls and wall cores, BCs commonly combine base fixity in the global model with explicit representation of hold downs, shear connectors, and wall to diaphragm interfaces so that rocking and shear slip are reflected in the lateral system stiffness [10]. Core systems are typically idealized as cantilevering wall assemblies fixed at the base and connected to the floors through collectors or links that are either rigid or semi rigid depending on the intended detailing, and case material shows that the chosen floor to core coupling strongly influences mode order and torsional participation in tall and mid-rise timber [25][29]. Modal studies also note that mass modelling and analysis setup interact with these BCs.

Including self-weight and an appropriate portion of imposed loads avoids systematic overestimation of eigenfrequencies, and extracting enough modes to reach a high cumulative effective modal mass in each principal direction improves comparability across configurations [41] [42][45] [43][44].

1.3.2.5 Reporting Conventions

Common reporting includes the ordering of the lowest modes with short notes on dominant shapes, participation factors and cumulative effective modal mass in each principal direction, and a concise record of the modelling choices that affect torsion. The latter usually covers base restraint, diaphragm assumption, connection stiffness representation, mesh rules, and mass model [43][44].

As a summary, the literature supports a parametric study with controlled geometry and transparent modelling. Recommending to model a fixed foundation, include self-weight and a stated fraction of imposed load, model the diaphragm and floor to core coupling as detailed, extract modes to about 90% cumulative EMM, and confirm results by calibrating diaphragm in plane stiffness and connections and by running sensitivity checks on base restraint, diaphragm rigidity, and floor to core coupling so that torsional trends reflect geometry rather than modelling artifacts.

1.3.3 Relationships Between the Fundamental Mode and Factors Affecting Torsion

The relationship between plan layout, stiffness distribution, and eccentricity becomes visible directly in the modal response, particularly in the fundamental mode. The following subsections summarize how torsional and translational modes are identified using participation factors, and how geometry, mass–stiffness modelling, loading direction, and stabilizing system choices can shift mode order and promote torsional dominance.

1.3.3.1 Mode Identification

For timber and hybrid structures, recent full-scale vibration tests confirm that participation factors provide a reliable way to distinguish between torsional and translational modes. If rotational (RZ) participation dominates while translational components (UX, UY) are small, the first mode is torsional. Conversely, dominance in UX or UY indicates a translational mode [10]. This avoids misreading cases where irregular geometry changes the order of frequencies and is directly relevant for asymmetric mid-rise timber buildings.

1.3.3.2 From Factors to Modal Responses

Plan geometry and core placement shape torsional demand and the influence appears directly in the modal response. Studies on timber and hybrid systems report that accurate eigenfrequency results depend more on modelling and analysis choices

than on the used software. To capture the governing behaviour researchers extract a sufficient number of modes and check effective modal mass and participation to verify that the modal basis is adequate for response prediction [46, 47, 48].

1.3.3.3 Sensitivity to Mass and Stiffness

Prior work on wind induced vibrations in timber buildings shows that natural frequencies and the balance between torsional and translational modes are highly sensitive to how mass and stiffness are represented, particularly the distribution of structural elements, connections, and secondary components. Full scale testing of a seven storey CLT building shows that wind-induced vibrations are closely linked to the eigenfrequencies and mode shapes of the building, and that reliable prediction of these properties depends on how mass distribution and connection stiffness are represented in the numerical model [49][50].

1.3.3.4 Geometric Patterns Linked to Torsional First Modes

Re-entrant corners are the most common geometric trigger. L- and T-shaped plans often show torsion as the dominant low mode. This is most evident when the legs are unequal or when wind acts along one arm. For T-shaped plans the largest torsion occurs when wind runs along the flange and mainly engages the web [19][20][21][18]. Cross- or plus-shaped plans can also bring torsion into the first mode when the re-entrant wings are deep because corner suction and channeling remain strong even if the mass layout is symmetric [33]. Comparative datasets show that rectangles usually are more torsion prone than squares, while triangles show the highest torsional offsets, and circles the lowest. Rectangles can excite torsion to the first mode when combined with stiffness or core offsets [22][14][16].

1.3.3.5 Directional Effects

Torsional dominance often appears for oblique approach winds, rather than winds aligned with a symmetry line in the building. This behaviour is clear in L- and T-shaped plans, and in plus-shaped plans with deep corners where separation at the internal corner drives peaks near quartering winds [18][20][33].

1.3.3.6 Structural System Choices

Offset or peripheral cores tend to increase RZ participation in the low modes, while a central core reduces it [25]. Semi-rigid diaphragm models and realistic connection slip make translation to torsion coupling visible in the modal basis, which can bring a torsional first mode forward in otherwise borderline cases. Fully rigid diaphragm assumptions can mask this behaviour [26][27].

1.3.4 Conclusion of Literature Review

Taken together, literature demonstrates that wind-induced torsion in mid-rise timber buildings arises from geometric irregularity, CM–CR offsets, and aerodynamic effects at oblique wind angles. Plans with re-entrant corners such as L- and T-shapes and deep plus-shaped plans are repeatedly linked to high torsional demand. Central core placement and sufficient diaphragm stiffness reduce modal torsion and edge accelerations [16][21][33][25][26]. Mitigation strategies therefore emphasize compact plan forms, central placement of stabilizing cores, and sufficient diaphragm stiffness to limit eccentricities. In regions such as Sweden, where wind is a governing action for mid-rise timber buildings, torsional response should be addressed explicitly from the earliest design stages rather than treated as a secondary effect [5][23][14][18][51][52].

Wind response is governed by eigenfrequencies and mode shapes. Participation factors give a robust basis for identifying torsional or translational dominance in the first mode. Credible studies include self-weight and a stated fraction of imposed load in the mass model, extract enough modes to reach high cumulative EMM, and document base restraint, diaphragm representation, and connection stiffness. Full scale testing and model updating confirm the need for realistic diaphragm in plane stiffness and floor to core coupling [10][41][42][46][50].

1.3.4.1 Identified Research-Gaps

Evidence for when the fundamental mode becomes torsion-dominated in mid-rise timber buildings remains limited, and no consolidated framework currently links plan irregularity and the positions of the stabilizing elements to the onset of torsional dominance. In addition, BC assumptions are not reported consistently across studies, which makes direct comparison difficult. This thesis addresses these gaps through a controlled parametric study of rectangular and L-shaped plans, where leg ratios and eccentricity are systematically varied under a consistent mass and stiffness modelling approach. Furthermore, while existing literature emphasizes eccentricity, particularly that arising from core placement, less attention is given to the role of shear wall placement and the contribution of torsional stiffness itself, which are therefore examined explicitly in this work.

2

Theory

2.1 Wind-Induced Response of a Building

Wind-induced response provides the practical context for why torsional behaviour is critical in building design. Although this thesis does not model wind mechanics explicitly (e.g., pressure fields, aerodynamic interference, or aeroelastic effects), it is still important to outline how wind can activate torsion through the interaction between lateral loading, eccentricity between CM and CR, and the modal properties of the building. The following subsections summarize the basic mechanisms of wind excitation and torsional response, to motivate why eccentricity and torsional stiffness are treated as the key parameters in the analyses presented later.

2.1.1 Torsional Response

Torsional response arises when lateral loads act with an eccentricity relative to the structure's center of rigidity (CR), producing rotation about the vertical axis in addition to translation. The eccentricity may originate from geometric irregularity, uneven stiffness distribution, or a mismatch between the center of mass (CM) and CR. Even small misalignment between CM and CR can generate a significant torsional moment when the building is subjected to lateral loading.

A simplified expression for the torsional moment is:

$$M_t = F \cdot e \tag{2.1}$$

Where: M_t is the torsional moment about the vertical axis [Nm],
F is the resultant lateral wind force [N], and
e is the eccentricity [m] between the applied load path and the center of stiffness (CR).

Once torsion is activated, the torsional moment is resisted by the lateral force-resisting system through the floor diaphragm, which transfers combined translational and torsional actions to the vertical stabilizing elements. Load distribution becomes non-uniform because stiffer elements attract larger forces, while more flexible elements undergo larger deformations. Since torsional effects increase with distance from CR, perimeter elements may experience considerably higher shear forces and bending moments than elements closer to the center. Diaphragm behaviour is therefore important because rigid diaphragms provide a more controlled redistribution of

forces, whereas flexible diaphragms allow for larger in-plane distortions and a less predictable torsional load path.

From a design perspective, torsional response is mitigated through regular plan layouts, centrally located and continuous stabilizing systems, and diaphragms with sufficient in-plane stiffness. Design standards also account for uncertainties by including accidental eccentricity, typically implemented as a prescribed offset of the applied lateral loads.

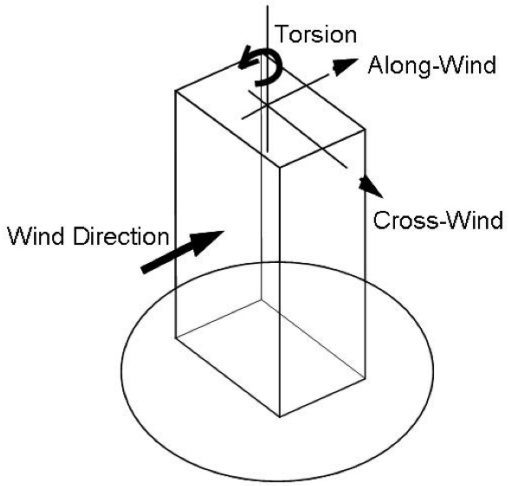

Figure 2.1: Wind-induced response on a building [1].

2.1.2 Excitation and Vibrations

Wind loading contains both a mean (quasi-steady) component and a fluctuating component driven by turbulence. While the mean component can often be approximated as a steady lateral force, the fluctuating pressures vary with time, height, and façade geometry, producing dynamic excitation of the structure. Turbulent wind contains energy across a broad range of frequencies. When a significant portion of this energy overlaps with one of the natural frequencies of the building, resonant amplification may occur and the corresponding vibration mode can dominate the response.

In symmetric buildings, the fundamental mode shape is typically lateral sway in one principal direction. In asymmetric plans, or in systems with stiffness or mass offsets, the modal response may instead take the form of torsional or coupled lateral-torsional motion already among the lowest modes. This is critical for serviceability because low-order modes contribute most to global response and are more easily excited by wind; torsional or coupled behaviour therefore tends to amplify accelerations and displacements at the plan edges and produces uneven motion across the floor plate.

For timber buildings, wind-induced vibrations and torsional coupling require particular attention because timber systems typically have lower mass and stiffness compared with concrete and steel. These characteristics tend to reduce natural frequencies and damping, increasing sensitivity to the fluctuating energy content of wind. In mid-rise timber buildings, even modest eccentricities between mass and stiffness centers may therefore be sufficient to shift the dominant response towards torsional or coupled lateral-torsional behaviour, increasing the importance of stabilizing system placement, diaphragm stiffness, and overall plan regularity.

2.2 Modal Analysis

A modal analysis is used to describe the dynamic structural behaviour of a building by identifying its natural frequencies (eigenfrequencies) and corresponding mode shapes. Using finite element analysis (FEA), the structure is idealized as a dynamic system governed primarily by mass and stiffness distributions. Together, these properties determine how the building prefers to vibrate and the characteristic deformation patterns associated with each natural frequency.

Reviewing eigenfrequencies and mode shapes is particularly important when a building is subjected to dynamic external loads such as wind, since resonance or significant vibration can occur if loading contains energy near the natural frequencies of the structure. The lowest (fundamental) mode is often the most influential for the global response because it is associated with the smallest energy required to excite the structure, and therefore tends to dominate the overall motion.

2.2.1 Eigenfrequency

An eigenfrequency is the frequency at which a system oscillates freely after being disturbed and then left to vibrate on its own. Each eigenfrequency is associated with a corresponding deformation pattern, known as the mode shape (eigenmode), which describes how the structure moves when vibrating at that frequency.

For a simple single-degree-of-freedom mass–spring system, the natural frequency can be expressed as:

$$f_n = \frac{1}{2\pi}\sqrt{\frac{k}{m}}[Hz] \tag{2.2}$$

Where: k is the stiffness [N/m], and
m is the participating mass [m].

When a system is disturbed by applied forces, forced vibrations occur. If the excitation frequency approaches the natural frequency of the system, the vibration response can increase significantly. This phenomenon is called resonance and may lead to amplified displacements and accelerations.

2.2.2 Mode Shapes

In building structures, the lowest modes are often characterised by global lateral translations in the principal horizontal directions (x and y), as illustrated by the 1st and 2nd modes in Figures 2.2 and 2.3. At higher frequencies, the dynamic response typically becomes more complex and may include torsional behaviour or coupled translational–torsional patterns, as shown by modes 3–6 in Figure 2.3. These mode shapes are independent of external loading and describe how the structure would deform if it was excited at one of its eigenfrequencies.

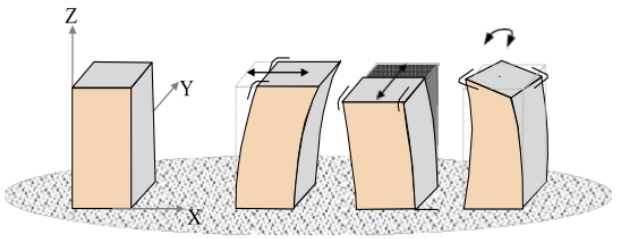

Figure 2.2: The first three theoretical mode shapes of a building [2], translation in x, and y, and then torsion.

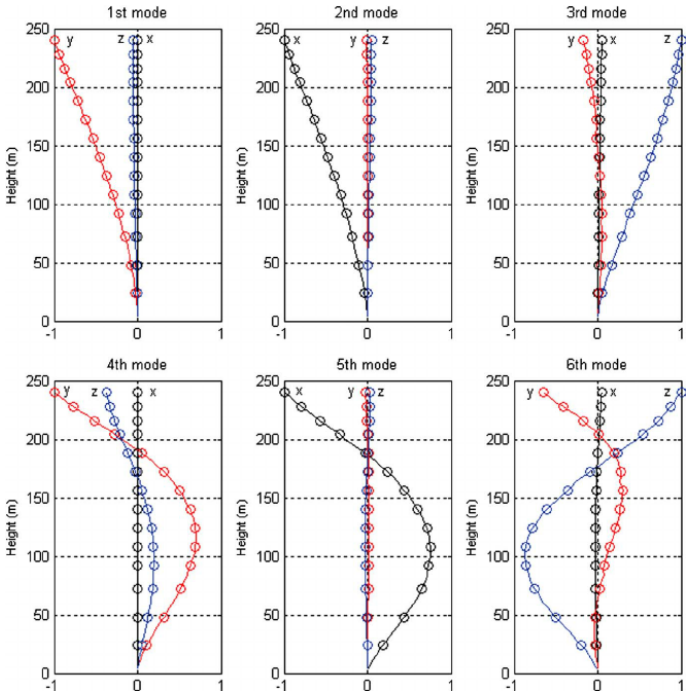

Figure 2.3: The first six mode shapes of a building under wind-induced forces [3]. Mode 1 showing translation in y, mode 2 showing translation in x, and mode 3-6 showing torsional or coupled mode shapes.

The characteristics of each mode shape are governed primarily by the distributions of stiffness and mass. In buildings with a symmetric layout and stabilizing elements located near the center, translational and torsional modes are often clearly separated. In contrast, plan irregularity, asymmetric stiffness, or eccentric placement of stabilizing systems can result in coupled lateral–torsional modes and more complex deformation patterns. In particular, when the center of mass (CM) and center of rigidity (CR) do not coincide, the resulting eccentricity couples lateral motion with rotation about the vertical axis.

2.2.3 Mode Shape Identification

In a modal analysis, each eigenmode represents a characteristic deformation pattern that the structure tends to vibrate in at a specific natural frequency. For buildings with a rigid diaphragm behaviour, the in-plane motion of a floor can be described as a translational, torsional, or a combination of both. Depending on how dominant the translational and rotational components are, the mode shape can be classified as predominantly translational, predominantly torsional, or coupled. This section introduces reference cases that are later used to interpret and classify the extracted FEM modes.

To illustrate the idealised cases, consider the reference rectangle in Figure 2.4, representing a rectangular building plan with the center of mass (CM), the center of rigidity (CR), and four corner points. The same CM–CR offset is used in all illustrations to keep the setup consistent, even though such eccentricity would typically produce a coupled mode in practice.

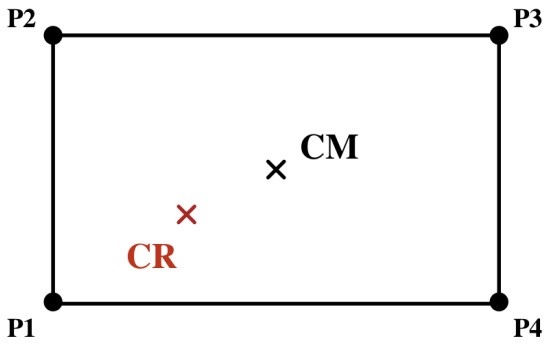

Figure 2.4: Reference rectangle.

2.2.3.1 Translation

A purely translational mode shape corresponds to rigid-body translation of the diaphragm without any rotation. In this ideal case, all points of the diaphragm move with the same displacement vector (same direction and amplitude). Therefore, the in-plane displacements at any set of points on the diaphragm are equal, i.e.

$$u_1 = u_2 = u_3 = ... = u_i. \tag{2.3}$$

For a geometrically and structurally symmetric plan, the fundamental mode is generally dominated by lateral translation, typically aligned with one principal direction. The idealized translational response may therefore be represented as pure translation in the x-direction, pure translation in the y-direction, or translation with simultaneous components in both directions.

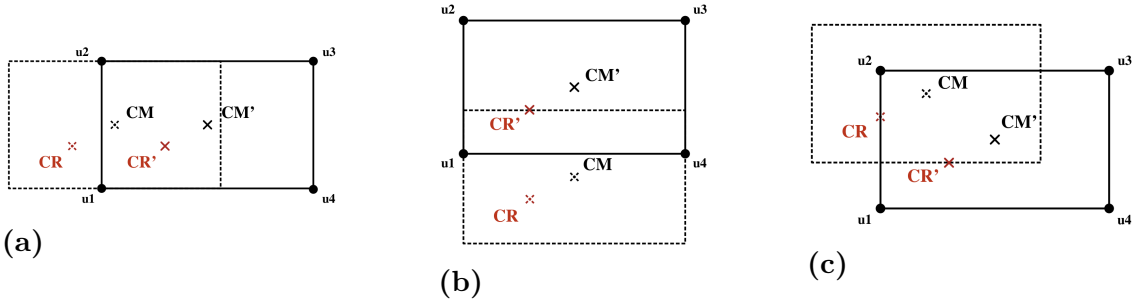

Figure 2.5: Idealised translational motion of the reference rectangle. The solid outline shows the deformed configuration (mode shape) and the dotted outline shows the reference configuration from Figure 2.4. CM and CR denote the original positions, while CM' and CR' denote the positions in the deformed configuration. The quantities u_1, u_2, u_3, and u_4 represent the in-plane displacements of the corner points P_1, P_2, P_3, and P_4. The mode shapes correspond to (a) pure translation in the x-direction, (b) pure translation in the y-direction, and (c) combined translation in both the x- and y-direction.

2.2.3.2 Torsion

A purely torsional mode corresponds to rigid-body rotation of the diaphragm about a vertical axis, without net translation. For building floors, this rotation is commonly interpreted relative to the CR. In the idealized pure torsion case, the diaphragm rotates about CR, meaning that CR itself does not translate, and the positions CR and CR' coincide. The in-plane displacement magnitude at any point increases with its distance to CR. Hence, corner points (often the most distant points) experience the largest displacements. Figure 2.6 illustrates this idealized torsional mode shape for the reference rectangle.

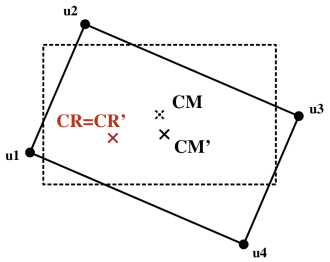

Figure 2.6: Pure torsional rotation of a rigid diaphragm about the CR. CM and CR denote the positions before rotation, while CR', CM', and u_1–u_4 indicate the corresponding positions after rotation.

2.2.3.3 Coupled Mode Shape

In practice, many building modes are neither purely translational nor purely torsional. A coupled lateral-torsional mode occurs when the diaphragm undergoes both translation and rotation in the same mode shape. In such cases, displacements are not uniform across the plane, and points further away from the instantaneous axis of rotation experience larger total displacements due to the superposition of translation and rotation.

Nevertheless, a coupled mode can be interpreted as the sum of a translational component and a torsional component. If the CR is known, the rotational part may be described as rotation about the CR. Since rotation about CR does not produce displacement at CR itself, the displacement of CR in the x- and y-directions therefore represents the translational part of the mode. By subtracting this translational contribution from the displacements at selected points, the remaining displacement field represents the torsional contribution. This decomposition provides a practical basis for quantifying torsional participation and for classifying modes as predominantly translational or predominantly torsional. Figure 2.7 illustrates how the coupled mode shape (left) can be decomposed into a translational component and a torsional component.

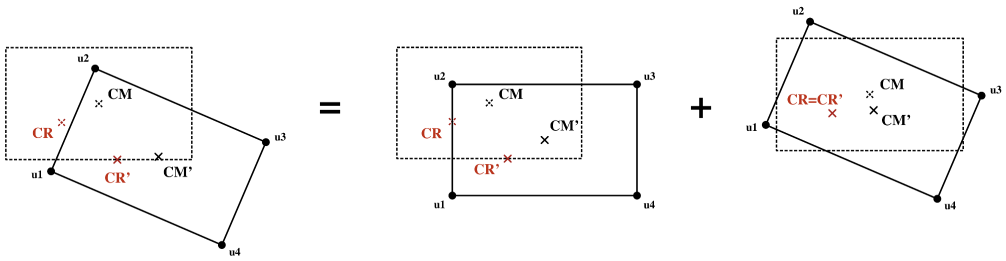

Figure 2.7: Coupled mode shape, illustrating the combined translational and torsional contributions.

2.2.4 Effective Modal Mass

The effective modal mass (EMM) is an indication of how much of the structure's total mass that is participating in a specific mode shape. A mode with a larger EMM generally contributes more to the dynamic response in that direction and is therefore more significant to consider. In practice, the cumulative EMM is often checked, and enough modes are included so that approximately 90% of the mass is captured in each principal direction to ensure that the dynamic behaviour of the building is adequately represented.

2.3 Plan Properties Governing Torsion

This section defines the geometric and stiffness-based plan properties used in this thesis to quantify torsional sensitivity, including CM, CR, eccentricity, and torsional stiffness about the CR.

2.3.1 Center of Mass

For plan layouts that are not geometrically or structurally symmetric, the CM should be determined explicitly rather than assumed to coincide with the geometric center. The CM coordinates in the floor plane are obtained as mass-weighted averages of the element coordinates:

$$x_{CM} = \frac{\sum m_i \cdot a_i}{\sum m_i} \tag{2.4}$$

$$y_{CM} = \frac{\sum m_i \cdot b_i}{\sum m_i} \tag{2.5}$$

Where: m_i is the element mass,
a_i is the x-coordinate of the element's centroid,
b_i is the y-coordinate of the element's centroid.
a_i & b_i are distances with respect to a chosen reference.

2.3.2 Bending Stiffness

To assess lateral stability and torsional response, the bending stiffness of the stabilizing elements must be considered. For a rectangular cross-section, the second moment of area about the principal axes is:

$$I_{x,i} = \frac{b \cdot h^3}{12}[m^4] \tag{2.6}$$

$$I_{y,i} = \frac{h \cdot b^3}{12}[m^4] \tag{2.7}$$

Where: b is the cross-section width [m], and
h is the cross-section height [m].

In this work, the directional bending stiffness terms $S_{x,i}$ and $S_{y,i}$ are used to describe the lateral stiffness contribution of element i in the x- and y-directions. The corresponding total bending stiffness in each direction that is denoted by K_x and K_y.

2.3.3 Center of Rigidity

The center of rigidity (CR), also referred to here as the center of rotation, can be computed as stiffness-weighted averages represented by the directional stiffness contributions $S_{x,i}$ and $S_{y,i}$:

$$x_{CR} = \frac{\sum S_{y,i} \cdot a_i}{\sum S_{y,i}} \tag{2.8}$$

$$y_{CR} = \frac{\sum S_{x,i} \cdot b_i}{\sum S_{x,i}} \tag{2.9}$$

Where: $S_{x,i}$ is the lateral stiffness contribution of element i in the x-direction„
$S_{y,i}$ is the lateral stiffness contribution of element i in the y-direction, and
a_i, b_i are the centroid coordinates of element i, with respect to a chosen point.

2.3.4 Torsional Stiffness about the CR

The torsional stiffness of the floor system about the CR can be estimated by summing the stiffness contributions multiplied by the squared lever arms to the CR:

$$K_\theta = \sum(S_{y,i} \cdot x_i^2) + \sum(S_{x,i} \cdot y_i^2)[m^6] \tag{2.10}$$

Where: $S_{x,i}, S_{y,i}$ are the directional stiffness contributions,
x_i is the distance in x from element i to the CR, and
y_i is the distance in y from element i to the CR.

2.3.5 Eccentricity

Plan eccentricity occurs when the CM and CR do not coincide. When lateral loads act through the CM while the stiffness is centered elsewhere, a torsional moment is induced about the vertical axis, which increases edge displacements and may lead to larger demands in certain stabilizing elements. Eccentricity may be caused by

geometric irregularities, uneven stiffness distribution, and/or non-uniform mass distribution.

The magnitude of eccentricity is defined as the distance between CM and CR:

$$e = \sqrt{(x_{CR} - x_{CM})^2 + (y_{CR} - y_{CM})^2}[m] \tag{2.11}$$

Where: (x_{CM}, y_{CM}) are the coordinates of the CM, and
(x_{CR}, y_{CR}) are the coordinates of the CR.

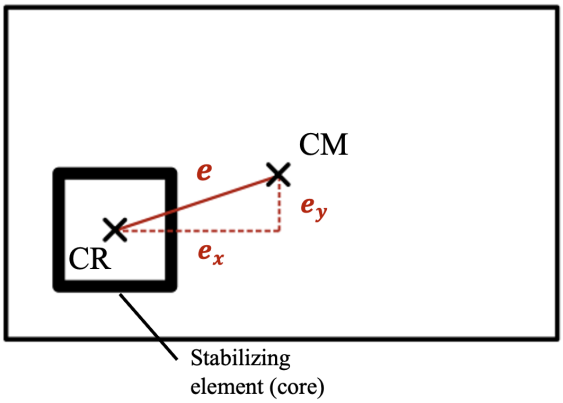

Figure 2.8: Eccentricity in a reference rectangular plan.

2.4 Parametric Modelling

Parametric modelling is a design approach where parameters of the design is defined and modelled so that these can be changed during the process and automatically updating the entire model. This modelling approach allows for flexible design because it is easy to make changes whenever in the process.

2.4.1 Grasshopper

Grasshopper is a visual programming environment integrated into Rhinoceros 3D which allows users to create parametric or rule-based models instead of modelling every component individually. Instead of traditional text-based coding, Grasshopper uses node-based workflow where different components are connected to each other with wires to define relationships between data, geometry and operations. This allows for parametric modelling because changes in input parameters automatically update the resulting geometry.

Although Grasshopper contains a large library of components, parametric structural models can typically be constructed using a limited set of fundamental component categories, described below:

- **Parameter:** Parameter components store and pass data such as numbers, text, lists, points or curves. They do not perform operations but act as containers that help structure the model. Typical examples include *Number*, *Point*, *Curve*, and *Panel*. Parameter components are used to control geometric dimensions, material properties and load magnitudes.

- **Math and Logic:** These components perform numerical operations such as addition, multiplication, conditional filtering, and comparisons. They enable the creation of relationships between variables, for example by scaling dimensions, iterating through alternative configurations or controlling the placement of structural elements.

- **Geometry:** Geometry components generate or modify geometric entities such as points, curves, surfaces or solids. Examples include *Construct Point*, *Move*, *Extrude*, and *Boundary Surface*. In this thesis, these components are used to construct floor plans, place structural elements and define analytical geometry to be exported to FEM-Design.

- **Data Management:** Grasshopper operates heavily with lists and data trees. Components such as *Merge*, *Flatten*, *Graft*, and *List Item* control how information is grouped and passed through the system. Proper data management is essential to ensure that structural elements and loads are mapped correctly when exported to the analysis model.

- **Plug-ins and Toolboxes:** Grasshopper can be extended through external plug-ins. In this work, the FEM-Design API components provide the connection between the parametric model and the finite element model, enabling automated creation of structural objects, assignment of materials and sections, and definition of load cases and combinations. Additional toolboxes (e.g., TT Toolbox) may be used to simplify workflows, add utilities for geometry/data handling, or provide domain-specific components depending on the modelling needs.

In this thesis, Grasshopper is used to generate variations of building layouts and stabilizing systems in order to perform a systematic parametric study of torsional wind response.

2.4.2 FEM-Design and the FEM-Design API

FEM-Design is a commercial finite element analysis (FEA) program developed by StruSoft for structural engineers. It provides tools for modelling, analysing and designing structures according to Eurocode. It includes calculations such as static,

dynamic, stability, eigenvalue analysis, and seismic analyses, as well as detailed element and material definitions for timber, concrete, steel, and other customized materials.

The FEM-Design API enables a direct link between Grasshopper and FEM-Design. In this workflow, Grasshopper is used to generate the parametric structural geometry and associated modelling data, while FEM-Design performs the numerical analysis. Since the model is parameter-driven, updates to geometric or material inputs in Grasshopper can be propagated to FEM-Design, allowing automated regeneration and re-analysis of multiple design variants.

3
Methods

The methodology of this thesis is centered around a parametric study focused on assessing the torsional wind response of mid-rise timber buildings featuring various plan geometries. Parametric models are developed in Grasshopper utilizing the FEM-Design API Toolbox, which allows direct definition and export of analytical models for finite element analysis (FEA) in FEM-Design. Two building configurations are examined: a rectangle and an L-shape, which represent typical types of plan irregularities. For each plan type, key parameters (e.g., aspect ratio and stabilizer placement) are varied both systematically in parametric sweeps and iteratively through targeted, practice-like adjustments to investigate their effects on torsional susceptibility. The building typology is a mid-rise office building with timber stabilizing units. Element dimensions are decided using Calculatis by Stora Enso, and all models undergo modal analysis in FEM-Design. Both input parameters and output results are cataloged in Excel to facilitate cross-comparison among cases.

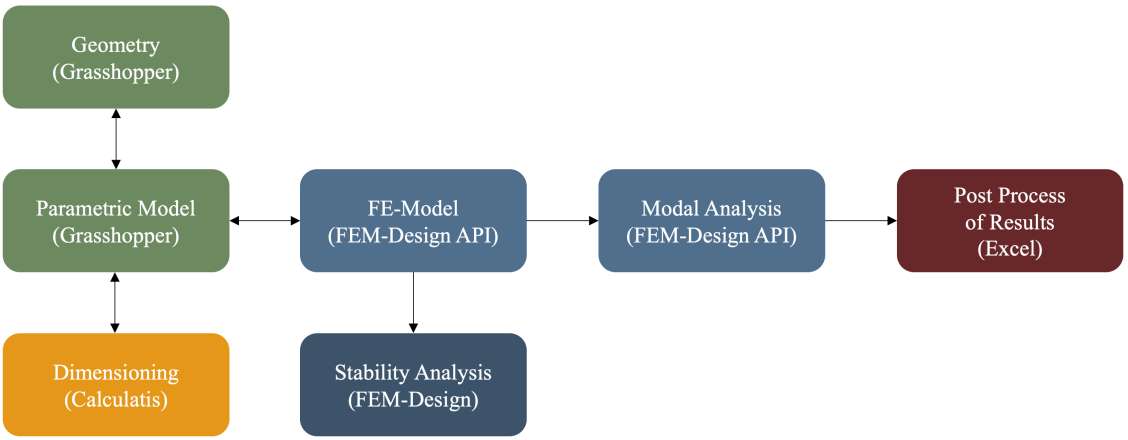

Figure 3.1: Illustration showing the workflow of the parametric model.

3.1 Building Design

The mid-rise timber buildings investigated in this study consist of a concrete foundation and a structure formed by CLT slabs, CLT shear walls, glulam columns, and glulam beams. The shear walls have both been used as a core, by placing them in a square, and as shear walls placed along the perimeter of the building.

To keep the parametric study efficient, the number of varying inputs is limited. Therefore, the element dimensions are held constant for all model variants, allowing the study to focus on parameters related to plan layout and geometric configuration rather than changes in member sizing.

3.1.1 General Layout

Two plan configurations are considered in the study: a rectangular plan and an L-shaped plan. The structural layouts are kept as comparable as possible within the geometric constraints of each configuration. A regular column grid defines the primary layout, with a centre-to-centre spacing of 6 m in both the x- and y-directions. The floor system is divided into 6 m x 6 m slab panels, which span in the short direction of each building part. Beams span 6 m in the long direction to support the slabs and transfer loads to the columns. Figure 3.2 illustrates the column grid, slab orientations, and beam layout for the two plan geometries. Black squares represent columns, solid black lines represent beams, and dashed lines indicate the slab divisions, with the spanning direction marked for each slab component. The base geometry for the L-shaped plan has x=54 m, y=54 m , and a width of 18 m, while the rectangular plan has dimensions 42×18 m. The buildings have 8 floors, with a storey height of 4 m.

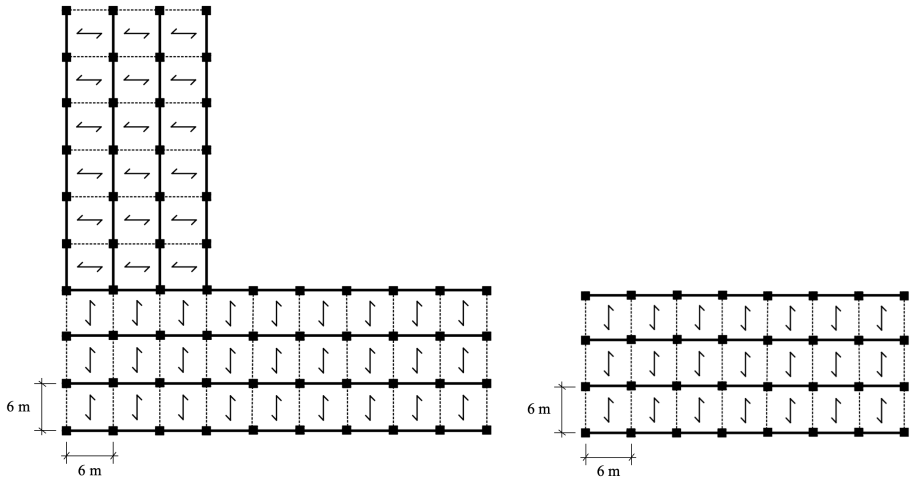

(a) L-shape **(b)** Rectangle

Figure 3.2: Illustrations of the column–beam grid with slab panels in between. Black squares indicate columns, solid black lines indicate beams, and dashed lines show the subdivision of the slab panels. The reference layouts correspond to (a) the L-shaped plan and (b) the rectangular plan.

The plan geometries and structural layouts are generated parametrically in Grasshopper (see Section 3.3.1), which enables systematic variation of key geometric parameters while maintaining the same modelling assumptions. In the parametric study, the x-length, particularly for the L-shaped plan, is varied in selected cases to investigate the influence of plan aspect ratio.

3.2 Loads & Dimensioning

Before evaluating torsional behaviour, the structural system is first verified to be globally stable. An unstable model can lead to unreliable modal results, where the apparent torsional response is dominated by numerical artefacts rather than structural behaviour

This section presents the adopted load magnitudes and load combinations, together with the preliminary element dimensions obtained using *Calculatis by Stora Enso*.

3.2.1 Load Combination

The load effects are evaluated using the ultimate limit state (ULS) fundamental load combination. For one leading variable action, the combination is written as:

$$\sum_j \gamma_G \, G_{k,j} + \gamma_Q \, Q_{k,1} + \sum_i \gamma_Q \, \Psi_{0,i} \, Q_{k,i} \tag{3.1}$$

Where:
- $G_{k,j}$ is the characteristic value of permanent action j (dead loads),
- $Q_{k,1}$ is the leading variable action,
- $Q_{k,i}$ are the accompanying variable actions,
- $\gamma_G = 1.0$ is the partial factor for permanent actions,
- $\gamma_Q = 1.5$ is the partial factor for variable actions, and
- $\Psi_{0,i} = 0.3$ is the combination factor for accompanying variable action i.

3.2.2 Dimensioning Loads

The actions included in the calculations are self-weight, complementary dead load, imposed load, and snow load. The characteristic values adopted in this study are summarised in Table 3.1. Snow load is based on Gothenburg conditions and a flat roof assumption.

Loads	$[kN/m^2]$
Self-weight	Material dependent
Complementary Dead Load	2.50
Imposed Load (Office, Cat. B)	3.0
Snow Load (Gothenburg, flat roof)	1.20

Table 3.1: Dimensioning loads used for stability analysis.

3.2.2.1 Self-weight

The self-weight of structural elements is obtained from the material density and gravitational acceleration. For an element with volume V, the characteristic dead load is:

$$G_k = \rho \, V \, g \tag{3.2}$$

Where: ρ is the material density $[kg/m^3]$,
V is the element volume $[m^3]$, and
g is the gravitational acceleration.

3.2.2.2 Complementary Dead Load

Complementary dead load includes non-structural permanent components such as finishes, installations, and suspended ceilings. In this study, a uniformly distributed complementary dead load of $2.5\,\mathrm{kN/m^2}$ is assumed, based on common practice for timber buildings in Sweden.

3.2.2.3 Imposed Load

Imposed load represents the variable actions from occupancy and usage. The imposed load is selected according to the EC category for office use (Category B) and applied to all office floors as $3.0\,\mathrm{kN/m^2}$. The roof is treated separately and is not assigned imposed office loading.

3.2.2.4 Snow Load

Snow load is also included as a variable action. The characteristic roof snow load is determined from the characteristic ground snow load and a roof shape coefficient:

$$s = \mu_1 \, s_k \tag{3.3}$$

Where: $s_k = 1.5\,\mathrm{kN/m^2}$ is the characteristic ground snow load for Gothenburg, and
$\mu_1 = 0.8$ is the roof shape coefficient for a flat roof.

3.2.3 Implementation in *Calculatis*

To establish a stable reference structural system and consistent member dimensions for all model variants, preliminary sizing and verification checks were carried out in *Calculatis by Stora Enso*. The software was used as an efficient design support tool to evaluate load effects and key requirements such as fire resistance for representative elements. The cross-sections obtained from these checks were then applied throughout the parametric study, ensuring that differences in torsional behaviour are driven by plan layout and geometric parameters rather than changes in member sizing.

Figure 3.3 shows an example of the load input and design setup for a GL30h beam in *Calculatis*, with a cross-section of 215×450 mm, service class 2, and fire resistance class R90. The self-weight of the beams is included automatically (LC1 in Figure 3.3), while additional permanent loads from elements above can be introduced separately (here represented by LC3). All *Calculatis* checks were performed for components at the bottom floor level, as these are generally the most highly loaded.

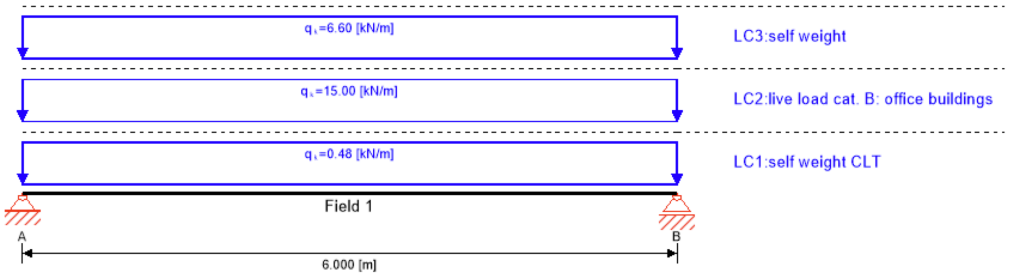

Figure 3.3: Example of beam loading and design setup in *Calculatis by Stora Enso*.

The resulting internal force diagrams for the same beam are presented in Figure 3.4, including the bending moment diagram and the shear force diagram.

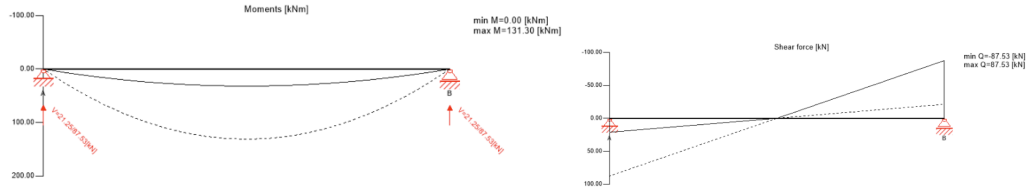

(a) **(b)**

Figure 3.4: Calculatis output for the beam in Figure 3.3 showing (a) the bending moment diagram, and (b) the shear force diagram.

Based on corresponding *Calculatis* calculations for the structural elements, the materials and cross-section dimensions adopted for the parametric study are summarised in Table 3.2.

Structural Element	Material	Cross-Section Dimension $[mm^2]$
Foundation	C30/37	500×6000
Slabs	CLT 220 L7s	220×6000
Shear Walls	CLT 200 L5s	200×4000
Columns	GL30h	330×360
Beams	GL30h	215×450

Table 3.2: Final dimensions of the structural elements.

For detailed *Calculatis* input and calculations, see Appendix A.

3.2.4 Stability Analysis in FEM-Design

Once the member dimensions were established in *Calculatis*, the structural model was generated using the FEM-Design API and analysed in FEM-Design. A stability analysis was performed to verify that the structural system provides sufficient global stiffness and to ensure that the subsequent torsional evaluation is based on

a numerically stable model. Table 3.3 summarizes the edge connection assumptions applied to the structural elements in the FEM-Design model.

Structural Element	Type of Connection
Foundation	Rigid
Slabs	Hinged
Shear Walls	Rigid
Columns	Hinged
Beams	Hinged

Table 3.3: Applied edge connection assumptions for the structural elements in the FEM-Design model.

The stability check confirms that the global lateral system behaves as intended and that no local mechanisms govern the response.

3.3 Parametric Modelling in Grasshopper with the FEM-Design API

All analytical models are created directly in Grasshopper using the FEM-Design API Toolbox. This workflow allows for the definition of geometry, structural elements, supports, and loads within Grasshopper, which are then recognized natively in FEM-Design without the need for manual reconstruction in the calculation program. The use of parametric modelling ensures consistent and repeatable model definitions across all studied variants and enables a systematic evaluation of torsional response for different geometric configurations.

3.3.1 Basic Geometrical Modelling

In this study, a single Grasshopper model was used for both the rectangular and the L-shaped configurations. The modelling set up for the two plan types differ only in the initial step where the base plan geometry is defined. One component group generates a rectangular outline, while an alternative group generates an L-shaped outline. All subsequent steps in the workflow are identical for both configurations. However, the rectangular reference plan uses a 42 m length to allow the core to be placed at the mid-grid location, enabling a zero-eccentricity baseline. The L-shaped reference plan instead uses 54 m leg lengths to provide sufficient room for systematic wall and core relocations along each leg while maintaining a consistent 6 m grid.

Several approaches can be used to construct the base geometry in Grasshopper. In this study, the plan outline is defined from a set of control points that serve as the geometric reference for the entire model. A point-based approach ensures that all elements are anchored to explicit coordinates, reducing the risk of small offsets between model parts that could otherwise affect connectivity or introduce numerical

inconsistencies in the analysis.

To enable parametric studies, key geometric variables are defined as adjustable inputs. *Number Sliders* are used to control point offsets and thereby govern fundamental dimensions such as building width and length. Since downstream geometry and element placement are derived from these control points, changes to a single parameter (e.g., plan length or width) propagate automatically through the model while maintaining correct connectivity.

After defining the base plan geometry, a 6×6 m grid is generated by subdividing the plan edges at 6 m intervals and connecting corresponding points to form horizontal and vertical grid lines. Intersection points and grid segments are then used to define the structural layout: intersections locate the columns, 6 m segments define beams and shear walls, and grid cells define the slab panels. As a result, the structural layout remains coherent and automatically adapts when geometric parameters (such as plan length or width) are varied. To conform the grid, all plan dimensions are chosen as multiples of 6 m. Figure 3.2 shows the grid layout on both plan shapes.

3.3.2 FEM-Design API

After defining the parametric plan geometry and 6×6 m structural grid in Grasshopper, the FEM-Design API is used to generate the analytical model by assigning materials and cross-sections and constructing the structural elements (foundation, slabs, shear walls, columns, and beams) directly from the grid. The model is then assembled and linked to FEM-Design, where the modal analysis is executed through the API. The detailed set up is shown in Appendix B.

3.3.3 Extracting Results in Grasshopper

After running the modal analysis, results are retrieved in Grasshopper using *FEM-Design.GetCaseCombResults*. The desired output is selected via the *ResultsType* component.

Eigenfrequency results are extracted by selecting *EigenFrequencies*, which returns mode number, eigenfrequency, period, modal mass, and mass participation factors. In this study, the extracted eigenfrequencies and corresponding mode numbers are used for comparison between configurations (Figure 3.5).

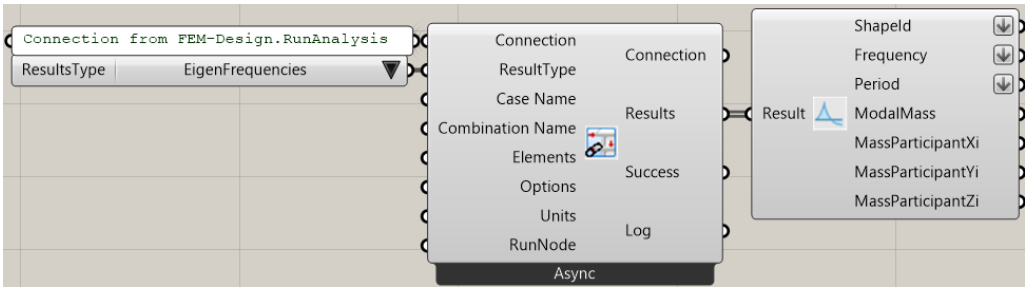

Figure 3.5: Extraction of eigenfrequency results using the reults type *EigenFrequencies*.

Nodal displacements are extracted using the result type *NodalVibration*. The relevant outputs are the mode number, node ID, and translational displacements. Rotational values reported at individual nodes are not used, since the objective is to quantify the global lateral-torsional behaviour of the plane. To simplify post-processing, one result component is used per mode.

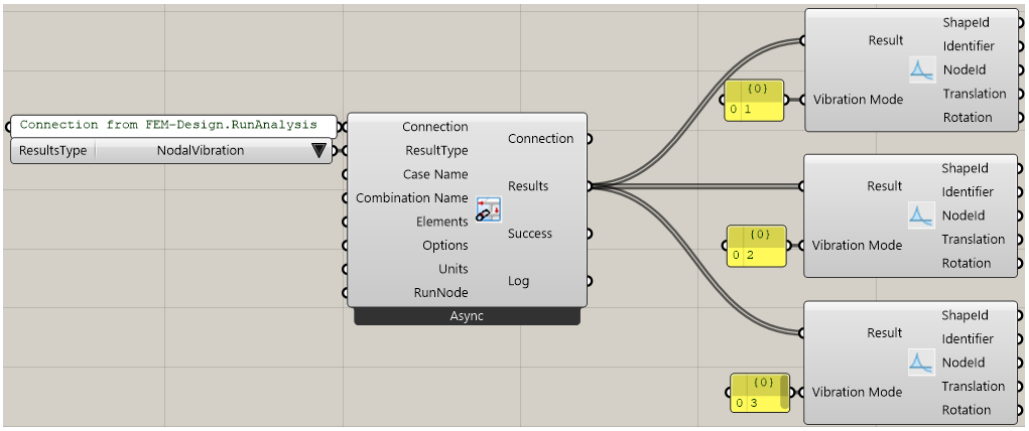

Figure 3.6: Extraction of nodal vibration results using the results type *NodalVibration*.

The primary response measure used in the torsional evaluation is the in-plane translational displacement of selected nodes. A rigid diaphragm behaviour is assumed, meaning each floor translates as a unit without significant in-plane distortion. The foundation is modelled with a rigid support, resulting in negligible displacement at the base and the largest response at the top floor. Therefore, three nodes at the top floor are selected to represent floor motion, as illustrated in Figure 3.7. The extracted x- and y-displacements at these points, together with the centre of rigidity (CR), are used to classify each mode as predominantly translational, predominantly torsional, or coupled.

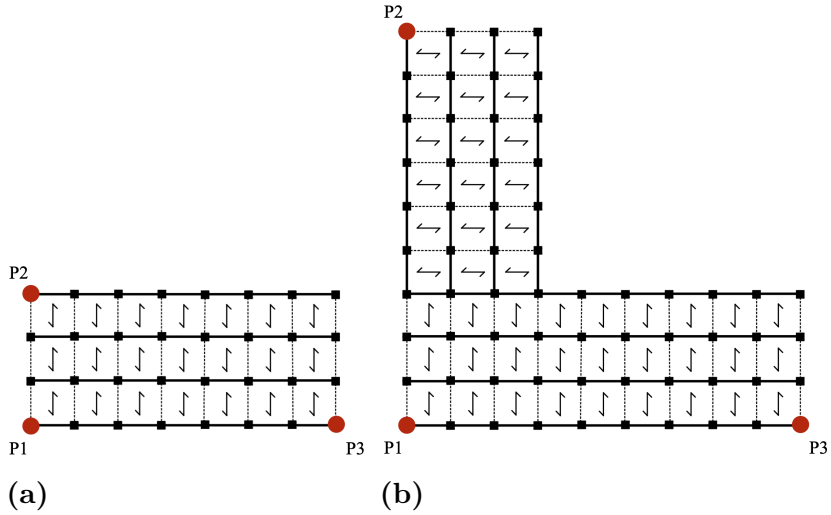

Figure 3.7: Selected result points at the top floor for (a) the rectangular plan and (b) the L-shaped plan. P_1 is located at the bottom-left corner, P_2 at the top-left corner, and P_3 at the bottom-right corner.

3.3.4 TT Toolbox

The TT Toolbox was used to automate the parametric study and streamline post-processing. It enables the Grasshopper definition to be iterated over many input combinations, while systematically collecting the resulting geometry, stiffness measures, and modal-analysis outputs into a structured dataset for export to Excel.

3.3.4.1 Looping the Model

Parametric variations are executed using the TT Toolbox component *Colibri Inputs (Iterator)*, which iterates over selected input parameters and runs the full model and analysis for each configuration.

3.3.4.2 Exporting Data to Excel

Results from all iterations are collected and exported using TT Toolbox components that provide a direct link to Excel. The exported dataset includes:

- Geometric input and derived quantities: Height, width, length, CM, CR, etc.
- Shear Wall Placements and layout descriptions.
- Stiffness properties: Bending stiffness, torsional stiffness. (These are calculated using the equations presented in Section 2.3)
- Eigenfrequency results: Mode number, frequency, etc.
- Nodal Vibrations results: Lateral nodal displacements.

3.4 Parametric Study

The parametric study investigates how plan configuration influences the tendency for torsional response in the fundamental mode. Based on the literature review, two

factors are treated as the primary drivers of torsion: (i) eccentricity, defined by the distance between the CM and the CR, and (ii) torsional stiffness (K_θ). The study is therefore structured to (a) vary eccentricity while keeping torsional stiffness as constant as possible, (b) vary torsional stiffness while keeping eccentricity close to zero (where feasible), and (c) vary both simultaneously to identify possible interaction effects.

Two plan geometries are investigated a rectangular plan and an L-shaped plan. The tested scenarios are summarized below, while detailed layouts and corresponding results are presented in Chapter

3.4.1 Rectangular Plan

The rectangular plan is used as the reference geometry since it can be designed fully symmetric in both geometry and stabilizing layout, allowing eccentricity to be reduced to zero. A symmetric base case is first established with a stabilizing system arranged such that CR coincides with CM. This provides an "ideal" dynamic reference, where the lowest modes are expected to be dominated by lateral translation in the principal directions, followed by a torsional mode.

The rectangular configurations are then evaluated through three main scenario groups:

- **Case A - Eccentricity induced by core placement:** The plan geometry and the shear wall layout are kept symmetric, while a core is relocated to different positions. This shifts CR relative to the (approximately fixed) CM and introduces controlled eccentricity, allowing the influence of eccentricity on the fundamental mode to be studied.
- **Case B - Torsional stiffness variation through shear wall placement:** To isolate the effect of torsional stiffness, configurations are created where the stabilizing system remains symmetric such that eccentricity is kept close to zero. The shear walls are then moved within the plan to change their lever arms relative to CR and thereby modify the K_θ, while maintaining a symmetric mass–stiffness arrangement.
- **Case C - Imbalance in bending stiffness between principal directions:** Additional configurations are used to introduce differences between the global bending stiffnesses K_x and K_y. These cases examine whether directional stiffness imbalance affects the modal ordering and torsional participation, both for near-zero eccentricity configurations and for layouts where eccentricity and torsional stiffness vary simultaneously.

3.4.2 L-shaped Plan

For the L-shaped plan, a near-zero eccentricity reference case is generally difficult to obtain. Depending on leg lengths, the CM may lie outside the plan outline, while a stable CR typically remains within the perimeter. As a result, coupled lateral-torsional behaviour is expected to occur more frequently than for the rectangular

plan. The objective for the L-shaped study is therefore to determine how geometric irregularity and stabilizer layout influence the onset of torsional dominance, and to identify layouts that maintain a predominantly translational fundamental mode where possible.

All L-shaped configurations include shear walls, with variations in placement and, in selected cases, length. The investigated scenarios are grouped as follows:

- **Case A - Aspect ratio effects:** The x-leg length is varied to study geometric influence. In Case A1 the stabilizing system is kept fixed, so CR remains essentially constant while CM shifts with the changing geometry, increasing eccentricity. In Case A2 a selected shear wall is moved with the x-leg, allowing CR to partially track the CM shift and increasing torsional stiffness through larger lever arms, enabling direct comparison with the fixed-stabilizer case.
- **Case B - Shear wall placement sensitivity (within geometry vs. along façades):** For a fixed L-shaped geometry, shear walls are systematically relocated to quantify how stabilizer placement affects both eccentricity and torsional stiffness. The study distinguishes between moving walls *within* the leg geometry (typically reducing effective lever arms and increasing torsional sensitivity) and moving walls *along the façades* (preserving large lever arms and generally promoting translational behaviour).
- **Case C - Effect of bending-stiffness imbalance:** The shear-wall relocation study is repeated with an imposed imbalance between the principal-direction bending stiffnesses ($K_x \neq K_y$). The purpose is to evaluate how directional stiffness asymmetry modifies torsional sensitivity, particularly near the transition region where small layout changes can switch the governing mode.
- **Case D - Core placement combined with aspect ratio:** A core is introduced in the common (overlapping) region and moved to different positions while the x-leg length is varied. Together with alternative perimeter wall layouts, these cases assess how core location and short-/long-leg geometries interact to shift CR and modify torsional participation in the lowest modes.

3.5 Mesh Convergence Study

Prior to the parametric analyses, a mesh convergence study was performed by varying the mesh size and evaluating the first three eigenfrequencies of a reference model. The results show convergence at mesh sizes of approximately 0.5 m, as illustrated in Figure 3.8. An average mesh size of 0.5 m was therefore adopted as a balance between accuracy and computational efficiency.

In the FEM-Design API, the *Fine mesh* option was used, for both the convergence study and the analysis, which introduces additional nodes within each mesh element and thereby refines the displacement field compared to a mesh defined only by corner nodes.

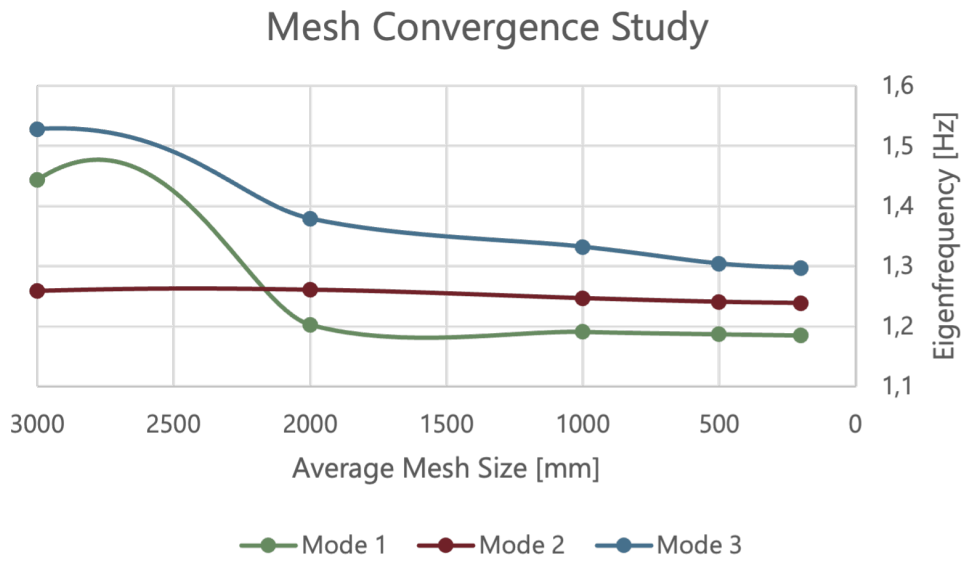

Figure 3.8: Mesh convergence graph illustrating the mesh size on the x-axis and the eigenfrequencies on the y-axis.

3.6 Post Process of Results

This section describes how the modal results from FEM-Design are post-processed to identify the governing behaviour of each configuration and to enable consistent comparison across the parametric study. For each model, the first three eigenmodes are extracted and classified as translation or torsion-dominated based on the motion of the (assumed rigid) floor diaphragm. The resulting mode classifications and eigenfrequencies are then related to key plan properties, eccentricity and torsional stiffness, using normalized measures that allow trends to be evaluated across both rectangular and L-shaped geometries.

3.6.1 Identification of Mode Shape

After each analysis, the first three modes are classified as predominantly translational or predominantly torsional. The desired reference behaviour is lateral translation in the first two modes, with the first torsional mode appearing as the third mode. This mode ordering is not expected for all configurations, particularly when eccentricity or stiffness irregularity introduces lateral-torsional coupling.

As described in Section 2.2.3, the in-plane motion of a rigid diaphragm can be interpreted as the superposition of a translational component and a rotational component (Figure 2.7). To quantify these contributions for coupled modes, the center of rotation must be known in both the undeformed configuration, CR, and the deformed configuration, CR', together with the undeformed and deformed coordinates of se-

lected result points. Given CR and the coordinates of points P_i in the undeformed plan and P_i' in the deformed mode shape (here denoted u_i), the location of CR' can be determined using trilateration, i.e., by computing an unknown point from its known distances to multiple reference points. Figure 3.9 illustrates the coupled mode shape and the point definitions used in the procedure.

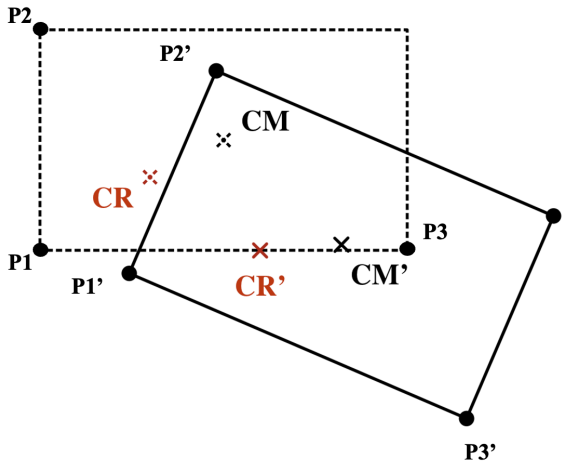

Figure 3.9: Coupled mode shape showing the original shape in the dashed figure and the mode shape in the solid lines, with corresponding points marked in the figure.

3.6.1.1 Determination of CR' using trilateration

For a rigid diaphragm, in-plane deformation of the floor plate is assumed negligible. Consequently, rigid-body motion preserves the distances between points on the diaphragm and the CR. The distance from each selected point to CR in the undeformed configuration is therefore equal to the distance from the corresponding deformed point to CR' in the mode shape. This geometric constraint allows the deformed center of rotation, CR', to be determined from the deformed positions of selected result points using trilateration.

Figure 3.10 separates the undeformed plan from the coupled mode shape. Three points are selected on the diaphragm, P_1, P_2, and P_3, with known undeformed coordinates and corresponding deformed coordinates extracted from the mode shape. The deformed point coordinates are denoted as:

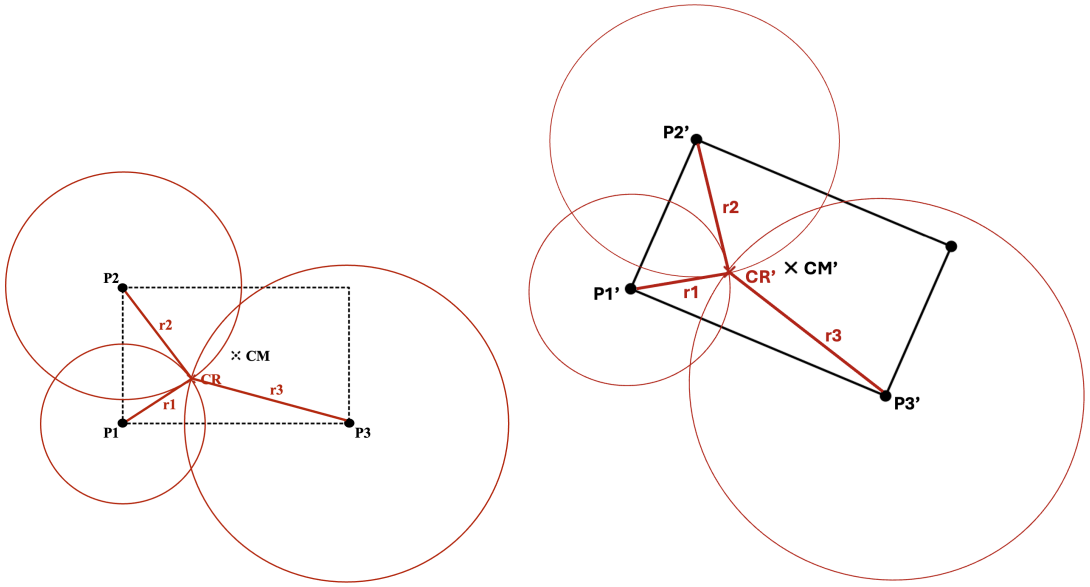

(a) Undeformed plan shape **(b)** Coupled mode shape

Figure 3.10: Trilateration setup of the coupled mode shape.

The deformed point coordinates are denoted as:

$$P_i' = (u_{i,x}, u_{i,y}), \qquad i = 1, 2, 3.$$

The deformed center of rotation, CR, is calculated in four steps as follows:

1. **Distances from CR to the undeformed points:**
   From the undeformed configuration, the squared distances from $CR = (CR_x, CR_y)$ to each point $P_i = (P_{i,x}, P_{i,y})$ are:
   $$r_i^2 = (P_{i,x} - CR_x)^2 + (P_{i,y} - CR_y)^2, \qquad i = 1, 2, 3. \tag{3.4}$$
   Only r_i^2 is needed; the square root is not required.

2. **Circle equations in the deformed configuration:**
   Since the diaphragm is assumed rigid, the same distances apply in the deformed configuration. Thus, $CR' = (x, y)$ must satisfy:
   $$(u_{i,x} - x)^2 + (u_{i,y} - y)^2 = r_i^2, \qquad i = 1, 2, 3. \tag{3.5}$$

3. **Linear system for CR':**
   Expanding Eq. (3.5) for $i = 1, 2, 3$ and subtracting the equation for $i = 1$ from the equations for $i = 2$ and $i = 3$ eliminates the quadratic terms x^2 and y^2, resulting in two linear equations in x and y:

$$2(u_{2,x} - u_{1,x})\, x + 2(u_{2,y} - u_{1,y})\, y = r_1^2 - r_2^2 + (u_{2,x}^2 - u_{1,x}^2) + (u_{2,y}^2 - u_{1,y}^2), \tag{3.6}$$

$$2(u_{3,x} - u_{1,x})\, x + 2(u_{3,y} - u_{1,y})\, y = r_1^2 - r_3^2 + (u_{3,x}^2 - u_{1,x}^2) + (u_{3,y}^2 - u_{1,y}^2). \tag{3.7}$$

For compactness, define:

$$A = 2(u_{2,x} - u_{1,x}), \tag{3.8}$$
$$B = 2(u_{2,y} - u_{1,y}), \tag{3.9}$$
$$C = 2(u_{3,x} - u_{1,x}), \tag{3.10}$$
$$D = 2(u_{3,y} - u_{1,y}), \tag{3.11}$$
$$E = r_1^2 - r_2^2 + (u_{2,x}^2 - u_{1,x}^2) + (u_{2,y}^2 - u_{1,y}^2), \tag{3.12}$$
$$F = r_1^2 - r_3^2 + (u_{3,x}^2 - u_{1,x}^2) + (u_{3,y}^2 - u_{1,y}^2). \tag{3.13}$$

The system can then be written as:

$$Ax + By = E, \qquad Cx + Dy = F. \tag{3.14}$$

4. **Closed-form solution:**
   Using Cramer's rule, with determinant:

$$\Delta = AD - BC, \tag{3.15}$$

the deformed center of rotation is obtained as

$$x = \frac{ED - BF}{\Delta}, \qquad y = \frac{AF - EC}{\Delta}. \tag{3.16}$$

A unique solution exists if $\Delta \neq 0$, which requires that the three deformed points u_1, u_2, and u_3 are not collinear.

3.6.1.2 Decomposition of a Coupled Mode into Translation and Rotation

Once the deformed center of rotation $CR' = (x, y)$ has been determined using trilateration, the coupled mode shape can be decomposed into a translational component and a torsional (rotational) component. Under the rigid diaphragm assumption, the in-plane motion of the floor can be represented as rigid-body translation plus rigid-body rotation about the CR.

The translational displacement is taken as the displacement of the center of rotation between the undeformed and deformed configuration:

$$\mathbf{d}_T = \begin{bmatrix} d_{T,x} \\ d_{T,y} \end{bmatrix} = \begin{bmatrix} CR'_x - CR_x \\ CR'_y - CR_y \end{bmatrix}, \tag{3.17}$$

with translation magnitude of:

$$d_T = \sqrt{d_{T,x}^2 + d_{T,y}^2}. \tag{3.18}$$

To isolate the torsional part, the translational contribution is removed from the deformed point coordinates. For each selected point $P_i = (P_{i,x}, P_{i,y})$ with deformed coordinates $P_i' = (u_{i,x}, u_{i,y})$, the translation-corrected coordinates are defined as:

$$\theta_{x,i} = u_{i,x} - d_{T,x}, \qquad \theta_{y,i} = u_{i,y} - d_{T,y}, \qquad i = 1, 2, 3. \tag{3.19}$$

These points represent the configuration obtained if the diaphragm had undergone rotation only.

The rotational radius from CR' to each corrected point is:

$$r_i = \sqrt{(\theta_{x,i} - CR_x')^2 + (\theta_{y,i} - CR_y')^2}, \qquad i = 1, 2, 3. \tag{3.20}$$

The chord length between the undeformed point P_i and the corresponding rotation-only point $(\theta_{x,i}, \theta_{y,i})$ is:

$$c_i = \sqrt{(\theta_{x,i} - P_{i,x})^2 + (\theta_{y,i} - P_{i,y})^2}, \qquad i = 1, 2, 3. \tag{3.21}$$

Assuming circular motion about CR', the rotational displacement length is approximated by the arc length:

$$s_i = 2r_i \arcsin\left(\frac{c_i}{2r_i}\right), \qquad i = 1, 2, 3. \tag{3.22}$$

To get the largest rotational distance, a representative rotational amplitude is taken as the maximum arc length among the selected points:

$$s_{\max} = \max(s_1, s_2, s_2). \tag{3.23}$$

The relative shares of translation and torsion in the coupled mode are quantified as:

$$UT = \frac{d_T}{d_T + s_{\max}}, \qquad UR = \frac{s_{\max}}{d_T + s_{\max}}, \tag{3.24}$$

where $UT + UR = 1$. A mode is classified as predominantly translational if $UT > UR$, and predominantly torsional if $UR > UT$.

3.6.2 Presenting of Results

The identified mode classifications and corresponding eigenfrequencies are related to geometric and stiffness-based parameters. To enable comparison across different geometries, the following normalized measures are introduced:

1. **Frequency Ratio (FR):**
   To identify whether the fundamental mode is torsional or translational, a frequency ratio is introduced. The ratio compares the fundamental frequency, f_1, to the lowest *translational* frequency in the modal set, f_T (i.e., the first mode that is predominantly translational in either x- or y-direction):

   $$FR = \frac{f_1}{f_T}. \tag{3.25}$$

   If the first mode is translational, then $f_1 = f_T$ and $FR = 1$. If a torsional mode occurs before the first translational mode, then $f_1 < f_T$ and $FR < 1$, indicating torsional dominance in the fundamental mode.

If: $FR = 1$ the fundamental mode is translational,
$FR < 1$ the fundamental mode is torsional.

2. **Normalized Eccentricity (e/D):**
Eccentricity is defined as the distance between the CM and CR, see Eq. 2.11. To enable comparison between different plan sizes, the eccentricity is normalized by the plan diagonal D:

$$D = \sqrt{x^2 + y^2}, \tag{3.26}$$

$$\frac{e}{D}. \tag{3.27}$$

Where: x plan dimension in the x-direction,
y plan dimension in the y-direction,
e eccentricity between CM and CR (Eq. 2.11).

3. **Normalized Torsional Stiffness (R):**
The torsional stiffness is expressed using a normalized measure that relates torsional stiffness to the overall translational bending stiffness of the stabilising system. To obtain a length-scale parameter, the ratio is square-rooted:

$$R = \sqrt{\frac{K_\theta}{K_x + K_y}}. \tag{3.28}$$

Where: K_θ total torsional stiffness about the vertical axis,
K_x, K_y total bending stiffness in the x- and y-directions.

With this definition, larger R values indicate greater resistance to torsion relative to translation. Since torsional resistance increases when stabilizing elements are distributed further away from the CR, R also serves as an effective measure of how "spread out" the stabilizing system is in plan.

4

Results & Discussion

As discussed throughout this thesis, the torsional response of a building is governed primarily by two parameters: eccentricity and torsional stiffness. This chapter presents and analyzes the simulated configurations to clarify when one parameter dominates and when a combined e/D–R relationship can be used to interpret whether torsion appears in the fundamental mode.

Two plan geometries are investigated: rectangular and L-shaped layouts. Rectangular plans are geometrically symmetric and can easily be designed with symmetric stabilizing systems, often resulting in negligible eccentricity. L-shaped plans may also be geometrically symmetric when the legs are equal. However, even in geometrically symmetric L-shaped plans, achieving zero eccentricity is often more challenging than for rectangles. The CM position is strongly influenced by the L-shaped mass distribution and may lie close to (or even outside) the re-entrant region, while the CR is constrained by where the stabilizing elements can realistically be placed within the plan. As a result, CM–CR coincidence is possible, but it typically requires more deliberate stabilizer placement and tuning, and many practical L-shaped layouts therefore tend to exhibit non-zero eccentricity. Accordingly, eccentricity is introduced for the rectangular cases by modifying the stabilizing system, whereas it is treated as a characteristic outcome of the geometry for the L-shaped configurations.

In general, CM is governed mainly by plan geometry, since the floor slabs contribute substantially more mass than the shear walls. Changes in stabilizer placement therefore shift CM only marginally unless the geometry changes. In contrast, CR is governed by the vertical stabilizing system (shear walls and core) and is highly sensitive to stabilizer placement. The stabilizer layout therefore controls eccentricity through CR movement, while simultaneously influencing torsional stiffness through the resulting lever arms and stiffness distribution. This motivates examining whether systematic combinations of eccentricity and torsional stiffness can distinguish torsion- and translation-dominated fundamental behaviour.

These relationships are also relevant in a wind context. Wind loading is a primary excitation source for many mid- to high-rise buildings, and it is particularly important for torsion because wind pressures are non-uniform in space and time. Even when the mean resultant wind force acts near the plan center, fluctuating components and aerodynamic effects can introduce torsional moments that couple translational and rotational motion. Therefore, the dynamic characteristics identified in this chapter, especially whether the fundamental mode is translation- or torsion-dominated

and how close a configuration lies to the transition regions, provide direct insight into wind-induced serviceability (SLS) sensitivity, where occupant comfort and drift limits may be governed by along-wind, across-wind, and torsional vibrations.

4.1 Connection to Wind-Induced Response

Wind effects are strongly frequency-dependent, and the fundamental mode often governs serviceability (SLS) response due to its low frequency and typically low damping. Configurations where torsion appears already in the fundamental mode are therefore more likely to show noticeable wind-driven rotation. In this sense, the frequency ratio FR is not only a classification metric, but also an indicator of whether torsional dynamics may compete with translation under wind excitation.

Wind can excite torsion whenever a CM-CR offset exists, since even a primarily translational wind force then generates a torsional moment about CR. In addition, real wind pressure fields are not perfectly symmetric, so fluctuating pressures can introduce torsional components even when the mean resultant is close to the plan center. This makes the transition regions in the e/D-R plots, in the following sections, particularly relevant, because small stabilizer-layout changes can shift the governing behaviour and alter the expected wind response.

For rectangular plans, torsional wind sensitivity is minimized by limiting e/D (avoiding stabilizer asymmetry that shifts CR) and by maintaining large lever arms (high R). For L-shaped plans, eccentricity is often inherent, so robustness relies more strongly on achieving sufficiently high torsional stiffness through stabilizer placement toward the extremities and avoiding pronounced stiffness imbalance. Overall, the e/D-R zoning can be used as an early-stage wind-sensitivity overview, where configurations that reduce e/D and increase R are expected to be less prone to wind-driven torsional SLS response, whereas points near the mixed-response boundaries should be treated as wind-sensitive and verified with additional dynamic wind assessment.

4.2 Rectangular Plan Configurations

Since rectangular plans are geometrically symmetric, they provide a clear basis for investigating how torsional response can be induced by structural asymmetry in the stabilizing system. In this study, asymmetry is introduced primarily through variations in the layout of the core and shear walls. The investigated rectangular configurations include: (i) structural asymmetry introduced by core placement, (ii) the effect of shear wall placement on torsional stiffness under zero eccentricity, and (iii) the influence of bending-stiffness imbalance between the principal directions, evaluated both without and with eccentricity.

4.2.1 Case A: Effect of Structural Asymmetry caused by Core Placement

The core usually contributes significantly to the lateral stability of a building. When the core is moved away from the geometrical center of the plan, the stabilizing system becomes asymmetric and eccentricity is introduced through a shift in CR.

4.2.1.1 Case A1: Shear Walls Centered on Façades

In this configuration, a 42x18m rectangular plan is stabilized by four shear walls placed at the midpoints of each perimeter façade. This symmetric arrangement places the CR at the geometric center (GM). A core with stiffness equivalent to the shear walls is then added and relocated to multiple positions in order to introduce structural asymmetry and shift CR towards the core. The offset core also affects CM slightly, however, this influence is small compared to the induced change in CR and is therefore neglected in the interpretation. Figure 4.1 illustrates the stabilizing layout (including examples of core positions 1 and 2), while Figure 4.2a shows the tested core positions (1-17). The black squares indicate positions that coincide with shear wall locations and are therefore excluded to not change the overall stiffness of the plan. Several core placements are mirrored about the plan axes (e.g., positions 1, 6, 12, and 17) and consequently produce the same structural response, differing only by direction. These equivalent placements are therefore grouped and identified using the same letter in the figures and tables, see Figure 4.2b.

Relocating the core increases eccentricity by moving CR away from the centrally located CM. At the same time, the torsional stiffness is affected because the relative distances between stabilizing elements and CR change as the core position changes.

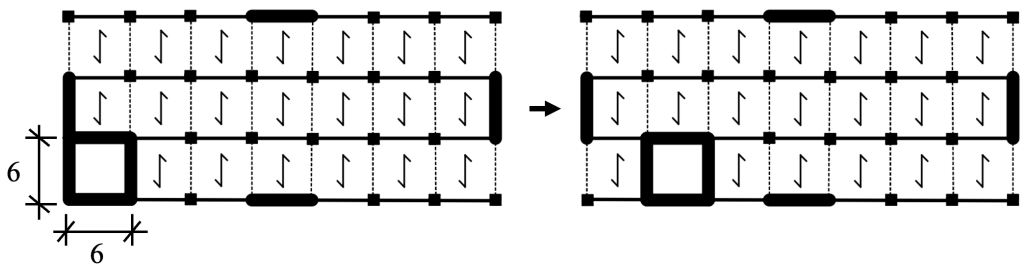

Figure 4.1: Plan configuration with four symmetrically placed shear walls (fixed) and a core moved to all feasible positions that do not coincide with the shear walls.

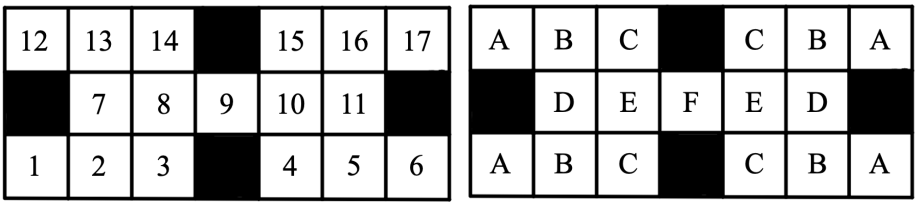

(a) Core Placements **(b)** Grouped Core Placements

Figure 4.2: (a) Tested core placements. (b) Core placements that are mirrored about the plan produce the same response and are therefore grouped together. Positions assigned the same letter indicate mirrored configurations with identical structural behaviour.

To evaluate the fundamental response, the mode shape is first classified using the Frequency Ratio (FR), as described in Section 3.6.2, Eq. 3.25. The FR is compared against (a) the normalized eccentricity, e/D (Eq. 3.26, 3.27), and (b) the normalized torsional stiffness, R (Eq. 3.28). An FR equal to 1 indicates a predominantly translational fundamental mode, while FR<1 indicates a predominantly torsional fundamental mode. Figure 4.3 shows FR plotted against both e/D and R. Torsional response occurs for the configurations with the largest eccentricity. It should be noted that these configurations also exhibit the largest torsional stiffness.

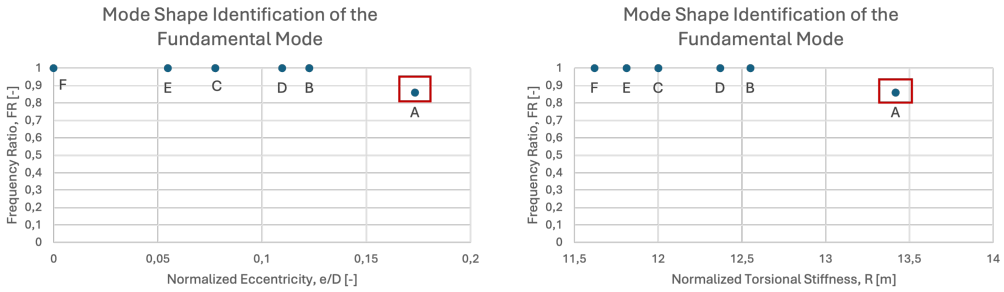

(a) **(b)**

Figure 4.3: The Frequency Ratio (FR) in relation to (a) the normalized eccentricity (e/D), and (b) the normalized torsional stiffness (R). Points are labeled with their corresponding letters as shown in Figure 4.2b, and the torsional mode shapes are highlighted with red boxes.

For this structural layout, eccentricity clearly governs the torsional response. When the core is located at position 9, CM and CR coincide and the eccentricity is zero, see Figure 4.4. No torsion is observed in the first mode of this configuration (Figure 4.5). As the core is moved further away from CM, the torsional contribution of the fundamental mode increases. Torsion in the first mode is observed only for the four most eccentric configurations, where the core is placed in the rear corners (1, 6, 13 and 17, group A). The corresponding CM and CR coordinates (Figure 4.4) further support that increasing eccentricity is the dominant factor in these cases.

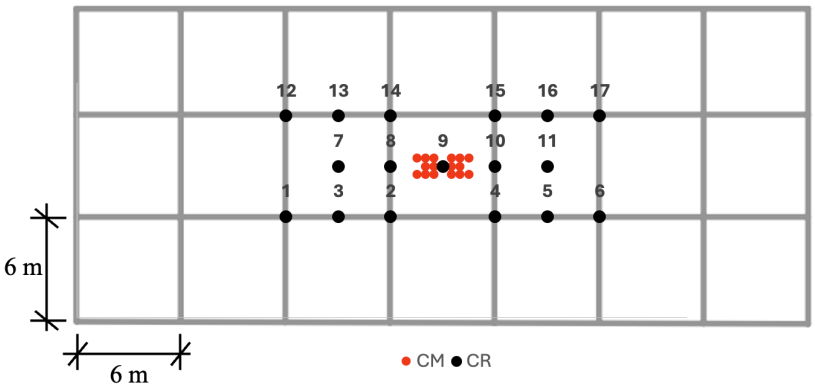

	CM	CR
1	(19.52, 8.51)	(12, 6)
2	(20.51, 8.51)	(18, 6)
3	(20.01, 8.51)	(15, 6)
4	(21.49, 8.51)	(24, 6)
5	(21.99, 8.51)	(27, 6)
6	(22.48, 8.51)	(30, 6)
7	(20.01, 9)	(15, 9)
8	(20.51, 9)	(18, 9)
9	(21, 9)	(21, 9)
10	(21.49, 9)	(24, 9)
11	(21.99, 9)	(27, 9)
12	(19.52, 9.49)	(12, 12)
13	(20.01, 9.49)	(15, 12)
14	(20.51, 9.49)	(18, 12)
15	(21.49, 9.49)	(24, 12)
16	(21.99, 9.49)	(27, 12)
17	(22.49, 9.49)	(30, 12)

Figure 4.4: Movement of the center of mass (CM) and center of rotation (CR) for the different core placements.

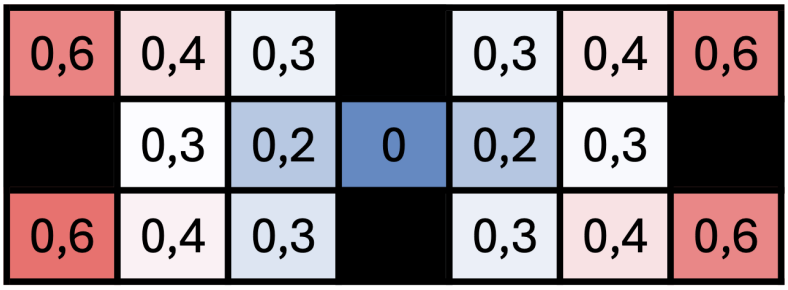

Figure 4.5: Heat map showing the torsional contribution of the fundamental mode. A value of 0 indicates pure translation and 1.0 indicates pure rotation. The mode is classified as predominantly torsional for values >0.5.

To investigate how the two primary influencing factors, eccentricity and torsional stiffness, relate to each other, their normalized values are plotted against one another, see Figure 4.6. The blue points represent the translational mode shapes, while the red point (A) denotes the torsional mode. The dashed lines indicate extensions from the critical points, and the dotted line shows the expected translational trend line. For the translational cases, the critical point is B, which is the last translational point before torsional behavior appears. Point B has the largest eccentricity among the translational points and also the largest torsional stiffness, with coordinates (0.12, 12.54). This suggests a relationship between R and e/D, where the normalized torsional stiffness is approximately 105 (104.5) times the normalized eccentricity. In the torsional configuration (A), the corresponding point has values (0.17, 13.42), implying a ratio of roughly 79 (78.94) instead which is about 25% lower than the translational relationship.

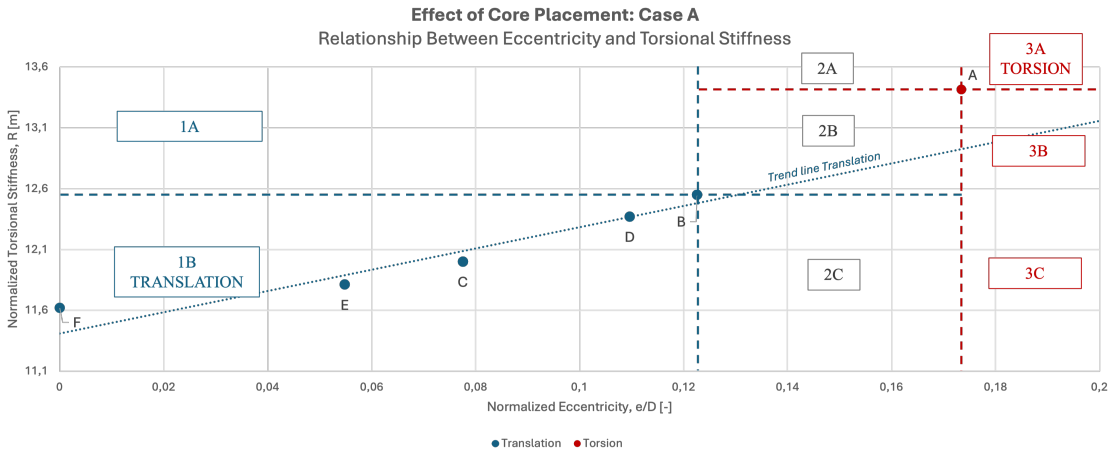

Figure 4.6: Relationship between normalized eccentricity and normalized torsional stiffness for the case with centrally placed shear walls along the facades (Case A1).

To better identify trends for this configuration, the plot can be divided into zones. Zone 1B shows translational behavior, and it is therefore reasonable to expect translational behavior in Zone 1A as well, since those points correspond to even higher torsional stiffness, which should increase resistance to torsional response. Clear torsional behavior is observed in Zone 3A. Considering point A, which marks the start of the torsional critical line, one would expect all points in Zone 3 to exhibit torsional response. Point A represents the stiffest configuration and still exhibits a torsion-dominated fundamental mode. This indicates that once eccentricity reaches the level of Point A, torsional behaviour is likely to govern even if torsional stiffness is increased, and configurations with the same or larger eccentricity should therefore be regarded as torsion-prone. Although no data points fall in Zones 3A–3C, in the present plot (a consequence of the specific configuration set-up), torsional response would, from a theoretical standpoint, be expected in Zones 3B and 3C at least, since these zones combine similarly high eccentricity with lower torsional stiffness than Point A. Zone 2 is less straightforward and can be viewed as a "grey zone," where a mix of torsional and translational mode shapes is expected. This region therefore requires greater attention during early design stages.

4.2.1.2 Case A2: Corner Shear Walls

To compare the moving core concept against a stiffer and more perimeter efficient stabilizing system, the shear walls are relocated toward the corners and the number of walls is increased, resulting in approximately doubled bending stiffness in both principal directions compared to the mid-façade case (Case A1) in Section 4.2.1.1. From torsional response theory the largest lateral displacements typically occur at the points furthest away from CR, often at plan corners. Placing shear walls at corners may therefore reduce torsional sensitivity by increasing lever arms and overall torsional resistance. Figures 4.7 and 4.8a show the stabilizing layout and the set of feasible core positions. Once again, core placements that would interact with the

shear walls are excluded, and mirrored core placements yield equivalent results (e.g., positions 1, 5, 13, and 17), see Figure 4.8b.

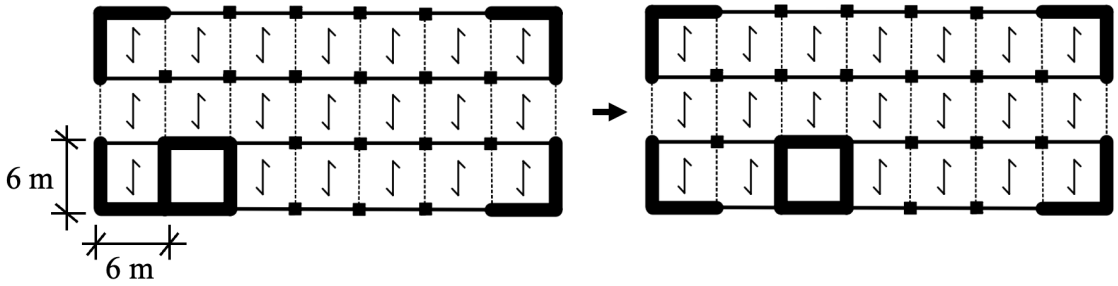

Figure 4.7: Plan configuration with corner shear walls and a moveable core.

	13	14	15	16	17	
6	7	8	9	10	11	12
	1	2	3	4	5	

(a) Core Placements

	A	B	C	B	A	
D	E	C	F	C	E	D
	A	B	C	B	A	

(b) Grouped Core Placements

Figure 4.8: (a) Feasible core positions for the corner shear wall configuration. (b) Core placements that are mirrored about the plan produce the same response and are therefore grouped together.

For all configurations with corner shear walls, the fundamental mode remains predominantly translational, see Figure 4.9.

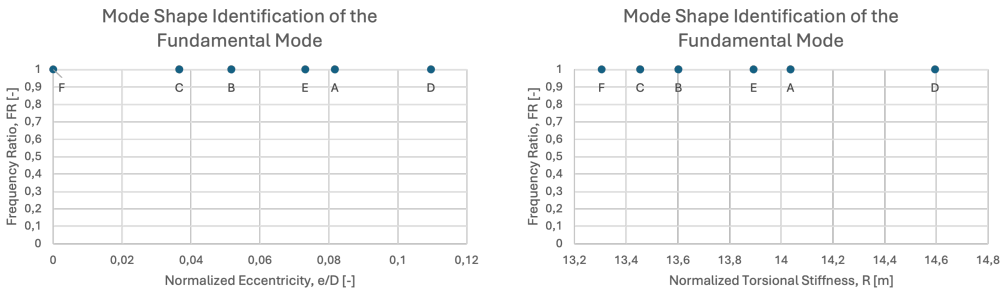

(a) **(b)**

Figure 4.9: The Frequency Ratio (FR) in relation to (a) the normalized eccentricity (e/D), and (b) the normalized torsional stiffness (R) for the corner shear wall configurations.

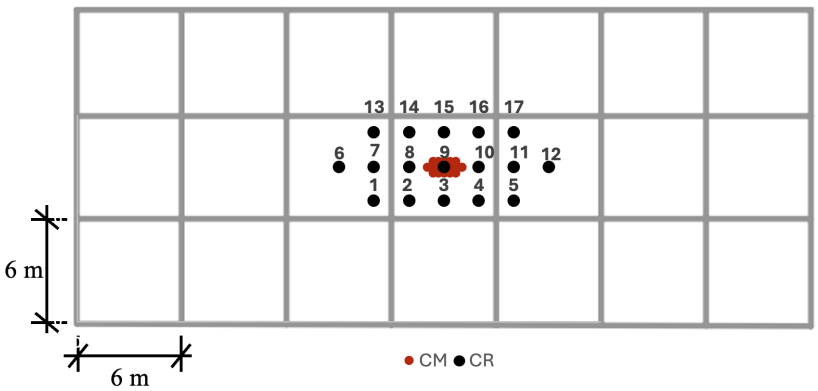

	CM	CR
1	(20.34, 8.67)	(17, 7)
2	(20.67, 8.67)	(19, 7)
3	(21, 8.67)	(21, 7)
4	(21.33, 8.67)	(23, 7)
5	(21.66, 8.67)	(25, 7)
6	(20.01, 9)	(30, 9)
7	(20.34, 9)	(15, 9)
8	(20.67, 9)	(17, 9)
9	(21, 9)	(19, 9)
10	(21.32, 9)	(21, 9)
11	(21.65, 9)	(23, 9)
12	(21.99, 9)	(15, 9)
13	(20.34, 9.33)	(15, 11)
14	(20.67, 9.33)	(18, 11)
15	(21, 9.33)	(24, 11)
16	(21.33, 9.33)	(27, 11)
17	(21.66, 9.33)	(30, 11)

Figure 4.10: Movement of the center of mass (CM) and center of rotation (CR) for the different core placements of Case B.

In Figure 4.11 the relationship between the normalized eccentricity and the normalized torsional stiffness for Case A2 is shown. All configurations exhibit translational behaviour, even as eccentricity increases. Considering point D, which has the largest eccentricity with coordinates (0.11, 14.59), the implied relationship between R and e/D corresponds to a normalized torsional stiffness roughly 133 (132.63) times larger than the normalized eccentricity.

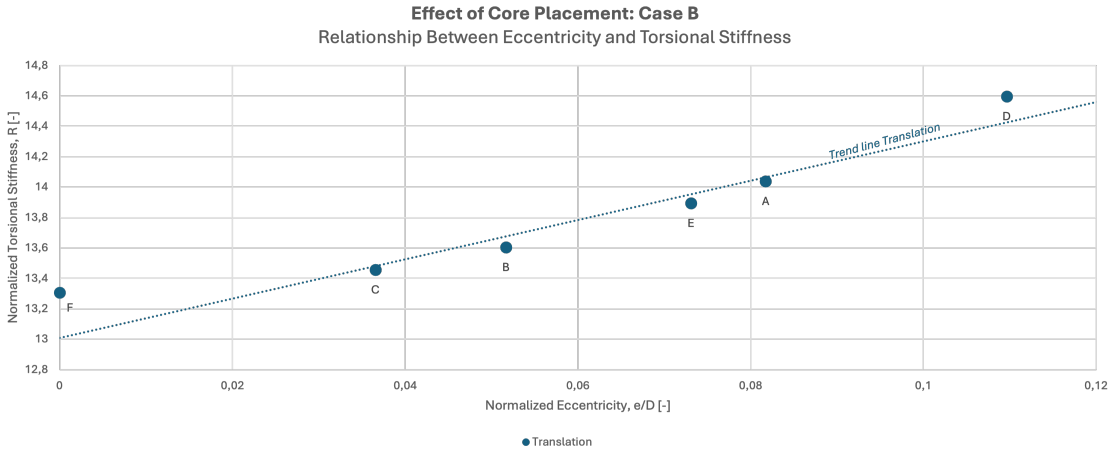

Figure 4.11: Relationship between normalized eccentricity and normalized torsional stiffness for the case with corner placed shear walls (Case A2).

4.2.1.3 Comparison between Case A1 and Case A2

In Subsections 4.2.1.1 and 4.2.1.2, it became evident that core placement plays a major role in otherwise seemingly symmetric rectangular buildings, even when shear walls are arranged symmetrically.

Figure 4.12 compares the two moving-core cases in a single plot. Blue markers denote translational configurations, while the red marker denotes torsional configurations. Circular markers represent Case A1 and square markers represent Case A2. The dashed lines indicate the critical points extended into critical boundaries, and the dotted lines show trend lines for the translational responses in each case.

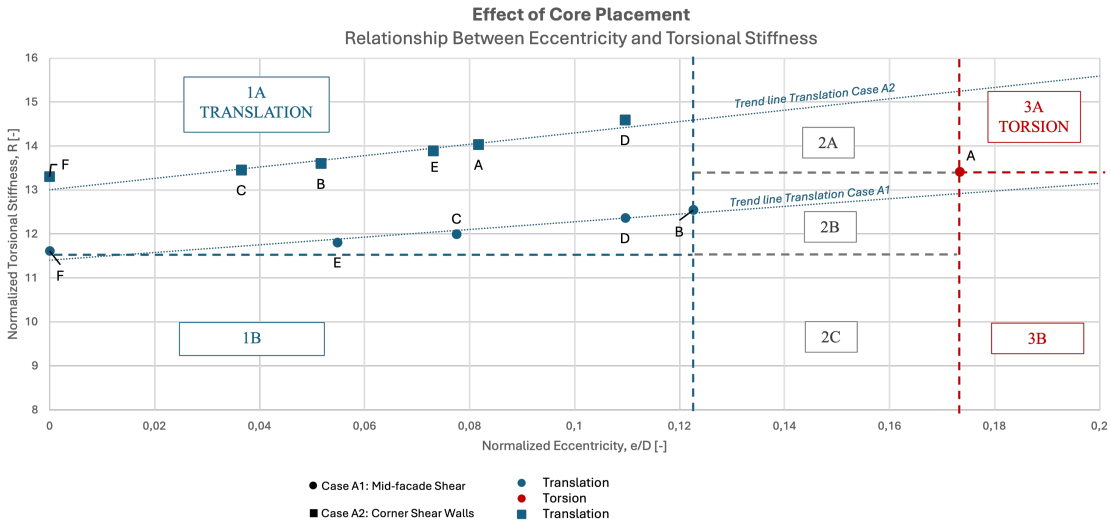

Figure 4.12: Relationship between eccentricity and torsional stiffness for the mid-façade and corner shear wall moving-core cases. Dotted lines show the translation trend lines, while dashed lines mark the critical translation and torsion values used to define zone boundaries., i.e. Zone 1A corresponds to translation while Zone 3A shows torsion.

For the translational configurations, both cases follow similar trends where torsional stiffness increases with eccentricity. This is expected, since moving the core away from the CM causes the CR to shift toward the core (see Figures 4.10 and 4.4), while the CM remains relatively unchanged due to the mass distribution, where the slabs have a greater influence than the vertical stabilizing elements. However, the corner shear wall layout in Case A2 produces higher torsional stiffness for the same core position, consistent with larger effective lever arms relative to the CR. This is reasonable because the shear walls in Case A1 act with shorter lever arms, whereas in Case A2 they are positioned further away from the CR and therefore contribute more strongly to torsional stiffness, increasing both the absolute and normalized values. The increased torsional stiffness in Case A2 is also consistent with the absence of any observed torsional response, highlighting the importance of torsional stiffness in controlling the dynamic behavior.

Comparing eccentricity between the cases, Case A1 generally exhibits larger eccentricities and is also the case in which torsional behavior occurs. The largest eccentricity among the translational modes is found in Case A1 (point B). Relative

to the maximum translational eccentricity in Case A2 (point D), point B has higher eccentricity but significantly lower torsional stiffness. Moreover, when comparing the points labeled D in both cases, which share the same eccentricity and both show translational response, it is clear that higher torsional stiffness at the same eccentricity further stabilizes the building. At the same time, the fact that torsion appears only in Case A1 suggests that eccentricity is a key driver of torsional response for these configurations. This is reinforced by the torsional point (A) in Case A1, that once the normalized eccentricity exceeds a certain level (here approx 0.17, noting that no data points exist in Zone 2), torsion may occur unless the relationship between also exceeds a threshold value.

These results also show that increasing eccentricity can simultaneously increase torsional stiffness, making the ratio between these factors particularly relevant. For Case A1, the corresponding ratios are approximately 105 for translational behavior and 85 for torsional behavior, while Case A2 yields a ratio of roughly 133, which is larger than for Case A1. With the limited number of configurations available here, it is not possible to define a definitive "critical" ratio, but the range between roughly 79 and 105 appears important and warrants further investigation.

Although these configurations were intended to isolate the effect of core placement, the comparison between the two cases also demonstrates that shear wall placement has a significant influence on torsional stiffness. In particular, the bending stiffness is doubled in Case A2 compared to Case A1, meaning the shear walls contribute more strongly to torsional stiffness in Case A2. This is consistent with the more concentrated CR movement in Case A2 (Figure 4.10) compared to the more distributed CR shift in Case A1 (Figure 4.4). Overall, the results indicate that placing stabilizing elements far from the CR increases lever arms, increases torsional stiffness, and reduces the likelihood of torsional behavior, when assuming the building still achieves adequate global stability.

Based on Figure 4.12, and the discussion above, the results suggest that low eccentricity combined with moderate torsional stiffness (Zone 1A in Figure 4.12) leads to a translational fundamental mode. At very large eccentricities, however, a torsional response may occur even when torsional stiffness is high (Zone 3A). In Zone 3A, the eccentricity is almost twice that of Zone 1A, while the torsional stiffness remains close to the translational trend line for Case A1 (see *Trend line Translation Case A1*). Thus, even if the torsional configurations meet or exceed this trend line in stiffness, the increase is not sufficiently large relative to the increase in eccentricity to prevent torsion from governing the fundamental mode.

It can also be expected that Zone 3B will exhibit torsional response, since its eccentricity is comparable to Zone 3A while its torsional stiffness is lower, as discussed in Subsection 4.2.1.1. Zone 2 represents a "grey zone," where the outcome is less distinct than in Zones 1A, 3A, and 3B. A mix of translational and torsional mode shapes is therefore expected, and configurations in this region require particular attention.

Finally, Zone 1B may also show a mix of translation and torsion because the torsional stiffness values are very low. One would expect trend lines similar to those for Cases A1 and A2 for the translational responses, but with the torsional critical boundary occurring at smaller eccentricities due to the reduced stiffness.

4.2.2 Case B: Effect on Torsional Stiffness caused by Shear Wall Placement

To isolate the influence of shear wall placement on torsional stiffness, eccentricity is set to zero in all cases in this section. With $e = 0$, CM and CR coincide at the geometrical center (GC) for all configurations. The core is omitted to ensure that the results reflect only the influence of the shear walls.

The base geometry is again a 42x18m rectangle. 4 cases are studied with two wall-length, (i) four shear walls of length 6 m (one grid length, Case 1 and 3), (ii) and four shear walls of length 18 m (three grid lengths, Case 2 and 4). The initial placement is central, as shown in the left sketches of Figure 4.13. The y-direction walls (SW2y and SW4y) are then moved in the x-direction (right sketches), while the x-direction walls (SW1x and SW3x) remain fixed. This setup examines how relocating the y-direction walls affects torsional stiffness. The gray lines denote how the shear walls move among the different model configurations, and the circled numbers correspond to each case's model number.

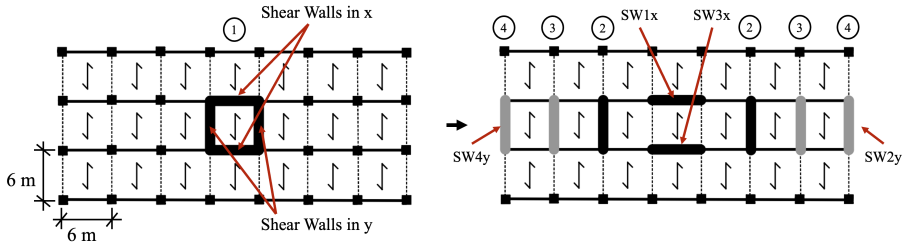

(a) Case 1

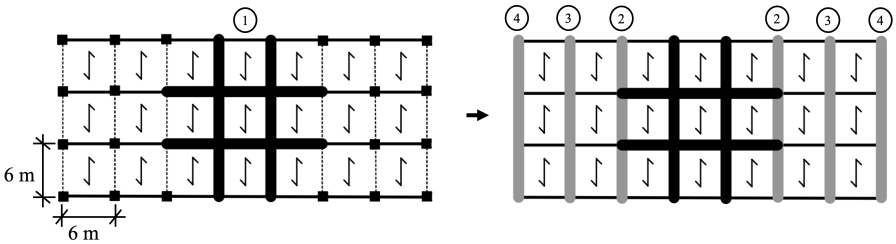

(b) Case 2

Figure 4.13: Plan layouts used to study the effect of shear wall placement on torsional stiffness with central x-direction walls. (a) Case 1 with shear walls with the length 6m, and (b) Case 2 with 18m long shear walls. The gray lines denote how the shear walls move among the different model configurations, and the circled numbers correspond to each case's model number.

The same cases are then repeated with the x-direction walls (SW1x and SW3x) relocated to the perimeter façade (Figure 4.14). This enables comparison to assess the influence of placing stabilizers closer to the façade while moving the y-direction walls.

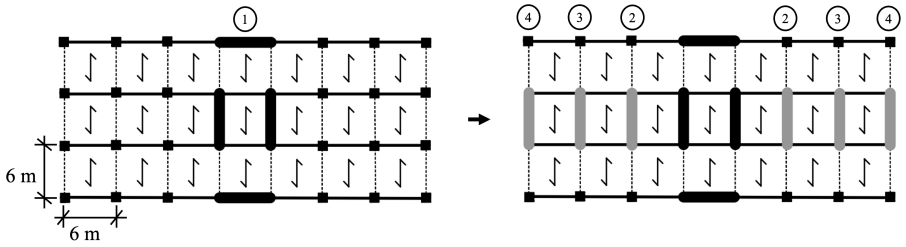

(a) Case 3

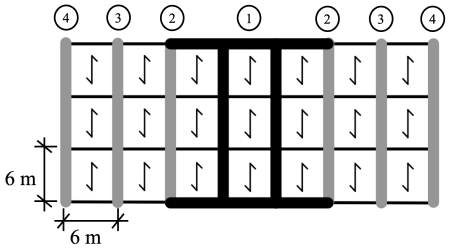

(b) Case 4

Figure 4.14: Plan layouts used to study the effect of shear wall placement on torsional stiffness when x-direction walls are placed at the façade. (a) Case 3 with 6m long shear walls, and (b) Case 4 with the shear walls spanning 18m. The gray lines denote how the shear walls move among the different model configurations, and the circled numbers correspond to each case's model number.

Figure 4.15 plots the normalized torsional stiffness (R) against the frequency ratio (FR). Since none of the configurations exhibit eccentricity, eccentricity-based plots are not relevant for this case. Blue, yellow, green, and red markers correspond to Cases 1–4, respectively, and each point is labeled as *Case x: Model no.* The torsional configurations are highlighted within the red square. All cases exhibit torsion in at least one configuration, Cases 1 and 2 show torsion in Models 1 and 2, while Cases 3 and 4 show torsion only in Model 1. Across all cases, the torsional configurations consistently have lower normalized torsional stiffness than the translational ones, indicating shorter effective lever arms to the CR in the torsional cases. The values of R1 (3m) and R2 (6.71m) represents the normalized torsional stiffness of the torsional cases.

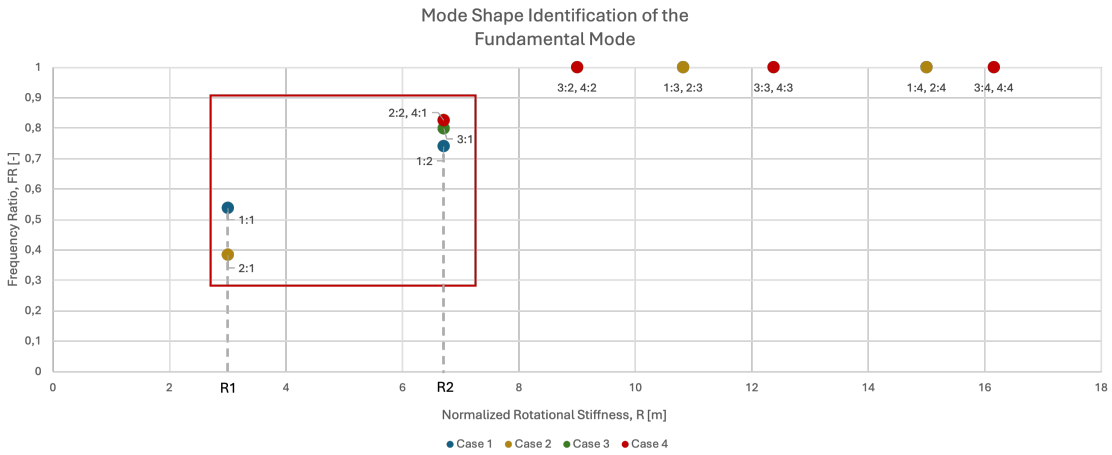

Figure 4.15: Mode shape identification for cases 1-4. The frequency ratio (FR) is plotted against normalized torsional stiffness (R). Labeling is the Case x:Model number according to Figures 4.13b and 4.14b. Points in the red box represents torsional behaviour, and R1 & R2 indicate the normalized torsional stiffnesses of the torsional modes.

To examine the torsional stiffness further, Figure 4.16 illustrates R as the average radius of the stabilizing system around a centrally located CR. Red markers denote the centered x-wall cases (Case 1 and 2), while blue markers denote the façade x-wall cases (Case 3 and 4). The first point in the centered x-wall cases ($R1 = 3$ m) represents the configuration without displacement in either direction. The second point in the same case represents a 6 m displacement in the x-direction, while the first point in case with the façade shear walls represents a 6 m displacement in the y-direction. These two points yield similar R, suggesting that, for equal displacement magnitudes, relocating shear walls in the x- or y-direction has limited influence on R for a geometrically and structurally symmetric rectangle. The remaining façade cases show larger R, as the increased distance to CR increases the average lever arms.

Torsion is observed for configurations with R up to 6.71 m (see table adjacent to Figure 4.16). Relating this to the plan dimensions, representative half-spans are $r_x = 42/2 = 21m$ and $r_y = 18/2 = 9m$. The value $R = 6.71$ m is smaller than both r_x and r_y. The first clearly translational configuration instead occurs at approximately $R = 9$ m, which matches r_y.

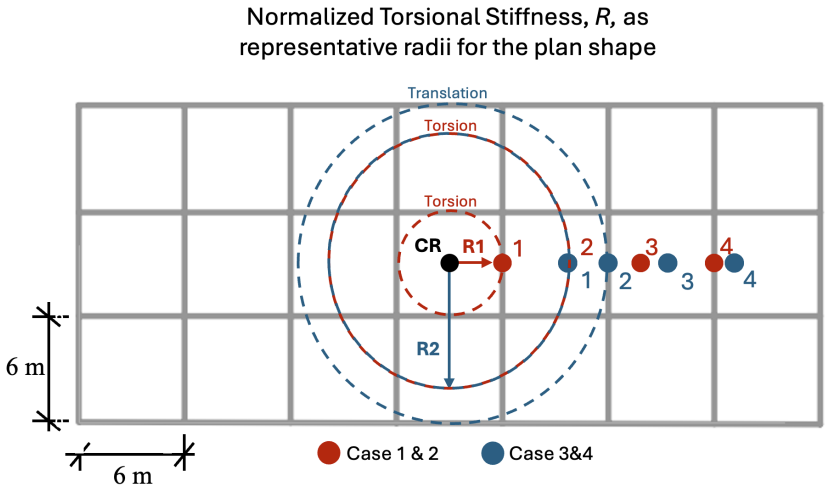

	Case 1 & 2	Case 3 & 4
	R [m]	R [m]
1	3.00	6.71
2	6.71	9.00
3	10.82	12.37
4	15.00	16.16

Figure 4.16: Normalized torsional stiffness, R, represented as the average radius of the stabilizing system of the plan. Red respresents the case where SW1x and SW3x (Case 1 & 2) are centered and the blue when they are placed of the facades (Case 3 & 4).

For cases with zero eccentricity, the same relationship between e/D and R cannot be established. Instead, the results can be interpreted using the R-FR plot in Figure4.15 and, for clarity, by dividing the configurations into zones as shown in Figure 4.17. In Zone 1, torsional response is clearly observed, whereas Zone 3 shows clear translational behavior. Zone 2 remains a "grey zone" where the response is less distinct and therefore requires additional caution in assessment and early design.

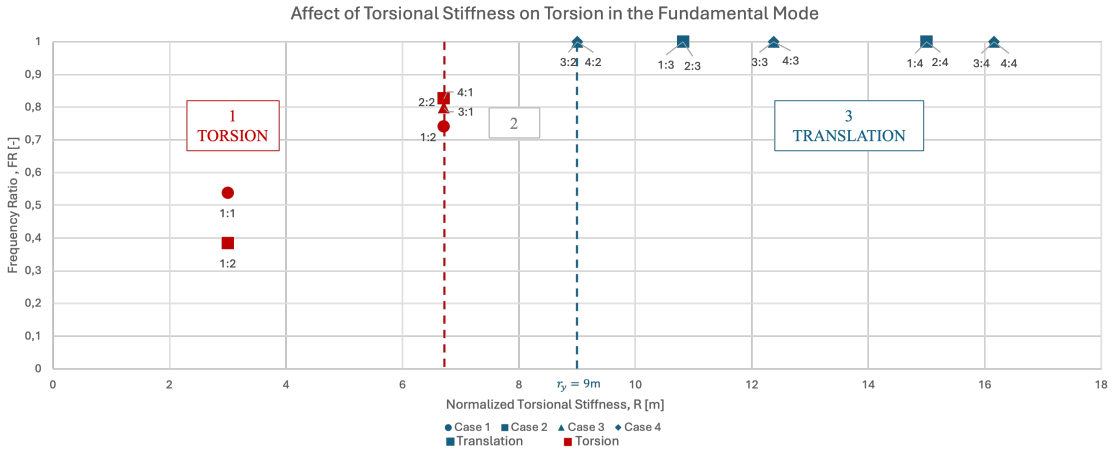

Figure 4.17: The affect of shear wall placement on the normalized torsional stiffness of the building.

Overall, for a rectangular plan with zero eccentricity and a symmetric structural sys-

tem, torsional response is governed primarily by torsional stiffness, which is strongly affected by the placement of the stabilizing elements. Positioning stabilizing units farther from the CR increases R and tends to reduce torsional response. When displacement magnitudes are comparable, the direction of relocation (x versus y) appears to have a limited effect. The results also suggest that torsional resistance improves once R reaches a representative plan radius (here, r_y). Based on this trend, configurations located in Zone 2 may also be expected to exhibit torsional response in the fundamental mode.

4.2.3 Case C: Effect of Structural Asymmetry caused by Imbalance in Bending Stiffness

Rectangular plans have a weak and a strong axis depending on their proportions. This section examines cases where the bending stiffnesses in the principal directions, K_x and K_y, are not equal.

4.2.3.1 Case C1: Without the Influence of Eccentricity

To isolate the effect of stiffness imbalance, the first configurations are evaluated with zero eccentricity. The study follows the approach in Section 4.2.2, but SW1x and SW3x are placed at the façades to reduce torsional sensitivity. The tested configurations are shown in Figure 4.18.

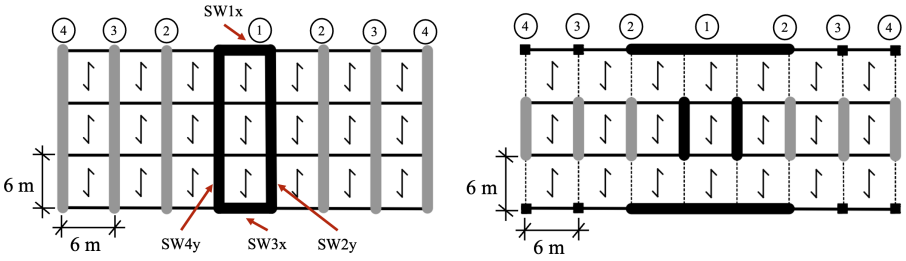

(a) Case C1a: Kx < Ky **(b)** Case C1b: Kx > Ky

Figure 4.18: Plan layouts used to study the influence of bending stiffness imbalance between principal directions: (a) higher stiffness in the y-direction ($K_x < K_y$) and (b) higher stiffness in the x-direction ($K_x > K_y$). Black walls indicate the first tested case and grey walls indicate subsequent configurations.

The mode-shape identification in Figure 4.19 shows that the fundamental mode is translational for both configurations, whereas torsion occurs in Mode 2. Since torsional motion appearing in Mode 2 still indicates that torsion occurs before an expected translational mode, Mode 2 is used for interpretation in this section.

Figure 4.19b also illustrates the previously observed trend of reduced torsional response with increased torsional stiffness (highlighted in the red box). Case C1a shows the largest torsional movement, while Case C1b produces the largest number of torsional cases.

Based on the moment of inertia relationship in Section 2.3.2, a rectangular plan has its strong axis along its long dimension. Since the plan is longer in the x-direction, the x-axis corresponds to the strong direction, and increasing stiffness in the weak direction (y-direction) is expected to be more effective in limiting torsional behaviour. This is consistent with the results, where $K_x < K_y$ (Case C1a) yields fewer torsional cases in Mode 2. However, the lowest torsional stiffness point belongs to the $K_x > K_y$ configuration (Case C1b), suggesting that torsional stiffness (and thus shear-wall placement and lever arms) can be more influential than stiffness imbalance when eccentricity is zero.

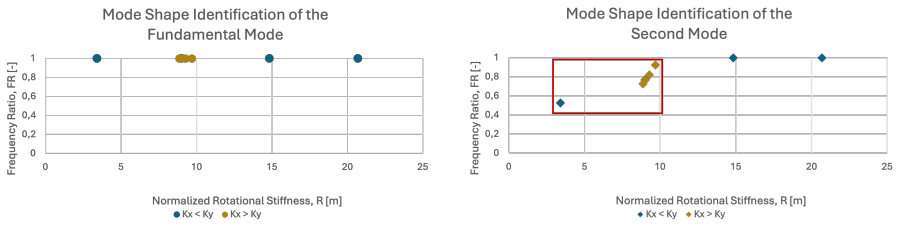

(a) Mode 1 **(b)** Mode 2

Figure 4.19: Mode shape identification of the two configurations. FR is plotted against normalized torsional stiffness R for (a) Mode 1 and (b) Mode 2.

4.2.3.2 Case C2: With Eccentricity

To examine whether stiffness imbalance becomes more pronounced in the presence of eccentricity, four asymmetric stabilizer layouts are tested (Figure 4.20).

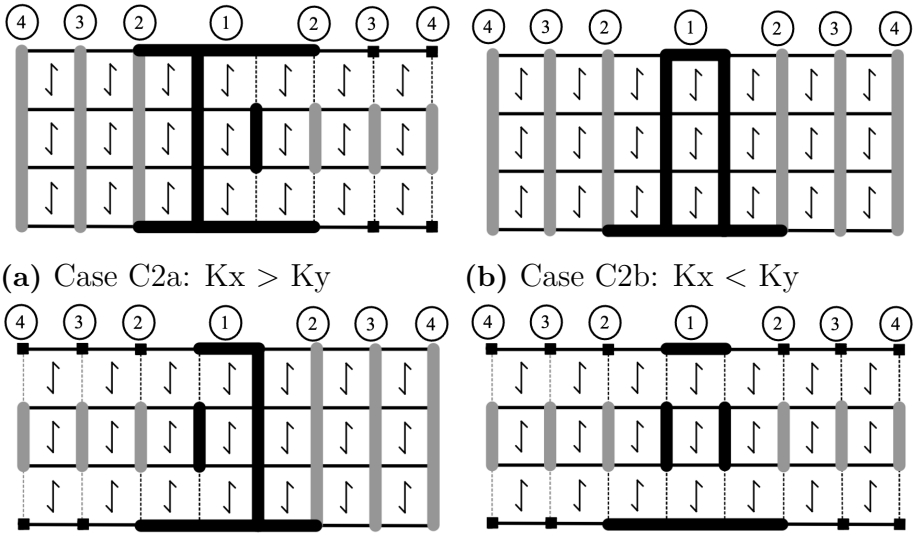

(a) Case C2a: Kx > Ky **(b)** Case C2b: Kx < Ky

(c) Case C2c: Kx = Ky **(d)** Case C2d: Kx > Ky

Figure 4.20: Plan configurations for the four tested cases.

Figure 4.21 shows the fundamental mode classification, with the frequency ratio FR plotted against (a) normalized eccentricity e/D and (b) normalized torsional stiffness

R. Cases C2a-d correspond to the plan configurations in Figure 4.20. Overall, the configurations that exhibit torsional response are generally associated with larger eccentricity, indicating that e/D remains a key driver for torsion in the fundamental mode.

In Figure 4.21a, Cases C2a (Kx>Ky) and C2c (Kx=Ky) show torsion for all configurations. These cases also exhibit generally higher eccentricity than Cases C2b and C2d, suggesting that increased eccentricity increases the likelihood of torsional response. For Case *a*, FR tends to decrease as eccentricity increases, implying a larger separation between the torsional and translational frequencies. This may suggest that torsional eigenmodes become increasingly dominant before a primarily translational mode appears. This behaviour is consistent with the fact that Kx>Ky strengthens the already strong axis of the rectangle (x-direction) rather than the weak axis (y-direction), which can amplify torsion sensitivity. Case *c*, despite having equal bending stiffness in the global x- and y-directions, also exhibits torsional behaviour. This indicates that equal global stiffness does not necessarily prevent torsion if the stiffness distribution within a direction is uneven.

Cases *b* and *d* behave differently. In these cases, the eccentricity remains essentially constant across the configurations. Even though bending stiffness is imbalanced, the CR does not shift significantly, and the CM is largely unchanged, consistent with earlier discussions in this thesis regarding the dominance of the slab mass distribution. Both B2 and B4 also have lower eccentricities than *a* and *c* and include translational fundamental modes. This further supports the observation that lower eccentricity reduces the likelihood of torsional response.

Considering Figure4.21b, the relationship between torsional stiffness and FR is less uniform across the cases. For *b* and *d*, higher torsional stiffness generally corresponds to a greater tendency toward translational behaviour, although the absolute R-values remain relatively low, especially in *d*. In contrast, *a* and *c* show torsional behaviour in all configurations, and the variation of FR with R is not consistent between them. In *c*, FR increases with increasing R, whereas in *a* the opposite trend is observed. This suggests that, for these configurations, torsional stiffness alone does not explain the observed response, but rather, the interaction between stiffness distribution and the induced eccentricity becomes decisive.

A key distinction between the two groups is the nature of the stiffness imbalance. In Cases *a* and *c*, there is an imbalance between the shear walls in the y-direction (the weak direction), meaning the shear walls along y are not equivalent. These cases appear particularly torsion-prone. In Cases *b* and *d*, the imbalance is instead primarily in the x-direction (the strong direction). The results therefore indicate that rectangular buildings may be more sensitive to stiffness imbalance in the weak direction than to a simple comparison of total global bending stiffness in x versus y. This also helps explain why Case *c* can exhibit torsion despite Kx=Ky. The global stiffness may be balanced, but the shear-wall distribution in the y-direction still introduces torsion-promoting asymmetry.

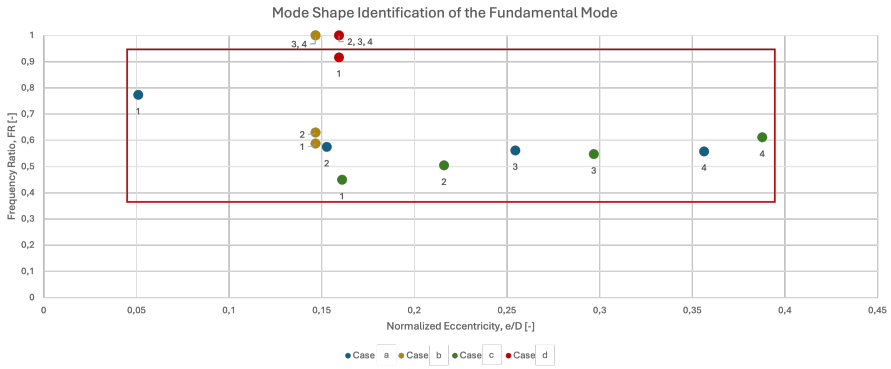

(a) Influence of Eccentricity

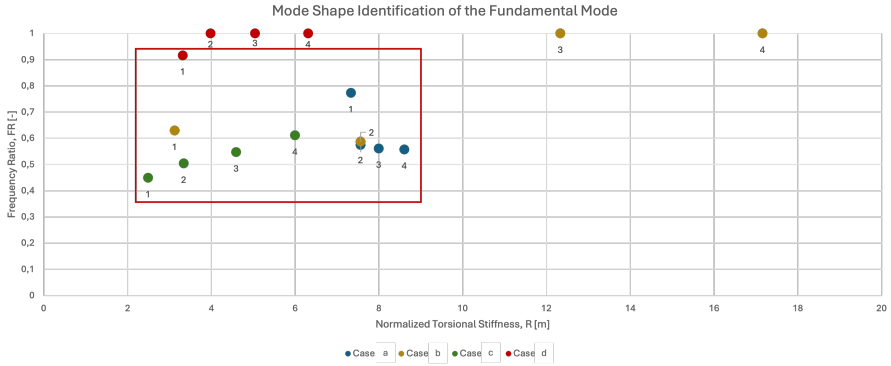

(b) Influence of Torsional Stiffness

Figure 4.21: Mode shape identification of the fundamental mode for the four plan configurations. FR is plotted against (a) e/D and (b) R. Cases a-d correspond to Figure 4.20d.

Finally, Figure 4.22 compiles all configurations in a single plot. Red markers denote torsional fundamental modes, while blue markers denote translational modes. The dashed lines indicate the critical points extended into critical boundaries. The Case B4 results are additionally encircled to emphasize that these points deviate from the trends observed in the other cases.

For Cases *a-c,* an overall tendency can be identified, increasing torsional stiffness is generally associated with reduced torsional response. However, no consistent relationship between R and e/D can be established across all cases. The implied ratios between these parameters vary substantially. For a the ratio spans roughly 24–144, for b torsion occurs at about 53 while translation is observed around 80, for c the maximum ratio is around 16, and for d it is approximately 47. If the exceptionally high ratios in B1 and the comparatively low values in d were absent, a clearer pattern might be inferred, but with the current results no robust threshold or universal trend can be defined.

The atypically low values for Case d are likely explained by its plan configuration. Only one shear wall has three spans (located along the bottom edge in the x-direction), while the remaining walls span only one bay, see Figure 4.20d. This

arrangement shifts the CR markedly toward lower y-values, while the CR position remains essentially unchanged across configurations, resulting in a nearly constant eccentricity. Under these conditions, the two x-direction walls contribute similarly to torsional stiffness, and although the y-direction walls contribute more due to their lever arms, the overall torsional stiffness does not reach the higher levels seen in the other cases. In this sense, the stiffness imbalance directly influences the response by strongly displacing the CR and thereby altering the torsional characteristics of the system.

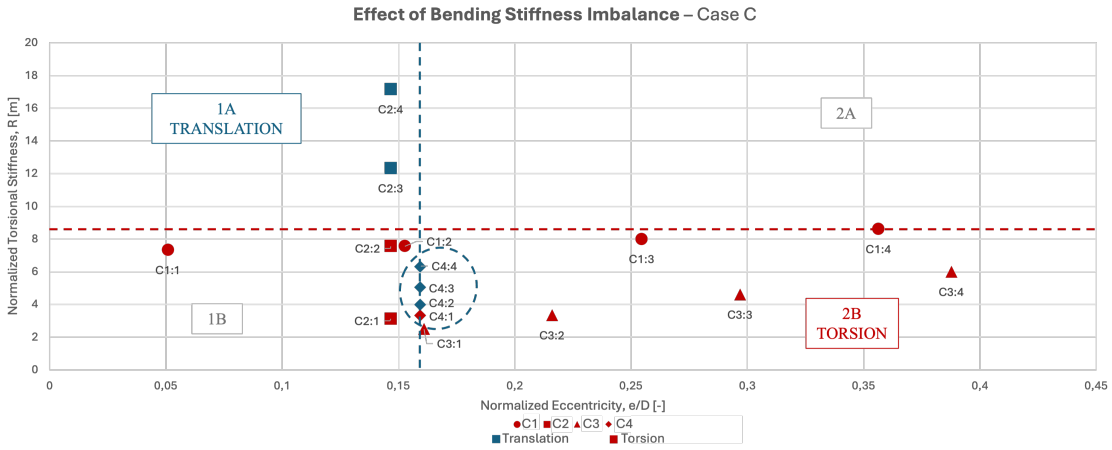

Figure 4.22: Effect of imbalanced bending stiffness on the torsional response of a rectangular building plan.

Based on the combined plot, Zone 1A can be interpreted as predominantly translational. Zone 1B represents a mixed response region, with the Case B4 results effectively defining the transition toward torsional behaviour. Zone 2B is clearly torsion dominated, characterized by low torsional stiffness combined with high eccentricity. For Zone 2A, a mixed response is expected since no clear relationship between R and e/D could be established. Configurations within these intermediate regions therefore require particular attention in early-stage design.

4.2.4 Summary of Torsional Response for Rectangular Plans

Figure 4.23 compiles all rectangular configurations in the e/D-R space. Blue markers denote translational fundamental modes and red markers denote torsional fundamental modes. Marker shapes distinguish the case groups: circles represent Case A (core placement), squares represent Case B (shear-wall placement), and triangles represent Case C (bending-stiffness imbalance). The dashed lines indicate the critical boundaries, and their intersections define the response zones (1A-2B).

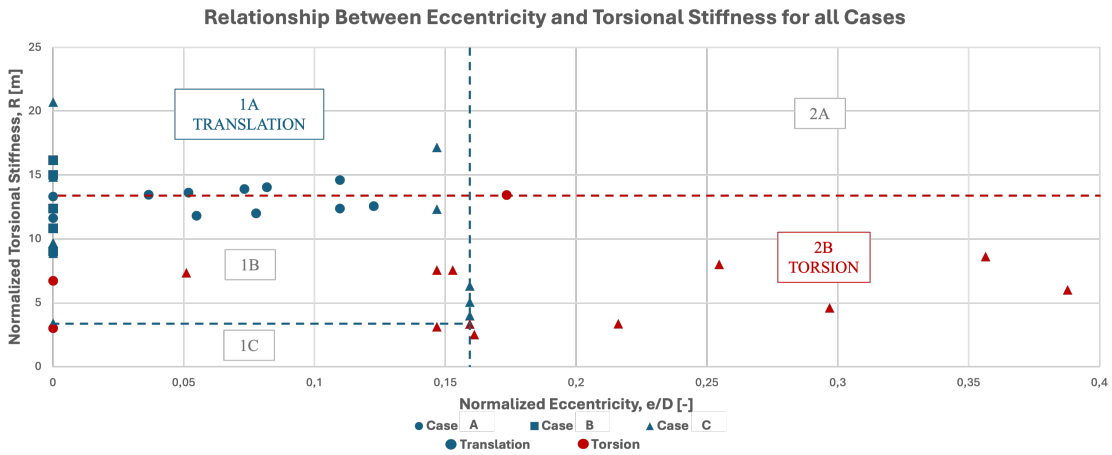

Figure 4.23: Relationship between normalized eccentricity and normalized torsional stiffness for all rectangular cases. Blue markers denote translation and red markers denote torsion. Dashed lines indicate the critical translation and torsion boundaries, and zones are defined by the intersections of these boundaries. Circular markers represent Case A (core placement), square markers represent Case B (shear-wall placement), and triangular markers represent Case C (bending-stiffness imbalance).

Overall, the results show that torsional response in rectangular plans is governed by the combined effect of eccentricity and the effective torsional resistance of the stabilizing system. When e/D increases, torsion becomes more likely, particularly when stiffness imbalance occurs in the weak direction (y-direction in this study). In Figure 4.23, configurations with $e/D \gtrsim 0.16$ cluster in the torsion-dominated region (Zone 2B). Conversely, sufficiently high torsional stiffness is associated with translational behaviour. Configurations with $R \gtrsim 13.5$ m remain translation-dominated (Zone 1A), even at moderate eccentricities.

Despite these tendencies, no universal R-e/D threshold can be defined, and some layouts (notably Case B4) deviate due to pronounced shifts of CR caused by the wall configuration. The figure therefore highlights distinct translation and torsion regions separated by intermediate "grey zones" where mixed behaviour is expected. Zone 1B is the main transition region in the combined dataset, where relatively small layout changes may switch the governing mode. A practical interpretation of this transition is that torsion becomes likely when R is not sufficiently large relative to e/D. For the present dataset, a representative boundary in Zone 1B can be approximated by

$$R \approx 84\,(e/D).$$

Configurations approaching this relationship should therefore be treated as torsion-sensitive and verified with additional dynamic assessment. Zones 2A and 1C may also be regarded as potentially torsion-prone due to their combination of relatively high eccentricity and/or low torsional stiffness. It should be noted, however, that

Zone 2A contains no data points in the present dataset. This reflects on the limited set of configurations tested, and to populate Zone 2A, cases deliberately designed to achieve both high eccentricity and high torsional stiffness would be required. The zoning is therefore based on the observed trends in the sampled configurations, rather than a systematic coverage of all possible layout combinations.

4.2.4.1 Dominant factors controlling torsion in rectangular plans

Across Cases A-C, the most influential drivers are:

1. **Eccentricity introduced by stabilizer asymmetry (CR shift):** Moving the core away from the plan center (Case A) directly increases e/D and is the most consistent trigger for torsion in the fundamental mode.
2. **Lever arms and torsional stiffness of the stabilizing system:** Even with $e = 0$ (Case B), torsion can occur when stabilizing elements are placed too close to CR (low R). Perimeter placement increases lever arms, increases R, and suppresses torsion.
3. **Stiffness imbalance in the weak direction and within-direction asymmetry:** Case C indicates that torsional sensitivity depends not only on the global comparison K_x versus K_y, but also on how stiffness is distributed within each direction. Imbalance affecting the weak direction (here, the y-direction) is particularly torsion-promoting.
4. **Pronounced CR shifts from uneven wall configurations:** Outliers (e.g., Case B4) show that specific wall layouts can shift CR strongly and deviate from otherwise smooth R–e/D trends, reinforcing that geometry alone is insufficient for prediction.

For early-stage design, Figure 4.23 supports two simple checks: (i) limit eccentricity, since torsion becomes highly likely beyond $e/D \approx 0.16$, and (ii) ensure adequate torsional stiffness through stabilizer placement with large lever arms (high R), noting that the transition region (Zone 1B) can be approximated by $R \approx 84\,(e/D)$.

4.3 L-Shaped Plan Configurations

Unlike the rectangular configurations, the L-shaped plan cases inherently tend to develop eccentricity due to their geometry. Even when the L-shape is geometrically symmetric (i.e., equal leg lengths), the CM may be located outside the plan outline, making it more difficult to align it with the CR through stabilizer placement. As a result, eccentricity is treated as a characteristic of the L-shaped geometry rather than a parameter that can be eliminated through symmetric structural layout.

In the following L-shaped results, the emphasis is therefore on how different stabilizing layouts influence the torsional response in a plan where eccentricity is typically unavoidable. The CM is primarily governed by the slab-dominated mass distribution and is mainly affected by the geometry of the L-shape, while CR is governed by the vertical stabilizing system and shifts with the placement of shear walls and/or the core. The results are presented by comparing mode-shape identification and the corresponding values of eccentricity and normalized torsional stiffness, in order

to evaluate under what conditions torsion appears in the fundamental mode for L-shaped plans.

The L-shaped plan configurations examined in this section include variations in aspect ratio (changing one leg length), shear wall placement both within the legs and along the façades, bending-stiffness imbalance between principal directions ($K_x \neq K_y$), and core placement combined with aspect ratio changes.

4.3.1 Case A: Effect of Change in Aspect Ratio

This section investigates how the aspect ratio of an L-shaped plan influences eccentricity and, consequently, torsional response. The aspect ratio is varied by changing the length of the x-leg (L_x) to 24, 30, 36, 42, 48, and 54 m, while keeping the y-leg length constant at 54 m. Two cases are considered to isolate the effect of geometry from the effect of stabilizer relocation.

In Case A1, the stabilizing system is kept fixed within the shared part of the L-shape while L_x is increased, see Figure 4.24a. Since the shear walls do not move, the CR remains constant. However, the CM depends on the plan geometry and therefore shifts toward the extended x-leg as L_x increases, which increases the eccentricity.

Case A2 is shown in Figure 4.24b. The x-leg is increased in the same manner as in Case A1, but the wall layout differs. In this case, SW1, SW3, and SW4 remain fixed, while SW2 is always placed at the end of the x-leg. Hence, increasing L_x causes both a geometric shift of CM and a shift of CR, since SW2 moves with the x-leg. Both cases share the same geometry sequence and the same overall bending stiffness.

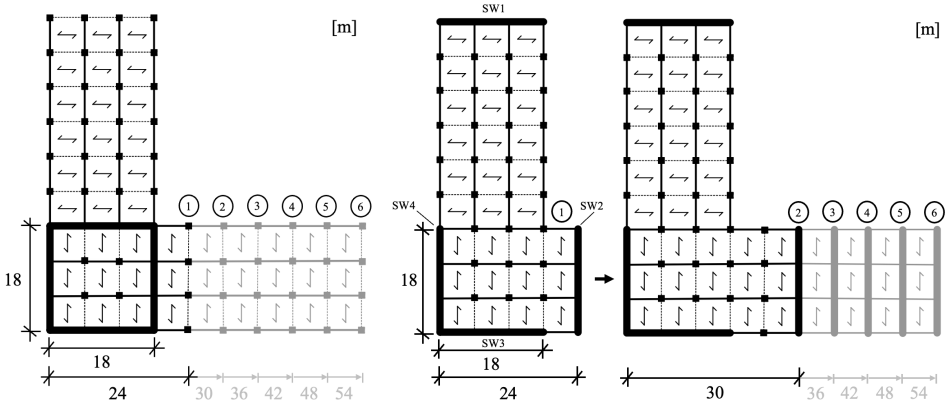

(a) Case A1 **(b)** Case A2

Figure 4.24: Tested configurations for the aspect-ratio study. Thick black lines indicate shear wall locations, grey lines indicate subsequent configurations, and circled numbers denote model numbers. In (a), L_x is increased while the shear walls remain fixed. In (b), L_x is increased and the shear wall on the x-leg (SW2) follows the extension and remains located at the x-leg end.

Mode shape identification is presented in Figures 4.25 and 4.26, where the frequency ratio (FR) is plotted against normalized eccentricity (e/D) and normalized torsional stiffness (R). Model numbers correspond to Figure 4.24, and torsional configurations are highlighted.

For Case A1, all configurations exhibit a predominantly torsional fundamental mode. The normalized eccentricity ranges from 0.176 to 0.228, while the normalized torsional stiffness remains constant at $R = 12.73$ for all models. In contrast, Case A2 shows translational fundamental modes for all configurations ($FR = 1$). Here, the normalized eccentricity is substantially smaller (0.036-0.117) and the torsional stiffness is markedly higher ($R = 29.54 - 38.18$). Thus, Case A1 combines higher eccentricity with lower torsional stiffness, which explains why torsion governs the fundamental mode, whereas the higher R and lower e/D in Case A2 suppress torsional response.

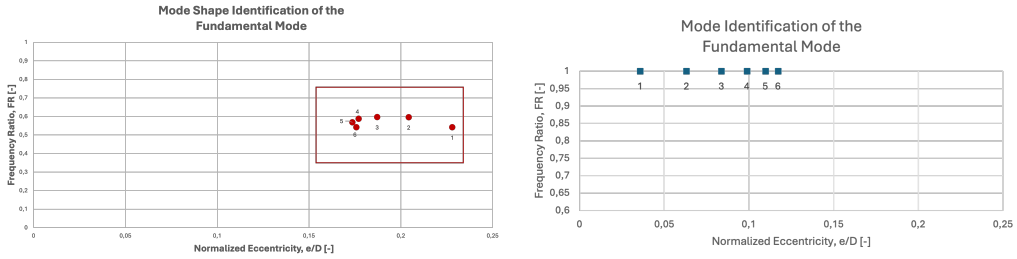

(a) Case A1 **(b)** Case A2

Figure 4.25: Normalized eccentricity (e/D) versus frequency ratio (FR). Values of $FR < 1$ indicate torsional behaviour. Case A1 exhibits torsion for all models, while Case A2 remains translational ($FR = 1$) for all configurations.

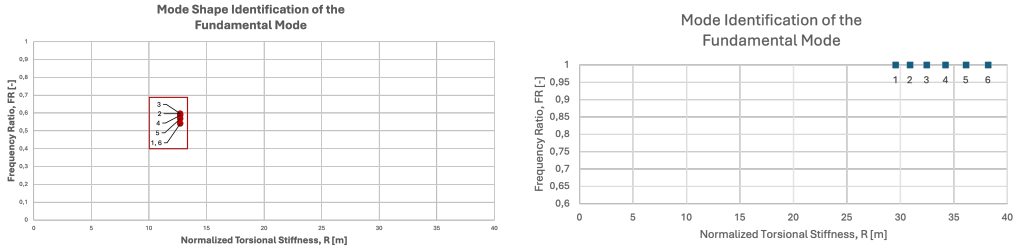

(a) Case A1 **(b)** Case A2

Figure 4.26: Normalized torsional stiffness (R) versus frequency ratio (FR). Values of $FR < 1$ indicate torsional behaviour. Case A1 shows torsion for all configurations, whereas Case A2 remains translational.

Figure 4.27 further illustrates that the torsional contribution in Case A1 increases with increasing L_x. Each colour block corresponds to one model, where the leftmost block represents Model 1 ($L_x = 24$ m) and the rightmost block represents Model 6 ($L_x = 54$ m).

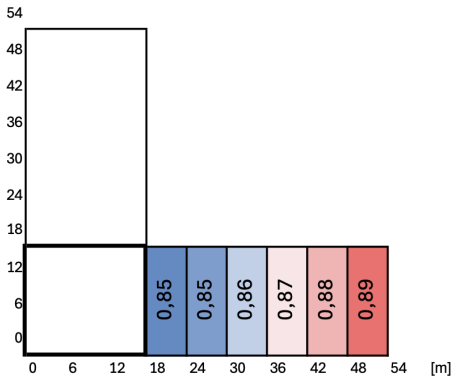

Figure 4.27: Heat map for Case A1 showing the torsional contribution of the fundamental mode (1.0 = pure torsion, 0.0 = pure translation). Values > 0.5 are classified as torsional. The leftmost block corresponds to Model 1 ($L_x = 24$ m) and the rightmost block to Model 6 ($L_x = 54$ m).

To explain the difference in eccentricity between the two cases, Figure 4.28 shows the movement of CM and CR across all configurations. CM shifts in a similar manner in both cases, consistent with the geometric extension of the x-leg. In Case A1, CR remains fixed, which causes the CM-CR distance to increase as L_x grows. In Case A2, CR moves in the x-direction as SW2 follows the extended leg, which partially tracks the CM shift and reduces the resulting eccentricity. Consequently, the CM and CR movements are more closely aligned in Case A2, consistent with the lower e/D values observed in Figure 4.25.

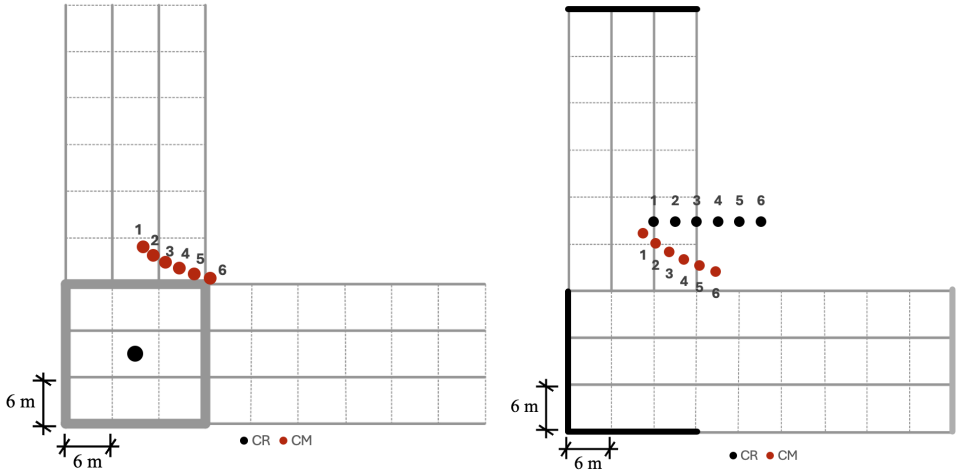

(a) Case A1 **(b)** Case A2

Figure 4.28: CM and CR positions across all models for the two cases (shown on the largest plan outline, i.e., Model 6). Black markers denote CR and red markers denote CM. Case A1 exhibits a fixed CR, while Case A2 shows a shifting CR due to the relocation of SW2.

Figure 4.29 summarizes the relationship between normalized eccentricity (e/D) and

normalized torsional stiffness (R) for Cases A1 and A2. Blue markers indicate translational response and red markers indicate torsional response, circles represent Case A1 and squares represent Case A2. The dashed lines correspond to the critical points extended into critical boundaries, and the intersections of these boundaries define the zones. Within this plot, Zone 1A contains only translational configurations, while Zone 3B contains only torsional configurations. Although the dataset is limited, the separation of these two zones supports the expected trend that reduced eccentricity and increased torsional stiffness both reduce the likelihood of torsion in the fundamental mode.

To quantify the relative influence of eccentricity and torsional stiffness, the ratio $R/(e/D)$ can be evaluated for representative points. For Case A2, Model 6 yields $R/(e/D) \approx 326$ (38.18/0.117), whereas for Case A1, Model 1 gives $R/(e/D) \approx 56$ (12.73/0.228). The largest ratio within Case A1 is approximately 73 (Model 5), which is still only about 22% of the Case A2 value. This indicates that low R relative to e/D is associated with torsional response, while substantially higher ratios are linked to translational behaviour.

The remaining zones are more difficult to interpret because the dataset is limited and several regions in Figure 4.29 are not populated. In this section, only two stabilizer layouts were studied and they represent two very different extremes. Case A1 keeps the shear walls concentrated near the intersection region for all L_x, which makes it difficult to increase torsional stiffness as the x-leg grows, while Case A2 already provides comparatively high torsional stiffness across all configurations, because one wall follows the x-leg and maintains larger lever arms. As a result, the tested points cluster in the clearly torsion-dominated and clearly translation-dominated regions, rather than filling the transition bands. Populating the "grey zones", especially Zone 2, would require additional intermediate layouts (e.g., combining features of A1 and A2 by keeping one wall near the intersection while moving the other, or fixing SW1 at the end of the y-leg while varying SW2 between a central and an end position) to better isolate the influence of aspect ratio and generate a denser point distribution.

Based on the current trends, Zones 1B and 2B are expected to show mixed behaviour. Zone 2C is likely torsion-prone, since the boundary between Zones 2B and 2C corresponds to relatively low ratios, $R/(e/D)$ values of roughly 56-109 values in this range are already associated with torsion in Case A1, and only limited increases are observed before shifting into the clearly translational behaviour of Case A2. Zone 2A is expected to be predominantly translational, since the intersection of the blue critical boundaries implies a minimum ratio on the order of $R/(e/D) \approx 170$. Zone 3A is expected to be torsion-dominated due to its high eccentricity.

Overall, all "grey zones" (Zones 1B, 2A–2C, and 3A) should be treated with caution, since mixed response is likely, and the present dataset is not sufficient to define sharp transitions.

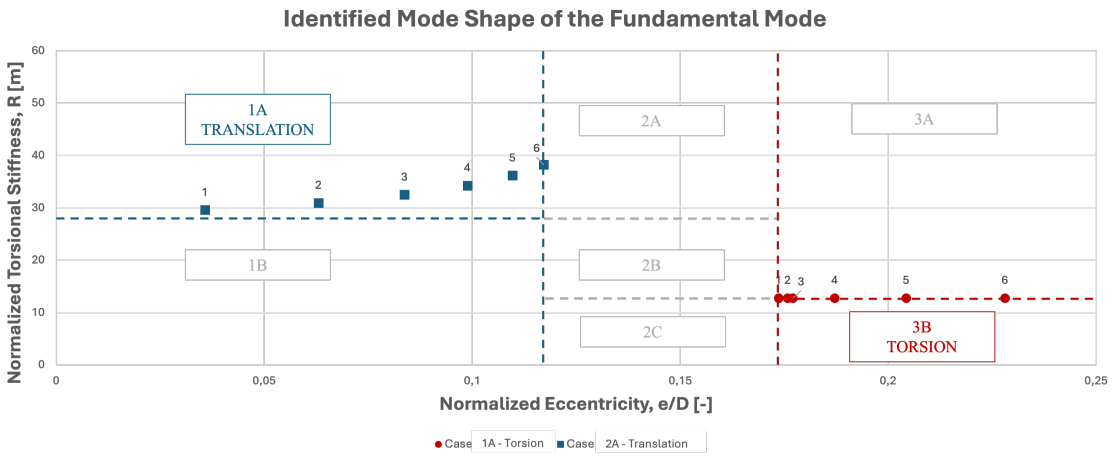

Figure 4.29: Relationship between normalized eccentricity and normalized torsional stiffness for the aspect-ratio cases. Blue markers denote translation and red markers denote torsion, circles represent Case A1 and squares represent Case A2. Dashed lines indicate critical values extended into zone boundaries. Zone 1A is predominantly translational, while the torsional configurations are concentrated in the torsion-dominated region, 3B.

4.3.2 Case B: Effect of Shear Wall Placements

The placement of stabilizing elements has a strong influence on torsional response. Depending on their location, shear walls may either increase torsional resistance or make the system more torsion-prone. The second set of cases in this L-shape study therefore evaluates how shear wall placement affects an L-shaped plan through changes in both eccentricity and torsional stiffness, and thereby the fundamental mode behaviour. For all configurations in this section, the plan dimensions are kept constant with $L_x = L_y = 54$ m and a constant leg width of 18 m. Two main scenarios are considered, Case B1, where shear walls are relocated within the leg geometry, and Case B2, where shear walls are moved along the building façades.

4.3.2.1 Shear Walls Within the Geometry

In Case B1, the shear walls are moved within the plan, thereby altering the stabilizing layout while keeping the geometry unchanged. Based on the aspect ratio study in Section 4.3.1, a more torsion-prone response is expected when stabilizing elements are positioned closer to the interior of the L-shape, whereas more translational behaviour is expected when they are placed further out along the legs. In this setup, SW1 is moved along the y-leg and SW2 along the x-leg in increments of one grid spacing (6 m). The investigated positions are shown in Figure 4.30, where SW1 spans positions 1-7 and SW2 spans positions A-G.

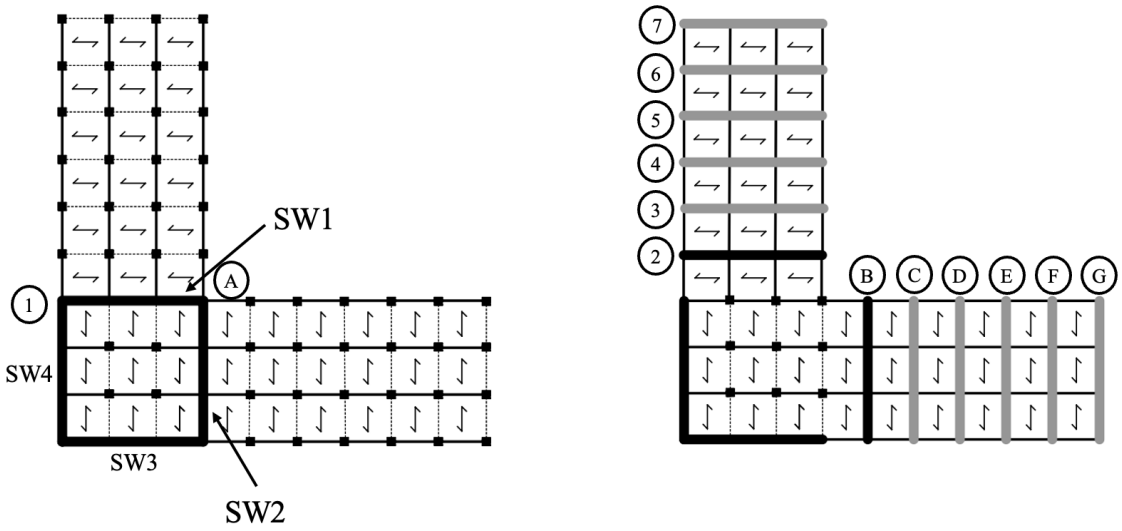

Figure 4.30: Tested configurations for shear walls inside the geometry. Thick black lines indicate shear wall locations, grey lines indicate subsequent configurations, and circled numbers denote model numbers. SW1 is moved along the y-leg for positions 1-7, while SW2 is moved along the x-leg for positions A-G.

To isolate directional effects, the response is first evaluated by moving only one wall at a time: (i) SW1 is moved along the y-leg while SW2 is kept fixed (Case B1a), and (ii) SW2 is moved along the x-leg while SW1 is kept fixed (Case B1b). Figures 4.31 and 4.32 show the corresponding mode shape classification using FR plotted against e/D and R, respectively.

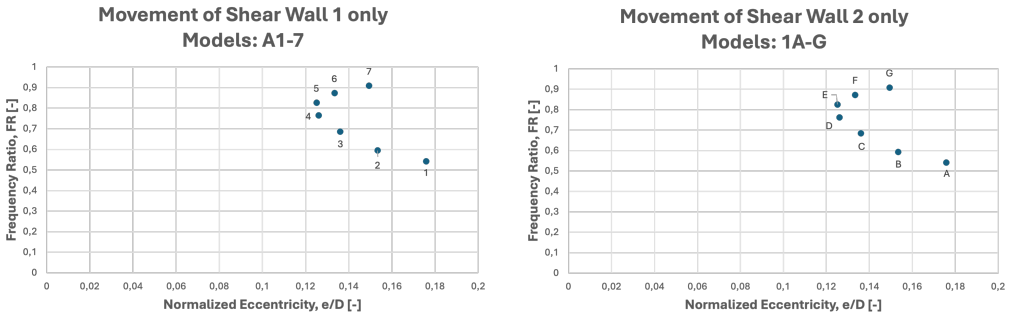

(a) Case B1a: Movement in y **(b)** Case B1b: Movement in x

Figure 4.31: Normalized eccentricity (e/D) versus frequency ratio (FR). Values of $FR < 1$ indicate torsional behaviour. Only movement in (a) y-direction, (b)x-direction.

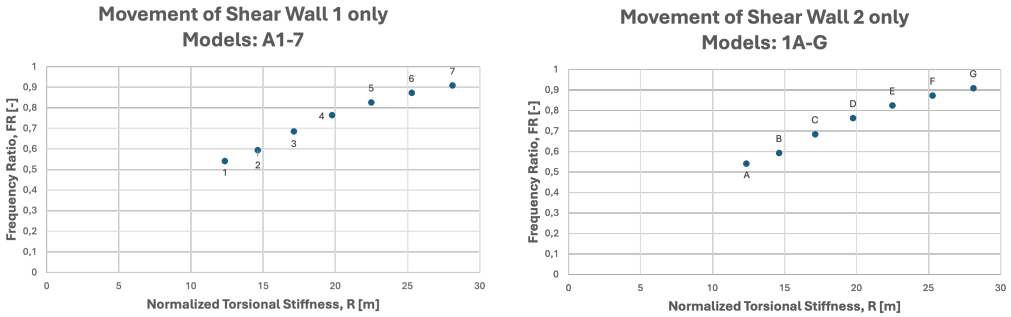

(a) Case B1a: Movement in y **(b)** Case B1b: Movement in x

Figure 4.32: Normalized torsional stiffness (R) versus frequency ratio (FR). Values of $FR < 1$ indicate torsional behaviour. Only movement in (a) y-direction, repectively (b) x-direction.

The two one-wall studies produce essentially the same response, indicating that shifting a single wall along x or along y has a comparable influence for this otherwise symmetric L-shape with equal global bending stiffness in the principal directions. In both cases, R increases as the moved wall is placed further away from the interior of the L-shape (Figure 4.32), which is consistent with increased lever arms relative to CR. The torsional contribution is also reduced as R increases, which follows the expected trend of improved torsional resistance with larger effective radii of the stabilizing system. Nevertheless, all one-wall configurations remain torsion-dominated in the fundamental mode ($FR < 1$ throughout), showing that relocating only one wall is insufficient to suppress torsion for this stabilizer layout.

A notable observation is that the eccentricity does not vary monotonically with wall relocation. Instead, Figure 4.31 shows a curved trend, where the eccentricity is largest for the initial configurations where the moving wall is closest to the common interior region of the L-shape, then decreases as the wall is shifted outward, and finally increases again after approximately Model 5/E. This behaviour is explained by the relative movement of CR with respect to CM. Figure 4.33a shows that CM (black arrows) shifts only slightly compared to CR, and that the turning point in the eccentricity trend occurs when CR passes closest to CM (around configuration 5/E), producing a local minimum in the CM-CR distance. Once CR moves beyond CM, the eccentricity increases again.

Figure 4.33b further confirms that moving the wall outward reduces the torsional contribution, consistent with the simultaneous increase in R.

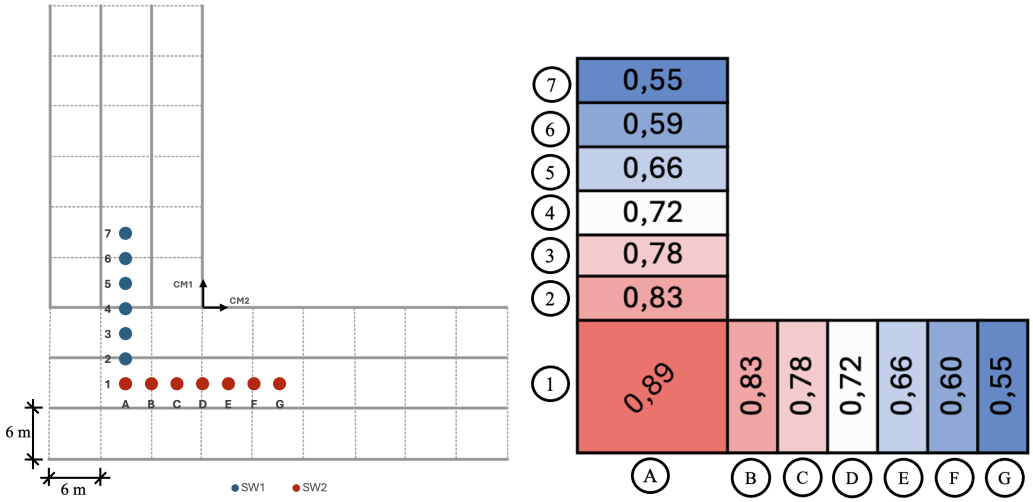

(a) Movement of CM and CR **(b)** Heat Map of Case B1a and B1b

Figure 4.33: (a) Movement of CM and CR for one-wall relocation in y (SW1) and x (SW2). Black arrows indicate CM movement (CM1 corresponds to SW1 relocation and CM2 to SW2 relocation). (b) Heat map showing reduced torsional contribution as the moving wall is placed farther from the interior region.

The persistent torsional response in the one-wall studies indicates that, even with symmetric plan geometry, asymmetry in the stabilizing system is sufficient to trigger torsion. To evaluate whether increased structural symmetry can mitigate this effect, SW1 and SW2 are next moved simultaneously by equal distances (i.e., symmetric relocation along both legs). Figure 4.34 shows FR plotted against e/D and R for these equal-movement configurations. Torsional modes are highlighted in the red box.

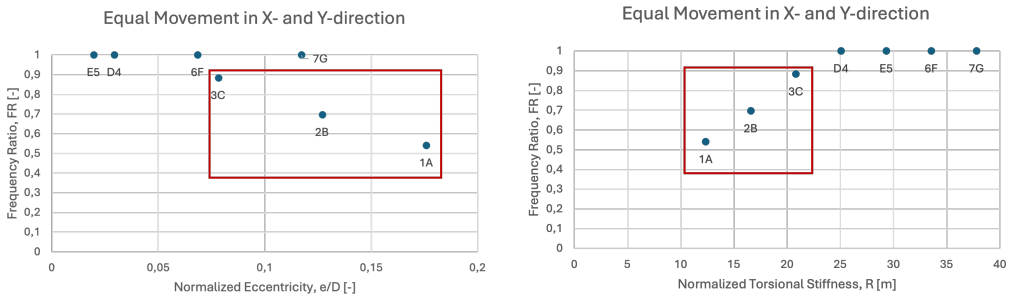

(a) **(b)**

Figure 4.34: (a) Normalized eccentricity, and (b) normalized torsional stiffness (R) versus frequency ratio (FR). Values of $FR < 1$ indicate torsional behaviour, for equal movement of SW1 and SW2.

The equal-movement configurations reduce torsion compared to the one-wall cases, but torsion is still observed for the first three models, where the moving walls remain closest to the interior region of the L-shape. These configurations also have the lowest torsional stiffness (Figure 4.34b), which is consistent with shorter effective

lever arms. The eccentricity trend again shows a decrease followed by an increase (Figure 4.34a), reflecting the same CM-CR proximity effect discussed above. Compared to Cases B1a/B1b, the equal-movement cases generally exhibit lower e/D and higher R, which explains the shift toward more translational behaviour.

Finally, Figure 4.35 combines (i) the one-wall relocation cases (circles), (ii) the equal-movement cases (squares), and (iii) all remaining feasible configurations for this setup (triangles). Blue markers denote translation and red markers denote torsion, and dashed lines extend the critical points into zone boundaries. The one-wall relocations occupy the lower right part of the plot, indicating comparatively larger eccentricity and lower torsional stiffness, and therefore a higher torsion tendency.

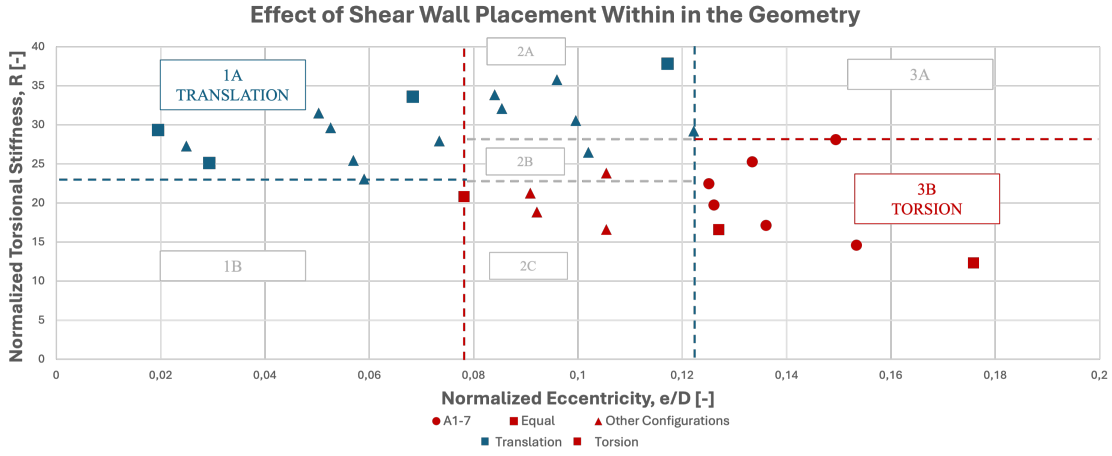

Figure 4.35: Relationship between normalized eccentricity and normalized torsional stiffness for the moving shear walls within the geometry cases. Blue markers denote translation and red markers denote torsion, circles represent Case B1a/B1b, squares represent equal movements in x and y, and triangles are the other cases thatcould be done with this set up. Dashed lines indicate critical values extended into zone boundaries. Zone 1A is predominantly translational, while the torsional configurations are concentrated in the torsion-dominated region, 3B.

The zoning in Figure 4.35 indicates predominantly translational behaviour in Zone 1A, characterized by low eccentricity and high torsional stiffness. The lower boundary of Zone 1A corresponds to an approximate ratio of $R/(e/D) \approx 295$, while Zone 2A remains translational for slightly lower ratios (down to roughly 235), consistent with its high torsional stiffness. Torsional configurations cluster in Zone 3C, where $R/(e/D)$ decreases substantially and reaches values as low as ~ 72 for the configurations with walls closest to the interior region. The remaining zones (Zones 1B, 2B-2C, and 3A) form "grey zone" regions where mixed behaviour is expected and should be treated with additional caution. Overall, although the absolute $R/(e/D)$ ratios in this shear-wall study are relatively high compared to other cases, the same qualitative trend remains where torsion is most likely when eccentricity is high rel-

ative to torsional stiffness, and it is mitigated as stabilizing elements are placed further away from CR, increasing lever arms and R.

4.3.2.2 Shear Walls Along the Façades

In the second shear wall study, the walls are relocated along the building façades rather than within the leg geometry. Placing the stabilizing elements on the perimeter maintains large lever arms to the CR, even when the walls are shifted toward the corner of the L-shape. Two cases are evaluated, one with shear walls spanning one grid length (6 m) and one with shear walls spanning three grid lengths (18 m). As shown in Figure 4.36, SW3 is moved along the outer y-façade and SW4 along the outer x-façade, and both walls are relocated by equal distances for each model. Thick black lines indicate the initial locations, while the grey lines indicate the remaining tested positions with corresponding model numbers.

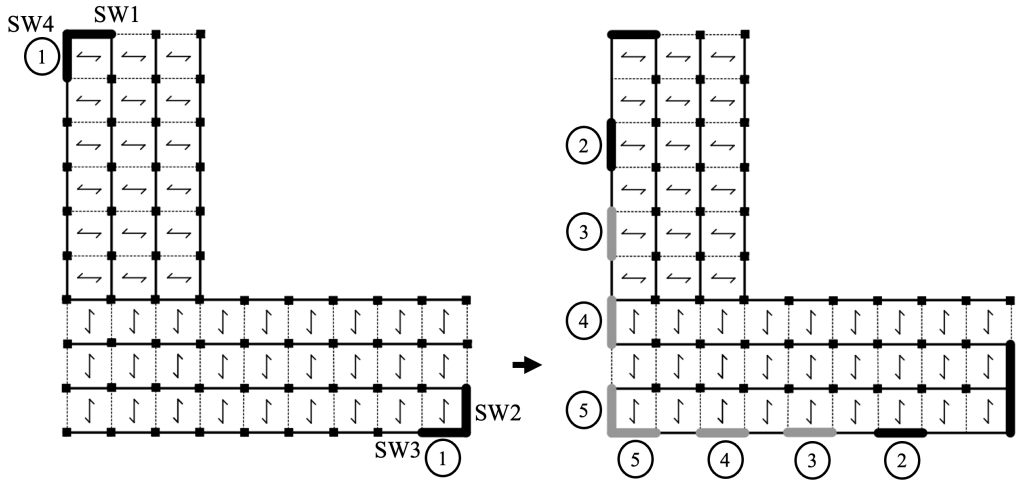

(a) Shear Walls 6 m

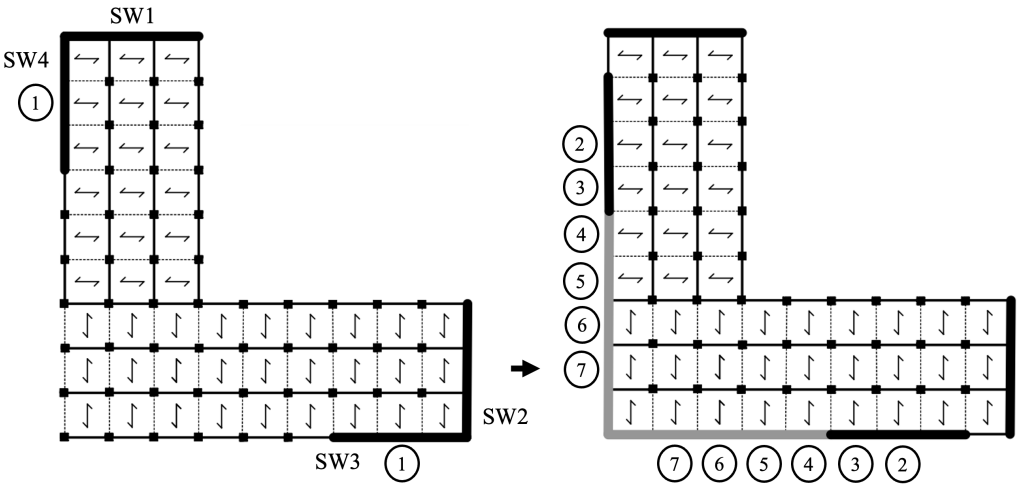

(b) Shear Walls 18 m

Figure 4.36: Plan configurations for moving shear walls along the facades, with (a) shear walls of 6m, and (b) shear walls of 18m.

All configurations in this study exhibit translational behaviour in the fundamental mode. The relationship between normalized eccentricity (e/D) and normalized torsional stiffness (R) is shown in Figure 4.37. Notably, the results collapse into one point per wall length, indicating that neither e/D nor R changes when SW3 and SW4 are moved along the façades in this symmetric manner. In other words, relocating perimeter walls along the outer edges does not reduce torsional resistance for the investigated L-shape, as long as the stabilizing system remains symmetric and the lever arms to CR remain large.

A possible explanation is that façade relocation mainly affects the response of each leg in its already strong direction. By viewing the L-shape as three connected rectangular parts (the two legs and the intersection region), each leg behaves similarly to a rectangle whose weak axis is aligned with the direction of SW1 and SW2. Shifting SW3 and SW4 along the façades therefore primarily modifies stiffness distribution along directions that are comparatively strong, and the global torsional response is consequently insensitive to these changes. This interpretation is consistent with the high ratios of $R/(e/D)$ observed for the two wall lengths, approximately 212 for the 6 m walls (0.127, 27), and 230 for the 18 m walls (0.117, 27), which are high compared to other tested configurations.

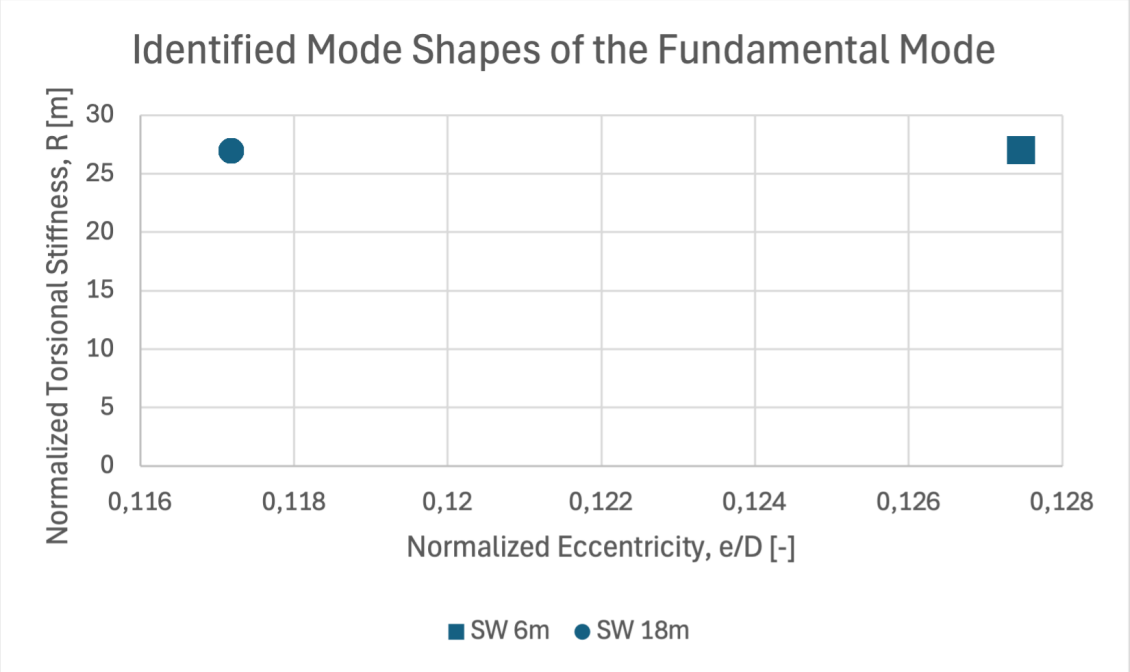

Figure 4.37: Relationship between normalized eccentricity and normalized torsional stiffness for shear walls moved along the façades. Squares indicate the 6 m wall case, while circles indicate the 18 m wall case.

Since all models within each wall-length case produce identical $(e/D, R)$ values, no trends or zone boundaries can be established for this study.

4.3.2.3 Conclusion on Shear Wall Placement

Figure 4.38 compiles all configurations in the e/D-R space and divides the response into zones using the critical boundaries. Zone 1A is translation-dominated, characterized by low eccentricity combined with relatively high torsional stiffness. Clear torsional behaviour is concentrated in Zone 3B, where eccentricity is high and R is insufficient relative to e/D. Zone 2 can be regarded as a "grey zone", however, for the present configurations it is split into distinct tendencies. Zone 2A exhibits translational response, characterized by high torsional stiffness and moderate eccentricity, whereas Zone 2C shows torsional response due to low R despite similarly moderate e/D. The remaining regions (Zones 1B, 2B, and 3A) constitute transition zones where mixed behaviour is possible. Zone 1B is expected to exhibit a mixed behaviour, with translation favoured at higher R and torsion becoming more likely as e/D increases. Zone 2B forms a transition band between the translation- and torsion-dominated regions, and Zone 3A may remain torsion-prone due to its high eccentricity even when R is elevated.

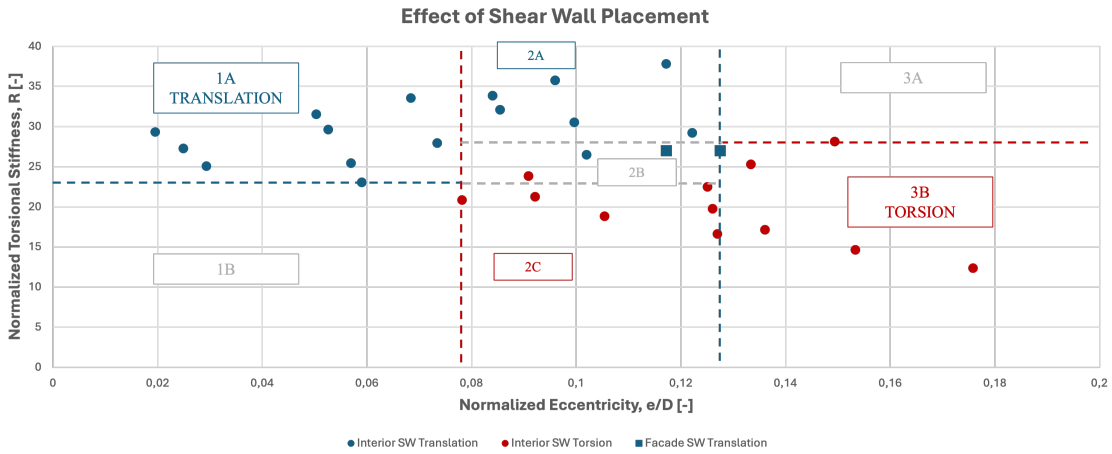

Figure 4.38: Relationship between normalized eccentricity and normalized torsional stiffness for all shear wall placement configurations.

In summary, moving shear walls within the geometry tends to reduce effective lever arms and shift configurations toward torsion-prone regions (notably Zones 2C and 3B), whereas relocating walls along the façades preserves large lever arms and keeps the response in translation-dominated regions. From a design perspective, torsional sensitivity is minimized by maintaining perimeter placement and/or ensuring sufficiently high R relative to e/D, while configurations located in the "grey zones" require additional attention in early-stage assessment.

4.3.3 Case C: Effect of Structural Asymmetry Caused by Imbalance in Bending Stiffness

L-shaped plans are inherently torsion-sensitive due to their geometric eccentricity and the resulting CM-CR offset. This sensitivity may be further affected when the bending stiffness differences between the principal directions, similar to the rectangular findings in Section 4.2.3. The purpose of this section is therefore to evaluate how an imbalance between K_x and K_y influences the torsional response of an L-shaped plan.
The geometry is kept constant with $L_x = L_y = 54$ m and a leg width of 18 m. The stabilizing layout follows the within-geometry setup in Section 4.3.2.1, where SW1 is moved along the y-leg (positions 1-7) and SW2 is moved along the x-leg (positions A-G) in 6 m increments. In contrast to Section 4.3.2.1, the present configurations are designed such that the global bending stiffness is imbalanced ($K_x < K_y$), introducing structural asymmetry through directional stiffness rather than through geometry.

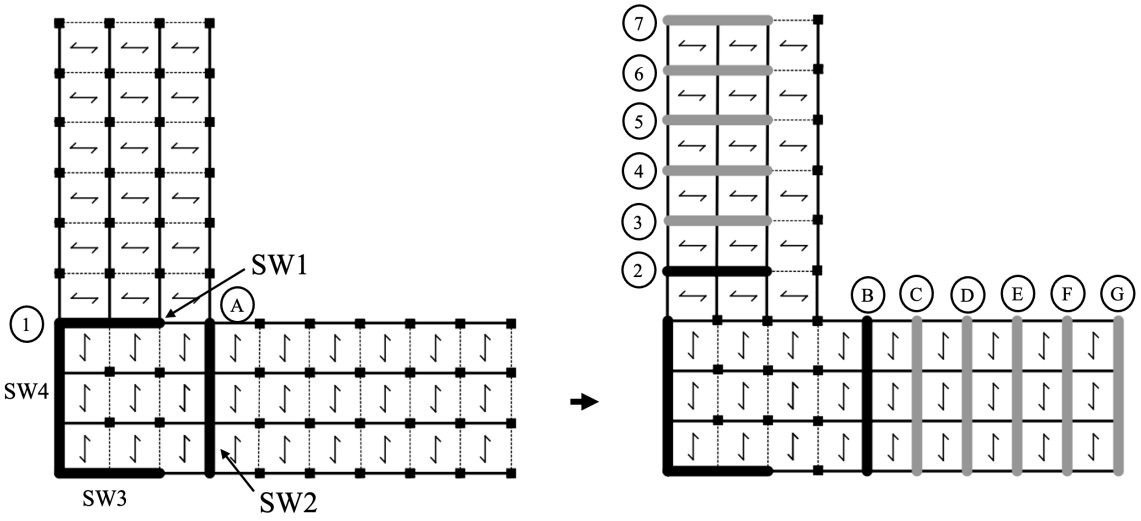

Figure 4.39: Tested configurations for bending stiffness imbalance. Thick black lines indicate shear wall locations, grey lines indicate subsequent configurations, and circled numbers denote model numbers. SW1 is moved along the y-leg for positions 1-7, while SW2 is moved along the x-leg for positions A-G.

As in Section 4.3.2.1, three subsets are first examined to isolate directional effects: (i) only SW1 is moved (y-direction), (ii) only SW2 is moved (x-direction), and (iii) SW1 and SW2 are moved simultaneously by equal distances (models A1, B2, C3, ..., G7). Figure 4.40 shows the mode shape identification, with FR plotted against normalized eccentricity (e/D) and normalized torsional stiffness (R). A clear difference compared to the equal-stiffness case (Section 4.3.2.1) is that relocation in the x- and y-directions no longer produces identical response patterns. This indicates that the stiffness imbalance ($K_x < K_y$) affects how sensitive the system is to shear wall relocation depending on direction.

The eccentricity trends broadly follow the same curved behaviour observed previously, e/D decreases as CR approaches CM and then increases again once CR passes CM. The curve is, however, less smooth for the SW2-only movement. This is mainly because translational response is reached earlier in some SW2 configurations when stiffness is higher in the associated direction, causing fewer torsion-dominated points to remain along the latter part of the curve. Interpreting the L-shape as two connected rectangular sub-plans, relocating SW2 mainly modifies the stabilizing system in the lower portion of the plan. Since SW2 is longer than SW1, its relocation provides a larger stiffness contribution in the weak direction of this bottom part, combined with the increasing lever arm as SW2 moves along the x-leg, this can promote a translational fundamental mode earlier than for the SW1 relocations. At the same time, the stiffness contribution in the strong direction is comparatively smaller for the SW2-movement case, since the associated walls (SW1 and SW3) are shorter. In contrast, shifting SW1 primarily affects the direction that remains relatively weak, resulting in a larger proportion of torsion-dominated configurations.

The R-FR plot in Figure 4.40(b) shows the expected stabilizing effect of increased torsional stiffness, configurations with low R are predominantly torsional and are typically associated with walls placed close to the L-intersection, while translation becomes increasingly common as R increases due to larger effective lever arms.

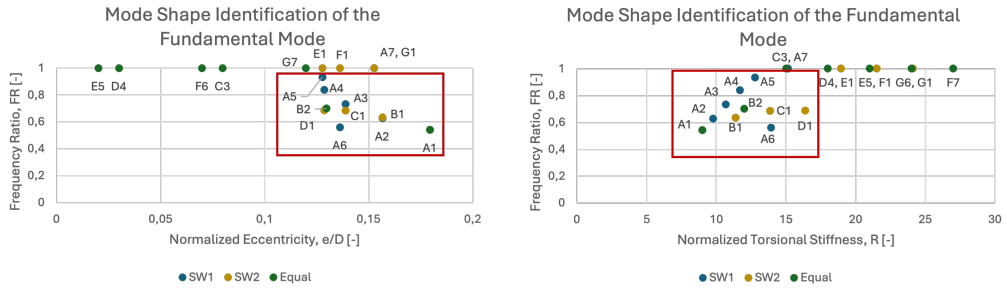

(a) **(b)**

Figure 4.40: (a) Normalized eccentricity and (b) normalized torsional stiffness (R) versus frequency ratio (FR) for bending-stiffness imbalance ($K_x < K_y$). Values of $FR < 1$ indicate torsional behaviour and are highlighted. Blue markers represent movement of only SW1 (y-direction), yellow markers represent movement of only SW2 (x-direction), and green markers represent equal movement in both directions (models A1, B2, ..., G7).

Figure 4.41 compiles all configurations in the e/D-R space, including SW1-only movement (circles), SW2-only movement (squares), equal movement (triangles), and remaining feasible placements (rhombs). Blue markers denote translation and red markers denote torsion. The critical points are extended into critical boundaries that divide the plot into zones (1A-3B). The overall trend is consistent with the previous sections, where translation occurs predominantly at low eccentricity and high torsional stiffness (upper-left region), whereas torsion occurs at higher eccentricity combined with lower torsional stiffness (lower-right region).

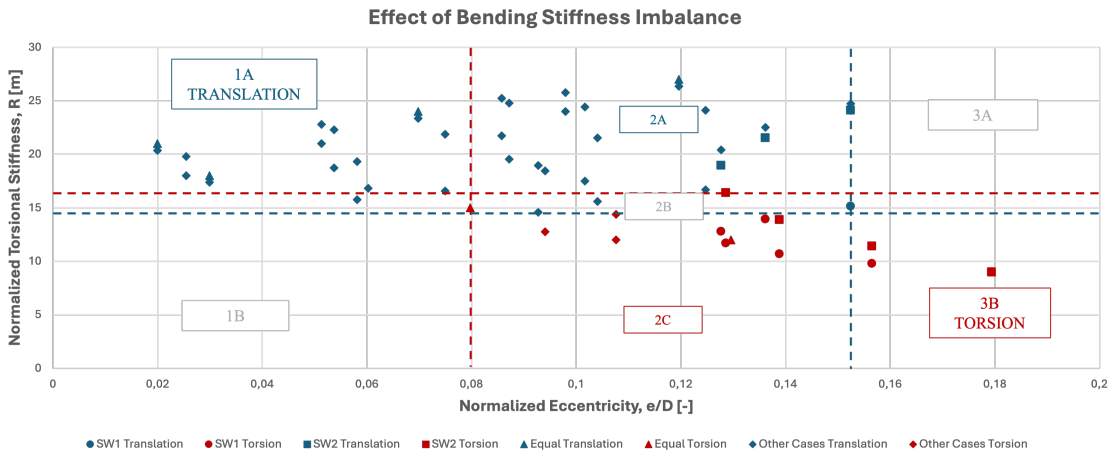

Figure 4.41: Relationship between normalized eccentricity and normalized torsional stiffness for all bending stiffness imbalance placement configurations.

The zone interpretation further clarifies this behaviour. Zone 1A is translation-dominated, Zone 3B is torsion-dominated, while Zone 2 represents the transition region. In the present dataset, Zone 2A contains only translational points and Zone 2C contains only torsional points, while Zone 2B exhibits mixed behaviour and therefore constitutes the primary boundary region between translation and torsion. Although the current simulations show relatively clear separation within Zone 2A and Zone 2C, these regions should still be regarded as part of the broader "grey zone" concept, as additional configurations could possibly populate them and introduce mixed response close to the critical lines. Zones 1B and 3A contain no points in the present plot, nevertheless, Zone 1B would be expected to transition from translation to torsion as eccentricity increases and/or R decreases, while Zone 3A would be expected to be torsion-prone due to high eccentricity unless counteracted by very high torsional stiffness.

Considering the ratio $R/(e/D)$ provides an additional perspective on the transition. Along the boundary region (Zone 2B) the ratio spans approximately 91-187.5, reflecting that the same absolute torsional stiffness can be sufficient at low eccentricity but insufficient at higher eccentricity. This spread also illustrates why a single "critical" ratio is difficult to define for the L-shape, since the governing behaviour depends on where the configuration lies relative to the critical boundaries rather than on one constant threshold.

Compared to the equal-stiffness study in Section 4.3.2.1, the stiffness-imbalanced configurations generally shift the response toward torsion for comparable placements, indicating that bending stiffness imbalance is less favourable for torsional performance in the L-shape. The imbalance ($K_x < K_y$) breaks the directional equivalence observed previously, that relocating stabilizing elements in the weaker direction triggers torsion more easily and results in torsion-dominated behaviour across a broader range of configurations. In practical terms, stiffness imbalance increases torsional sensitivity by affecting both the movement of CR and the overall rotational resistance of the system. As a result, configurations near the critical boundaries (especially Zone 2B) may change governing mode with relatively small placement adjustments. A key design implication is therefore that torsional robustness in L-shaped buildings depends not only on maintaining large lever arms (high R), but also on avoiding pronounced stiffness imbalance between directions, particularly when stabilizing elements are located close to the interior intersection of the L. If a stiffness imbalance is nevertheless required, it is likely preferable to orient the weaker direction along the strong axis of the rectangular sub-plans that together form the L-shape.

4.3.4 Case D: Effect of Core Placement Combined with Change in Aspect Ratio

As discussed previously, L-shaped plans inherently exhibit eccentricity due to their geometry and the resulting CM-CR offset, and torsion can therefore arise without introducing additional asymmetry (in contrast to the rectangular cases in Section 4.2). Nevertheless, it is of interest to examine how an added core, in combination with changes in aspect ratio, influences the torsional response. In the present study, a core is introduced and relocated within the intersecting part of the L-shape, while the aspect ratio is varied by changing the x-leg length from $L_x = 24$ m to $L_x = 54$ m in steps of one grid length (6 m), consistent with Section 4.3.1. For each L_x, the core is tested in nine positions (1-9) within the common region (Figure 4.42c). In addition, one 6 m shear wall is placed at each outer edge of the legs, with SW2 always located at the end of the x-leg and therefore moving as L_x increases. Two shear wall layouts are considered, in Case D1, the perimeter shear walls are shifted toward the long outer sides of the L-shape, while in Case D2 they are placed at mid-span along the leg edges. Figures 4.42(a) and (b) show the shear wall layouts and the changing x-leg lengths (models A-F), and Figure 4.42(c) shows the tested core positions (1-9). Solid black lines indicate the reference configuration and grey lines indicate the remaining tested configurations.

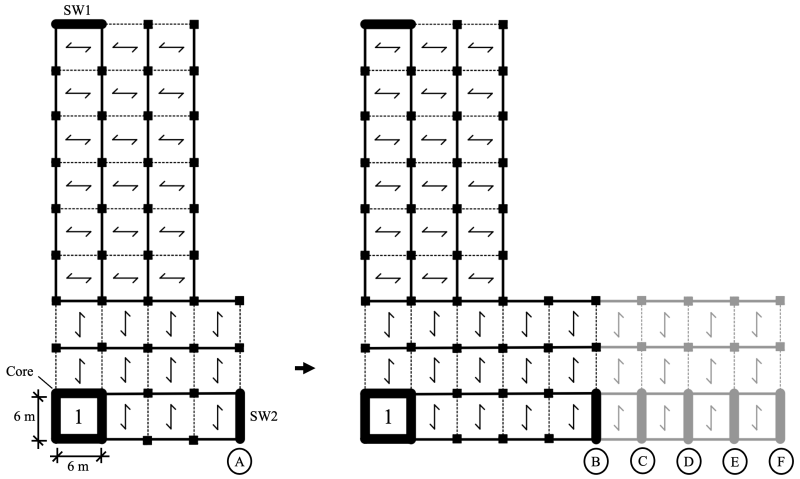

(a) Case D1: Change in Aspect Ratio

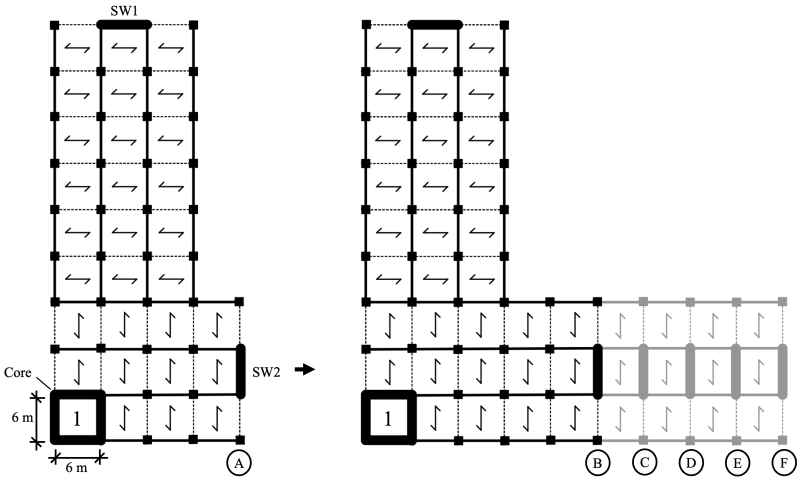

(b) Case D2: Change in Aspect Ratio

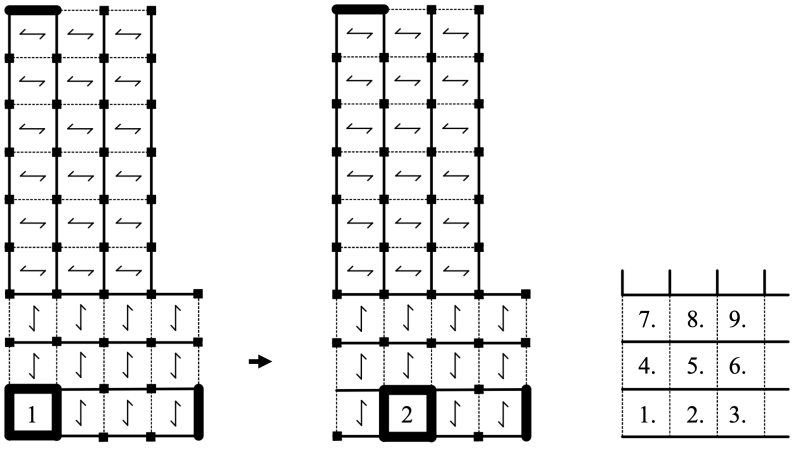

(c) Core Placements

Figure 4.42: Plan configurations for core placement combined with aspect ratio. (a) Change in x-leg length for Case D1, (b) change in x-leg length for Case D2, and (c) tested core positions (shown for Case D1; the same positions apply for Case D2). Solid black lines indicate the reference layout and grey lines indicate the other tested configurations.

Figure 4.43 presents the mode shape classification through the frequency ratio (FR) plotted against (a) normalized eccentricity (e/D) and (b) normalized torsional stiffness (R). The responses for Cases D1 and D2 are nearly identical, Case D2 yields slightly higher values, but the differences are small and do not affect the overall interpretation. Only three configurations exhibit torsion in the fundamental mode, A9, B9, and C9. These correspond to the combination of (i) the shortest x-leg lengths and (ii) core position 9, and they occur at relatively high eccentricity together with low torsional stiffness.

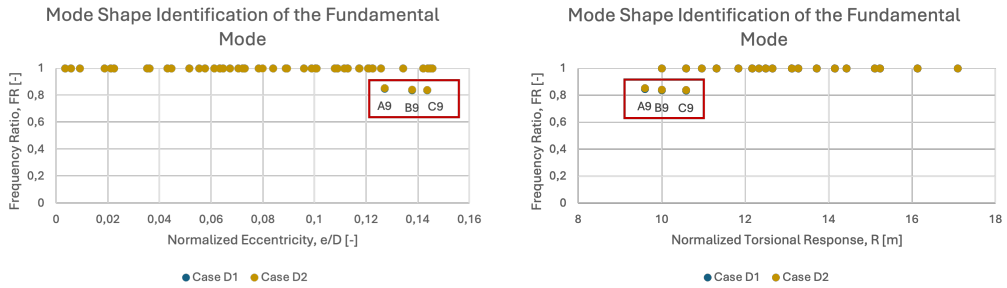

(a) **(b)**

Figure 4.43: (a) Normalized eccentricity (e/D) and (b) normalized torsional stiffness (R) versus frequency ratio (FR). Values of $FR < 1$ indicate torsional behaviour and are highlighted.

These observations are consistent with the aspect ratio trends identified in Section 4.3.1. When one leg is short and the stabilizing system is concentrated near the common region, the plan behaves similarly to a strongly eccentric rectangle, which increases torsion sensitivity. In the present configurations, SW2 is placed at the end of the x-leg, so for short L_x it remains close to the common region and therefore provides limited lever arm relative to CR. As L_x increases, SW2 is moved farther away, increasing torsional stiffness and reducing torsion sensitivity.

To further investigate the influence of core position, Figure 4.44 compares the torsional contribution across core placements 1-9 for the shortest (Model A) and longest (Model F) x-leg in Case D1. The heat maps show that core position 9 consistently produces the largest torsional contribution. Notably, core position 1 yields a non-negligible torsional component for Model A (approximately 23%), but essentially no torsional contribution for Model F. This suggests that for the longer x-leg the combined stabilizing system (perimeter shear walls with larger lever arms plus a corner-covering core placement) is sufficient to suppress torsion, whereas for the shorter x-leg the available lever arms are smaller and the same core position cannot provide the same stabilizing effect.

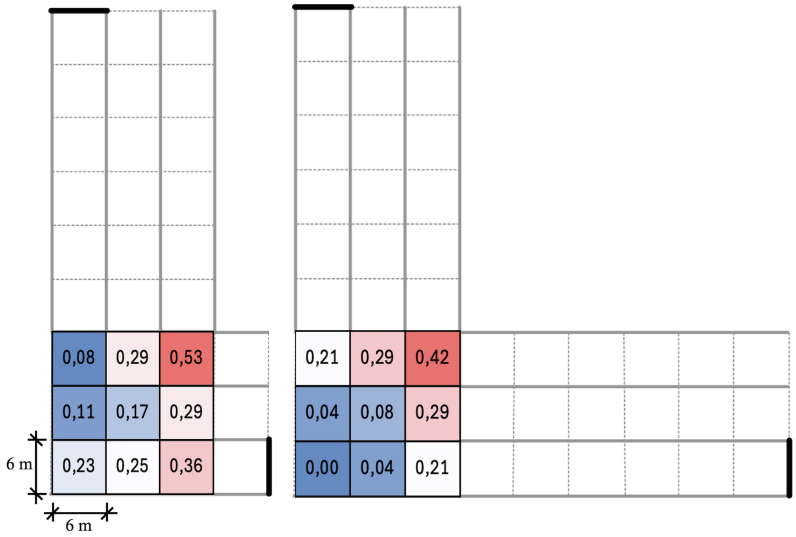

(a) Model A **(b)** Model F

Figure 4.44: Heat map for Case D1 showing torsional contribution of the mode shape (0.0 = pure translation, 1.0 = pure torsion). (a) Model A (L_x = 24 m) and (b) Model F (L_x = 54 m).

Figure 4.45 compiles all configurations (all core positions and all aspect ratios) in the e/D–R space. The three torsional configurations are located in the region of comparatively high eccentricity and low torsional stiffness, while the remaining configurations cluster in the translational region.

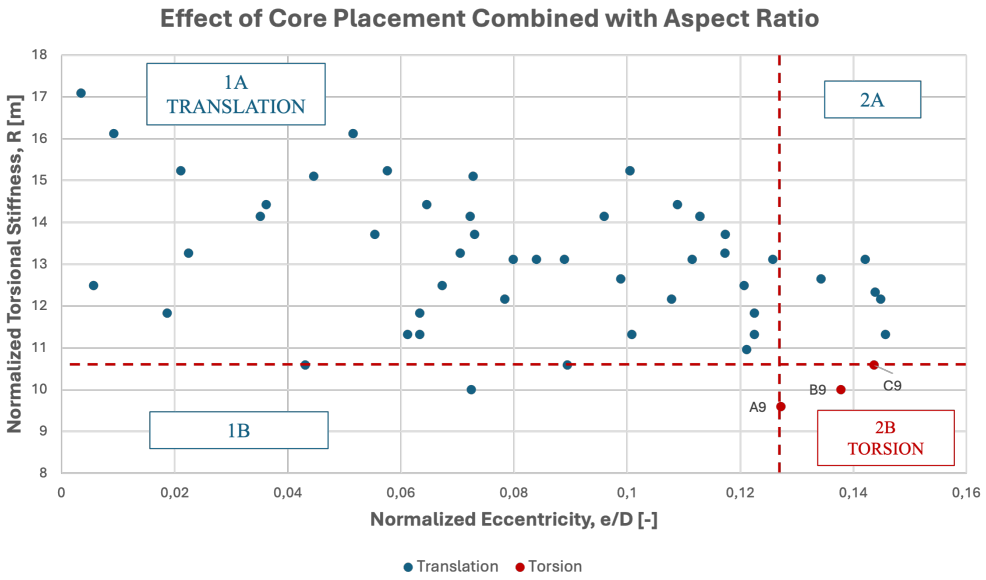

Figure 4.45: Relationship between normalized eccentricity and normalized torsional stiffness for all core positions and aspect ratios. Blue markers denote translation and red markers denote torsion. Dashed lines indicate critical boundaries.

Dividing Figure 4.45 into zones is less straightforward than for the other studies, since most configurations remain translational despite relatively high eccentricity, likely due to consistently high torsional stiffness from the perimeter shear walls and the additional stabilizing effect of the core. Zone 2B contains the torsional configurations, while Zone 1A is clearly translational. Zones 1B and 2A appear predominantly translational in the present dataset, leaving only limited evidence of intermediate "grey zone", however, several points lie close to the critical boundaries, suggesting that mixed behaviour may still occur and that the absence of data in some regions limits the robustness of zone-based conclusions.

Despite the limited number of torsional cases, two practical trends emerge. First, torsion is promoted by the combination of short-leg aspect ratios (small L_x) and unfavourable core placement (here, position 9), which together produce high eccentricity while limiting torsional stiffness. Second, increasing effective lever arms, either by extending the x-leg (moving SW2 outward) or by placing stabilizing elements to "cover" corners, improves torsional resistance and promotes translational behaviour. In early design, configurations that concentrate stabilizers near the interior corner of an L-shape should therefore be treated as torsion-sensitive, whereas distributing stabilizing elements toward the extremities (especially corners) provides a more robust torsional response.

4.3.5 Summary of Torsional Response for L-Shaped Plans

Figure 4.46 compiles all L-shaped configurations from Cases A-D in the e/D-R space. Blue markers denote translational fundamental modes and red markers denote torsional fundamental modes. The dashed vertical lines mark two critical eccentricity limits, while the dashed horizontal lines indicate two critical torsional-stiffness levels used to define the zone boundaries. From the figure, the critical torsional-stiffness values are $R_{\text{crit},1} = 10.0$ m and $R_{\text{crit},2} = 28.11$ m. The corresponding critical eccentricities are approximately $e/D = 0.078$ (left dashed red line) and $e/D = 0.152$ (right dashed blue line). Using these boundary values, the associated stiffness-eccentricity ratios are approximately $R/(e/D) \approx 128$ for $R_{\text{crit},1}$ and $R/(e/D) \approx 184$ for $R_{\text{crit},2}$.

Zone 1A (upper-left) is translation-dominated, showing low eccentricity combined with sufficiently high torsional stiffness leads to a translational fundamental mode. Zone 3B (lower-right) is torsion-dominated, showing high eccentricity together with low-to-moderate torsional stiffness produces torsion in the fundamental mode. Zone 2 represents the transition region, where the response depends on the balance between e/D and R. In particular, the plot shows a clear split within Zone 2, where configurations in Zone 2A (moderate e/D but high R) remain translational, whereas configurations in Zone 2C (moderate e/D but low R) are torsional. Zone 2B forms the primary boundary band where mode switching occurs. Zones 1B and 3A contain fewer points overall, but can be interpreted as mixed/transition regions where translation is favoured at high R and torsion becomes more likely as e/D increases.

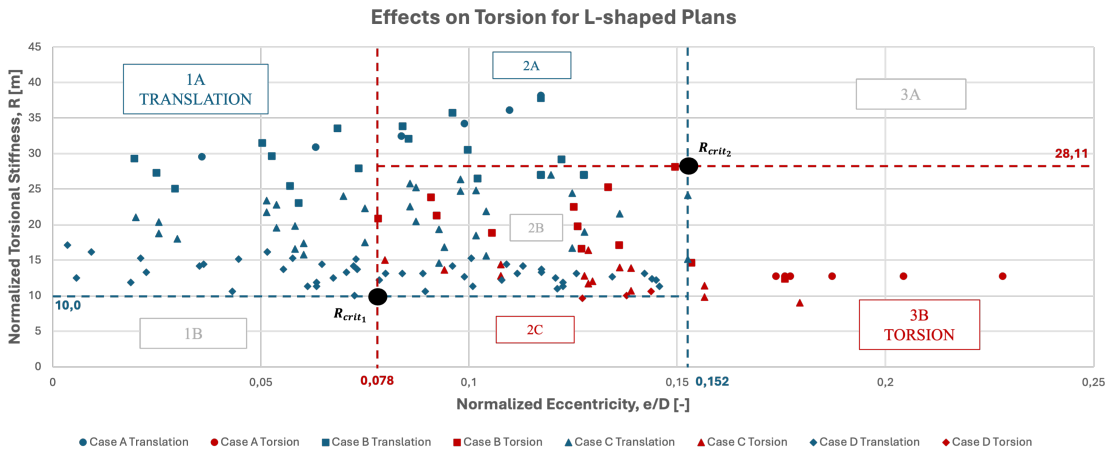

Figure 4.46: Relationship between normalized eccentricity and normalized torsional stiffness for all tested L-shaped configurations. Blue markers denote translational response and red markers denote torsional response. Dashed lines indicate the critical boundaries, and Zone 2B is highlighted as the mixed-response region. The markers $R_{\text{crit},1}$ and $R_{\text{crit},2}$ indicate the upper and lower $R/(e/D)$ boundary levels for Zone 2B, respectively.

Across all cases, two mechanisms dominate the L-shape behaviour: (i) **eccentricity is largely geometry-driven** (CM is governed by the slab-dominated mass distribution and can be difficult to align with CR), and (ii) **torsional stiffness is layout-driven** (CR position and lever arms depend on the stabilizing system).

- **Case A (Aspect Ratio)** shows that aspect ratio is a strong torsion driver when the stabilizing system does not track the geometric CM shift. In Case A1, keeping stabilizers fixed while increasing L_x increases e/D while keeping R low (around the lower band), placing the configurations deep in the torsion-prone region. In Case A2, letting SW2 move with the x-leg increases R and reduces e/D, shifting the response into the translational region.
- **Case B (Shear Wall Placement)** shows that lever arms are a key control variable. Moving walls within the geometry tends to reduce effective lever arms and moves points toward Zones 2C/3B, while façade/perimeter placement maintains large lever arms and keeps the response in translational zones (typically above $R_{\text{crit},2}$ for moderate e/D).
- **Case C (Bending Stiffness Imbalance)** increases torsional sensitivity by breaking directional equivalence, since relocating stabilizers along the weaker direction produces torsion more easily and over a wider range of placements. In the combined plot, this appears as more red points extending into the transition region (Zone 2B) for comparable eccentricities.
- **Case D (Core + Aspect Ratio)** indicates that adding a core can improve robustness primarily by increasing overall torsional resistance and by "covering" critical corners. However, unfavourable core placement combined with short-leg aspect ratios can still produce torsion (the torsional models occur for

short L_x and the same critical core position).

4.3.5.1 Which factors affect torsion the most in L-shaped plans

Based on Cases A-D and their location in Figure 4.46, the dominant factors (from strongest to weaker, in terms of shifting configurations into torsion-dominated zones) are:

1. **Geometric eccentricity level (e/D), driven mainly by aspect ratio and CM-CR separation.** Case A shows the clearest shift into torsion when e/D becomes high.
2. **Effective torsional stiffness / lever arms (R), governed by stabilizer placement.** Case B demonstrates that perimeter placement and larger lever arms can keep even moderate eccentricities translational, especially when $R \gtrsim R_{\text{crit},2}$.
3. **Structural asymmetry from stiffness imbalance ($K_x \neq K_y$). .** Case C broadens the transition region and makes mode switching easier near Zone 2B.
4. **Core Placement** as a modifier. Case D shows it can be beneficial, but becomes critical only for certain placements and short-leg geometries).

Figure 4.46 suggests two simple design oriented checks: (1) configurations with e/D approaching or exceeding the upper critical eccentricity (about 0.152) are torsion-prone unless torsional stiffness is very high; and (2) for moderate eccentricities (around the mid-zone), maintaining R above the upper critical stiffness level $R_{\text{crit},2} \approx 28.11$ m, corresponding to roughly $R/(e/D) \gtrsim 184$ at the boundary, is generally associated with translational behaviour, whereas values below $R_{\text{crit},1} \approx 10.0$ m—about $R/(e/D) \lesssim 128$ at the boundary—are consistently torsion-prone. Configurations that fall between these limits (especially Zone 2B) should be treated as sensitive and require additional verification in early design.

4.3.6 Future Work

The present study provides a clear modal classification of when torsion governs the fundamental mode as a function of plan geometry and stabilizer layout. A natural continuation is to refine and validate the transition regions, and to connect the modal findings to wind-driven serviceability performance.

First, the "grey zone" regions identified in the $e/D - R$ space should be investigated with a denser set of configurations. This would improve confidence in the critical boundaries and enable the development of more reliable design-oriented thresholds (e.g., "torsion is likely when e/D exceeds x, while R falls below y). Such refinement should include additional intermediate layouts near the boundary lines, as well as targeted variations in stabilizer placement and stiffness distribution to clarify whether the transition is gradual or abrupt for different mechanisms (core offset, wall lever arms, stiffness imbalance).

Second, the modelling assumptions could be refined to better represent real timber buildings. In particular, more realistic boundary conditions and connection

behaviour should be introduced, since stiffness reductions due to connections can significantly influence both bending and torsional response. A refined slab discretisation should also be studied, since floor plates are rarely continuous 6 m wide panels in practice, but instead consist of subdivided elements where stiffness is reduced through joints and secondary spanning effects. Introducing these refinements would allow the sensitivity of the results to modelling idealisations to be assessed.

Third, the analysis could move from mode classification to response magnitude. For representative torsion-prone layouts, dynamic wind-type loading could be used to compute peak accelerations and corner displacements, enabling quantification of how much torsion amplifies serviceability response compared to translation-dominated cases. This would also support more actionable recommendations by relating the identified torsion-prone regions to measurable performance indicators.

Finally, the applicability of the findings could be strengthened by generalizing the parametric scope. This includes studying additional building heights (more storeys and/or varying storey heights) and extending the plan types beyond rectangles and L-shapes (e.g., T- and U-shaped layouts). A wider set of stabilizer arrangements and structural variations would clarify whether the identified trends remain consistent or whether separate boundaries are required for different classes of irregularity.

5

Conclusion

This thesis investigated torsional tendencies in mid-rise timber buildings through a parametric study of rectangular and L-shaped floor plans. The results show that the likelihood of torsion governing the fundamental mode is controlled by the combined effect of (i) the CM-CR eccentricity, expressed as the normalized eccentricity e/D, and (ii) the effective torsional resistance of the stabilizing system, expressed as the normalized torsional stiffness R. While neither parameter alone provides a universal predictor, the combined e/D-R plots and associated zone definitions provide a consistent framework for interpreting when torsion is expected, when translation is robust, and where mixed behaviour (mode switching sensitivity) occurs.

5.1 Key Findings for Rectangular Plans

For rectangular plans, torsion is not inherent to the geometry and is primarily introduced through stabilizer asymmetry and unfavourable stiffness distribution. The combined dataset indicates that torsion becomes increasingly likely as e/D increases, particularly when stiffness imbalance occurs in the weak direction. Configurations with $e/D \gtrsim 0.16$ clustered in the torsion-dominated region, whereas sufficiently high torsional stiffness was associated with translational behaviour, with translation-dominated cases typically occurring for $R \gtrsim 13.5$ m. The main transition region (Zone 1B) can be interpreted as a balance problem, where torsion becomes likely when R is not sufficiently large relative to e/D. For the present rectangular dataset, a representative boundary in this transition region was approximated by

$$R \approx 84\,(e/D),$$

and configurations approaching this range should be treated as torsion-sensitive.

5.2 Key Findings for L-shaped Plans

For L-shaped plans, torsional sensitivity is driven more strongly by geometry because the plan form makes CM-CR alignment more challenging in practice, even though zero eccentricity can be achieved with carefully placed stabilizers. Across the studied cases, the same qualitative trend was seen where torsion occurred when eccentricity was high relative to torsional stiffness, and translation was promoted when stabilizers were placed toward the extremities to increase lever arms and R. In the compiled e/D-R plot, the mixed-response band (Zone 2B) was bounded

by two representative torsional-stiffness levels, approximately $R_{\text{crit},1} = 10.0$ m and $R_{\text{crit},2} = 28.11$ m, together with critical eccentricity limits around $e/D \approx 0.078$ and $e/D \approx 0.152$. Interpreted as ratios, the transition band corresponded roughly to $R/(e/D) \approx$ 128-184 at the zone boundaries, reinforcing that L-shaped plans require comparatively higher torsional stiffness to remain translation-dominated at moderate eccentricities.

5.3 Comparison Between Rectangular and L-shaped Behaviour

A central difference between the geometries is that rectangular plans can readily achieve low eccentricity through symmetric stabilizer layout, whereas L-shaped plans more often become torsion-sensitive unless stabilizers are deliberately arranged to both (i) control the CM-CR offset and (ii) maintain large lever arms to sustain high R. In rectangles, torsion is primarily triggered by stabilizer asymmetry and by stiffness imbalance in the weak direction, while in L-shapes, torsion is primarily governed by geometric irregularity (re-entrant corner effects and aspect-ratio changes) amplified by stabilizer placements that concentrate resistance near the interior. Consequently, the L-shaped configurations occupy a larger portion of the mixed-response and torsion-prone regions in the e/D-R space, and they require more deliberate stabilizer placement to reach translation-dominated behaviour.

5.4 Connection to wind sensitivity and practical implication

Wind loading is a primary excitation source for many mid- to high-rise timber buildings and is particularly relevant for torsional serviceability because fluctuating pressures and aerodynamic effects introduce time-varying torsional moments that couple sway and rotation. The modal tendencies identified in this thesis are therefore directly relevant as an early-stage indicator of wind-driven torsional sensitivity. Configurations that reduce e/D and increase R are expected to be less prone to wind-driven torsional response, while configurations close to the mixed-response boundaries should be treated as wind-sensitive and verified with additional dynamic assessment. For rectangular plans, torsional wind sensitivity is minimized by limiting e/D (avoiding stabilizer asymmetry that shifts CR) and by maintaining large lever arms (high R). For L-shaped plans, robustness relies more strongly on achieving sufficiently high torsional stiffness through stabilizer placement toward the extremities and avoiding pronounced stiffness imbalance, since geometric irregularity makes torsion harder to eliminate through symmetry alone.

5.5 Overall Takeaway

The primary contribution of this work is a unified interpretation of torsional tendency in terms of the combined (e/D, R) space. Although no universal threshold applies across all layouts, the zoning concept provides a practical screening tool for early design, where points deep in translation-dominated regions are typically robust, whereas points near the transition boundaries are sensitive to small layout changes and should be treated as torsion-prone under wind excitation.

Bibliography

[1] P. Mendis, T. Ngo, N. Haritos, A. Hira, B. Samali, and J. Cheung, "Wind loading on tall buildings," *Electronic Journal of Structural Engineering*, vol. Volume 7, pp. 41–54, 01 2007.

[2] R. R. S. Harish A. Kadam, "Parametric study of factors influencing mode shape of oscillation," *International Journal of Engineering Research and Applications*, vol. 12, no. 7, Series-I, pp. 153–165, 2022. Accessed: 2025-10-03.

[3] K. Tse, K. Kwok, and Y. Tamura, "Performance and cost evaluation of a smart tuned mass damper for suppressing wind-induced lateral-torsional motion of tall structures," *Journal of Structural Engineering*, vol. 138, pp. 514–525, 03 2012.

[4] RISE Research Institutes of Sweden, "Timber construction," 2025. Accessed: 2025-09-24.

[5] A. Kareem, "Wind induced torsional loads on structures," *Engineering structures*, vol. 3, pp. 85–86, 2016.

[6] M. Elsharawy, K. Galal, and T. Stathopoulos, "Design wind loads including torsion for rectangular buildings with horizontal aspect ratio of 1.6," *Journal of Structural Engineering*, vol. 140, no. 4, p. 06013006, 2014.

[7] T. Nguyen, T. Stathopoulos, and L. Tirca, "Wind-induced shear and torsion in low-rise and medium-rise buildings: Provisions of national building code of canada 2015," *Canadian Journal of Civil Engineering*, vol. 45, 01 2018.

[8] Structures Centre, "Structural torsion in asymmetric building design," 2023. Accessed: 2025-10-03.

[9] M. Nilsson and M. Kryh, "Wind-induced vibrations of a multi-storey residential building in cross-laminated timber in the serviceability limit state," master's thesis, Chalmers University of Technology, Göteborg, Sweden, 2012. Accessed: 2025-10-03.

[10] A. Aloisio, D. P. Pasca, Y. De Santis, T. Hillberger, P. F. Giordano, M. M. Rosso, R. Tomasi, M. P. Limongelli, and C. Bedon, "Vibration issues in timber structures: A state-of-the-art review," *Journal of Building Engineering*, vol. 76, p. 107098, 06 2023.

[11] *Eurocode 5: Design of timber structures – Part 1-1: General – Common rules and rules for buildings.* EN 1995-1-1:2004, Brussels: European Committee for Standardization (CEN), 2004. Accessed: 2025-10-03.

[12] *Eurocode 1: Actions on structures – Part 1-4: General actions – Wind actions.* EN 1991-1-4:2005, Brussels: European Committee for Standardization (CEN), 2005. Accessed: 2025-10-03.

[13] M. Elsharawy, T. Stathopoulos, and K. Galal, "Wind-induced torsional loads on low buildings," *Journal of Wind Engineering and Industrial Aerodynamics*, vol. s 104–106, p. 40–48, 07 2011.

[14] A. Kareem, "Lateral-torsional motion of tall buildings to wind loads," *Journal of Structural Engineering*, vol. 111, no. 11, pp. 2479–2496, 1985.

[15] R. Gonzalez Herrera and M. Gómez-Soberón, "Influence of plan irregularity of buildings," 10 2008.

[16] T. Awida, "Impact of building plan geometry on the wind response of concrete tall buildings," pp. 781–786, 01 2011.

[17] S. Rana, S. Das, V. Kumar, and R. Ahirwar, "Comparison study of responses generated in rectangular and octagonal shaped high rise buildings under wind loads," *International Journal of Research in Engineering and Technology*, pp. 2395–0056, 05 2022.

[18] Z. Zhang, M. Elsharawy, and T. Stathopoulos, "Aerodynamic torsional loads on l-shaped low-rise buildings.," 01 2014.

[19] nbspBhumika Pashine, nbspV. D. Vaidya, and nbspDr. D. P. Singh, "Wind analysis of multistoried structure with t shape and l shape geometry," *International Journal of Engineering Development and Research*, vol. 4, pp. 70–77, 2016.

[20] R. Ahlawat and A. K. Ahuja, "Wind loads on 't' plan shape tall buildings," *Journal of Academia and Industrial Research*, vol. 4, no. 1, pp. 27–30, 2015.

[21] Y. Li, Q. Li, and F.B.Chen, "Wind tunnel study of wind-induced torques on l-shaped tall buildings," *Journal of Wind Engineering Industrial Aerodynamics*, vol. 167C, pp. 41–50, 05 2017.

[22] G. Bitsuamlak and R. Merrick, "Shape effects on the wind-induced response of high-rise buildings," *Journal of Wind Engineering*, vol. 6, pp. 1–18, 01 2009.

[23] Y. T. Yong Chul Kim, Jun Kanda, "Wind-induced coupled motion of tall buildings with varying square plan with height," *Journal of Wind Engineering and Industrial Aerodynamics*, vol. 99, no. 5, pp. 638–650, 2011.

[24]

[25] H. Ilgin, "High-rise residential timber buildings: Emerging architectural and structural design trends," *Buildings*, vol. 14, p. 25, 12 2023.

[26] J. Vilotijević and M. Premrov, "Assessment of in-plane timber floor stiffness as structural diaphragms: A numerical approach to lateral load response," *Forests*, vol. 16, p. 56, 12 2024.

[27] G. D'Arenzo, D. Casagrande, and W. Seim, "Rigid or flexible? a numerical investigation on the in-plane behaviour of clt floor diaphragms," 08 2021.

[28] V. Žegarac Leskovar and M. Premrov, "A review of architectural and structural design typologies of multi-storey timber buildings in europe," *Forests*, vol. 12, no. 6, p. 757, 2021.

[29] G. Angelucci, F. Mollaioli, M. Molle, and S. Paris, "Performance assessment of timber high-rise buildings: Structural and technological considerations," *The Open Construction Building Technology Journal*, vol. 16, 09 2022.

[30] R. Tabatabaei, *Torsional Vibration of Eccentric Building Systems*. 09 2011.

[31] M. Botis and C. Camelia, "A method for reducing of the overall torsion for reinforced concrete multi-storey irregular structures," *Applied Sciences*, vol. 10, p. 5555, 08 2020.

[32] A. Singh, D.-P. N. Kontoni, and S. Mandal, "Wind-induced torsional loads and responses of tall buildings," *Research on Engineering Structures Materials*, vol. 10, no. 3, pp. 1281–1300, 2024.

[33] A. Kumar, R. Meena, R. Ahirwar, M. I. Khan, and J. Khatib, "Wind effects on re-entrant wing faces of plus plan shape building," 11 2023.

[34] M. Burton, K. Kwok, P. Hitchcock, and R. Denoon, "Frequency dependence of human response to wind-induced building motion," *Journal of Structural Engineering-asce - J STRUCT ENG-ASCE*, vol. 132, 02 2006.

[35] J. Golding, A. Mueller, and M. Gresty, "A motion sickness maximum around the 0.2 hz frequency range of horizontal translational oscillation," *Aviation, space, and environmental medicine*, vol. 72, pp. 188–92, 04 2001.

[36] H. Howarth, "Human exposure to wind-induced motion in tall buildings: and assessment of guidance in iso 6897 and iso 10137," 09 2015.

[37] B. Li, J. Cunyan, W. Lu, W.-H. Cai, and L. Jing, "A parametric study of the effect of building layout on wind flow over an urban area," *Building and Environment*, vol. 160, p. 106160, 05 2019.

[38] L. Kabošová, H. Achten, M. Kopřiva, and S. Kmet, "Parametric wind design," *Frontiers of Architectural Research*, vol. 7, 08 2018.

[39] R. Vaicaitis, M. Shinozuka, and M. Takeno, "Parametric study of wind loading on structures," *Journal of the Structural Division*, vol. 99, no. 3, pp. 453–468, 1973.

[40] S. N. Heo, Seokjae and W. Choi, "Serviceability evaluation of high-rise buildings exposed to typhoon proximity effects using iso10137 and iso6897," *Buildings*, vol. 13, no. 8, p. 2119, 2023.

[41] StruSoft, *FEM-Design Wiki: Analysis*, 2024. Accessed: 2025-09-25.

[42] StruSoft, *FEM-Design Applied Theory and Design*, 2022. Accessed: 2025-09-25.

[43] V. Karlberg, "Dynamic analysis of high-rise timber buildings," Master's thesis, Luleå University of Technology, 2017.

[44] E. Andersson, "Global analysis of a tall timber–concrete hybrid structure," Master's thesis, KTH Royal Institute of Technology, 2022.

[45] StruSoft, *FEM-Design Material Models: Timber*, 2024. Information on timber stiffness (E_0,mean) in eigenfrequency analysis. Accessed: 2025-09-25.

[46] B. Kurent, W. K. Ao, A. Pavic, F. Pérez Pérez, and B. Brank, "Modal testing and finite element model updating of full-scale hybrid timber-concrete building," *Engineering Structures*, vol. 289, p. 116250, 08 2023.

[47] I. Bouckaert, A. Piedboeuf, M. Godio, and J. Pacheco de Almeida, "Modal analysis and superposition for dynamic response of structures with discontinuities using hybridfem," *Finite Elements in Analysis and Design*, vol. 249, p. 104360, 2025.

[48] M. Nieto, M. Elsayed, and D. Walch, "Modal participation factors and their potential applications in aerospace: A review," 05 2018.

[49] P. Landel, *Wind-induced vibrations in tall timber buildings - Design standards, experimental and numerical modal analyses*. PhD thesis, Linnéuniversitetet, 06 2022.

[50] B. Kurent, B. Brank, and W. K. Ao, "Model updating of seven-storey cross-laminated timber building designed on frequency-response-functions-based modal testing," *Structure and Infrastructure Engineering*, vol. 19, pp. 1–19, 06 2021.

[51] M. Elsharawy, *Wind-Induced Torsional Loads on Low- and Medium-Rise Buildings*. PhD thesis, 06 2014.

[52] H. Alinejad, T. H.-K. Kang, S. Y. Jeong, and B. Ahn, "Engineering review of wind-induced torsional moment and response of buildings," *Journal of Structural Engineering*, vol. 149, no. 11, p. 03123001, 2023.

A

Appendix A

This appendix presents the preliminary stability and capacity checks performed using *Calculatis by Stora Enso*. The purpose of these calculations was to support the initial selection of member dimensions (slabs, shear walls, columns, and beams) used in the parametric FEM-Design models. The screenshots below document the governing inputs and utilisation results adopted in the study.

Preliminary member sizes were selected based on Calculatis checks for relevant limit states (e.g., bending, shear, deflection, and stability/buckling where applicable). The chosen dimensions were then used as fixed baseline properties in the numerical model to isolate the effect of stabilizer layout on torsional behaviour.

A.1 Slabs

Figures A.1–A.2 show the Calculatis output used to select the slab configuration and thickness.

System

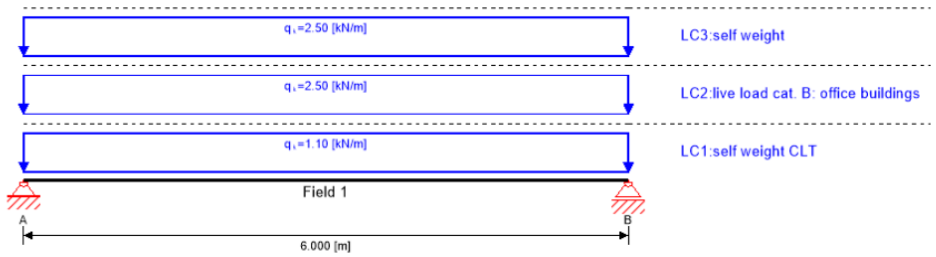

Section: CLT 220 L7s - 2; **Material**: C24 pine ETA (2022); **Service class**: service class 1; **Fire resistance class**: R 90

Utilization 111%

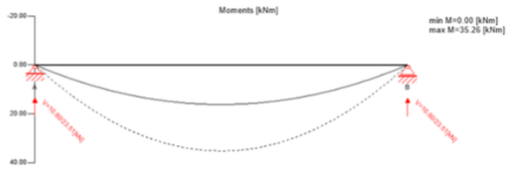

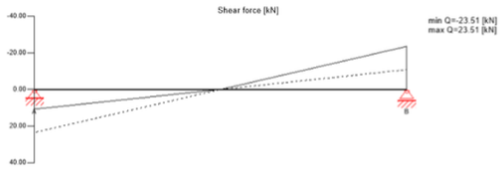

Flexural stress analysis						**28%**
$M_{y,d}$ =	35.26	kNm		$f_{m,k}$ =	24.00	N/mm²
$M_{z,d}$ =	0.00	kNm		$f_{m,k,z}$ =	24.00	N/mm²
$N_{t,d}$ =	0.00	kN		$f_{t,0,k}$ =	0.00	N/mm²
$\sigma_{t,d}$ =	0.00	N/mm²		$f_{t,0,d}$ =	8.96	N/mm²
$\sigma_{m,y,d}$ =	-4.79	N/mm²		$f_{m,y,d}$ =	16.90	N/mm²
$\sigma_{m,z,d}$ =	0.00	N/mm²	<	$f_{m,z,d}$ =	0.00	N/mm² ✓
Shear stress analysis						**6%**
V_d =	-23.51	kN		$f_{v,k}$ =	4.00	N/mm²
$\tau_{v,d}$ =	0.15	N/mm²	<	$f_{v,d}$ =	2.56	N/mm² ✓
Rolling shear analysis						**14%**
V_d =	-23.51	kN		$f_{r,k}$ =	1.60	N/mm²
$\tau_{r,d}$ =	0.14	N/mm²	<	$f_{r,d}$ =	1.02	N/mm² ✓

w_{inst} = w[char] ✓

Field	K_{def}	Limit	w_{limit}	$w_{calc.}$	Ratio
		[-]	[mm]	[mm]	
1	0.8	L/300	20.0	12.1	61%

w_{fin} = w[char] + w[q.p.]*kdef ✓

Field	K_{def}	Limit	w_{limit}	$w_{calc.}$	Ratio
		[-]	[mm]	[mm]	
1	0.8	L/250	24.0	19.1	79%

$w_{net,fin}$ = w[q.p.] + w[q.p.]*kdef ✓

Field	K_{def}	Limit	w_{limit}	$w_{calc.}$	Ratio
		[-]	[mm]	[mm]	
1	0.8	L/300	20.0	15.6	78%

Figure A.1: Calculatis output for slab sizing check (case 1).

Flexural stress analysis Fire						25%
$M_{y,d}$ =	19.58	kNm		$f_{m,k}$ =	24.00	N/mm²
$M_{z,d}$ =	0.00	kNm		$f_{m,k,z}$ =	24.00	N/mm²
$N_{t,d}$ =	0.00	kN		$f_{t,0,k}$ =	0.00	N/mm²
$\sigma_{t,d}$ =	0.00	N/mm²		$f_{t,0,d}$ =	16.10	N/mm²
$\sigma_{m,y,d}$ =	7.52	N/mm²		$f_{m,y,d}$ =	30.36	N/mm²
$\sigma_{m,z,d}$ =	0.00	N/mm²	<	$f_{m,z,d}$ =	0.00	N/mm² ✓
Shear stress analysis Fire						3%
V_d =	-13.05	kN		$f_{v,k}$ =	4.00	N/mm²
$\tau_{v,d}$ =	0.14	N/mm²	<	$f_{v,d}$ =	4.60	N/mm² ✓
Rolling shear analysis Fire						8%
V_d =	-13.05	kN		$f_{r,k}$ =	1.60	N/mm²
$\tau_{r,d}$ =	0.14	N/mm²	<	$f_{r,d}$ =	1.84	N/mm² ✓

Vibration analysis					111%
Criterion	Calc.	Cl. I	Cl. II	Cl. I	Cl. II
Frequency min	7.198	4.5	4.5	✓	✓
Frequency	7.198	8.0	6.0	×	✓
Acceleration	0.056	0.05	0.1	×	✓
Stiffness	0.14	0.25	0.5	✓	✓

Support reaction			
Load case category	k_{mod}	A_V	B_V
		[kN]	
self weight CLT	0.6	3.30	3.30
		3.30	3.30
live load cat. B: office buildings	0.8	7.50	7.50
		0.00	0.00
self weight	0.6	7.50	7.50
		7.50	7.50

Figure A.2: Calculatis output for slab sizing check (case 2).

A.2 Shear Walls

Figures A.3–A.4 present the Calculatis checks used to define the shear wall thickness and strength/stability assumptions adopted in the parametric study.

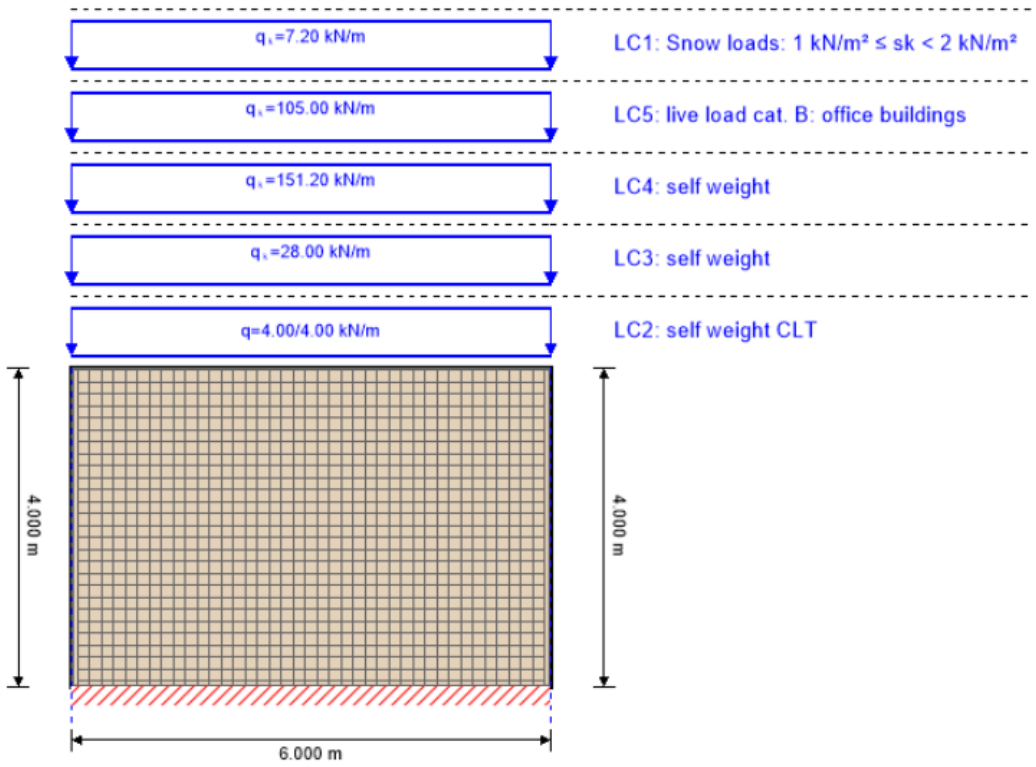

Global utilization ratio					
ULS	36 %	ULS Fire	32 %	SLS	0 %

Figure A.3: Calculatis output for shear wall sizing check (case 1).

Section: CLT 200 L5s

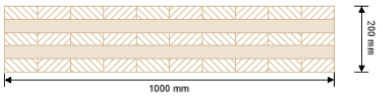

Layer	Thickness [mm]	Orientation	Material
1	40.0 mm	0°	C24 pine ETA (2022)
2	40.0 mm	90°	C24 pine ETA (2022)
3	40.0 mm	0°	C24 pine ETA (2022)
4	40.0 mm	90°	C24 pine ETA (2022)
5	40.0 mm	0°	C24 pine ETA (2022)
t_{CLT}	**200.0 mm**		

Section Fire: CLT 200 L5s

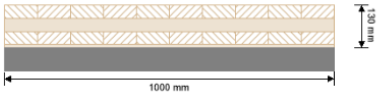

Layer	Thickness [mm]	Orientation	Material
1	40.0 mm	0°	C24 pine ETA (2022)
2	40.0 mm	90°	C24 pine ETA (2022)
3	40.0 mm	0°	C24 pine ETA (2022)
4	10.0 mm	90°	C24 pine ETA (2022)
t_{CLT}	**130.0 mm**		
Time	**90 min**		

Fire resistance class: R 90

Fire protection layering:
no additional fire protection

k_0 [-]	d_0 [mm]	$d_{char,0,h}$ [mm]	$d_{ef,h}$ [mm]	$d_{char,0,v}$ [mm]	$d_{ef,v}$ [mm]
1	7	63.0	70.0	0.0	0.0

Material values

Material	$f_{m,k}$ [N/mm²]	$f_{t,0,k}$ [N/mm²]	$f_{t,90,k}$ [N/mm²]	$f_{c,0,k}$ [N/mm²]	$f_{c,90,k}$ [N/mm²]	$f_{v,k}$ [N/mm²]	$f_{r,k\ min}$ [N/mm²]	$E_{0,mean}$ [N/mm²]	G_{mean} [N/mm²]	$G_{r,mean}$ [N/mm²]
C24 pine ETA (2022)	24.00	14.00	0.12	21.00	2.50	4.00	1.70	12,000.00	690.00	50.00

Figure A.4: Calculatis output for shear wall sizing check (case 2).

A.3 Columns

Figures A.5–A.7 show the Calculatis checks used to select the glulam column cross-section, including stability (buckling) verification for the assumed boundary conditions and member length.

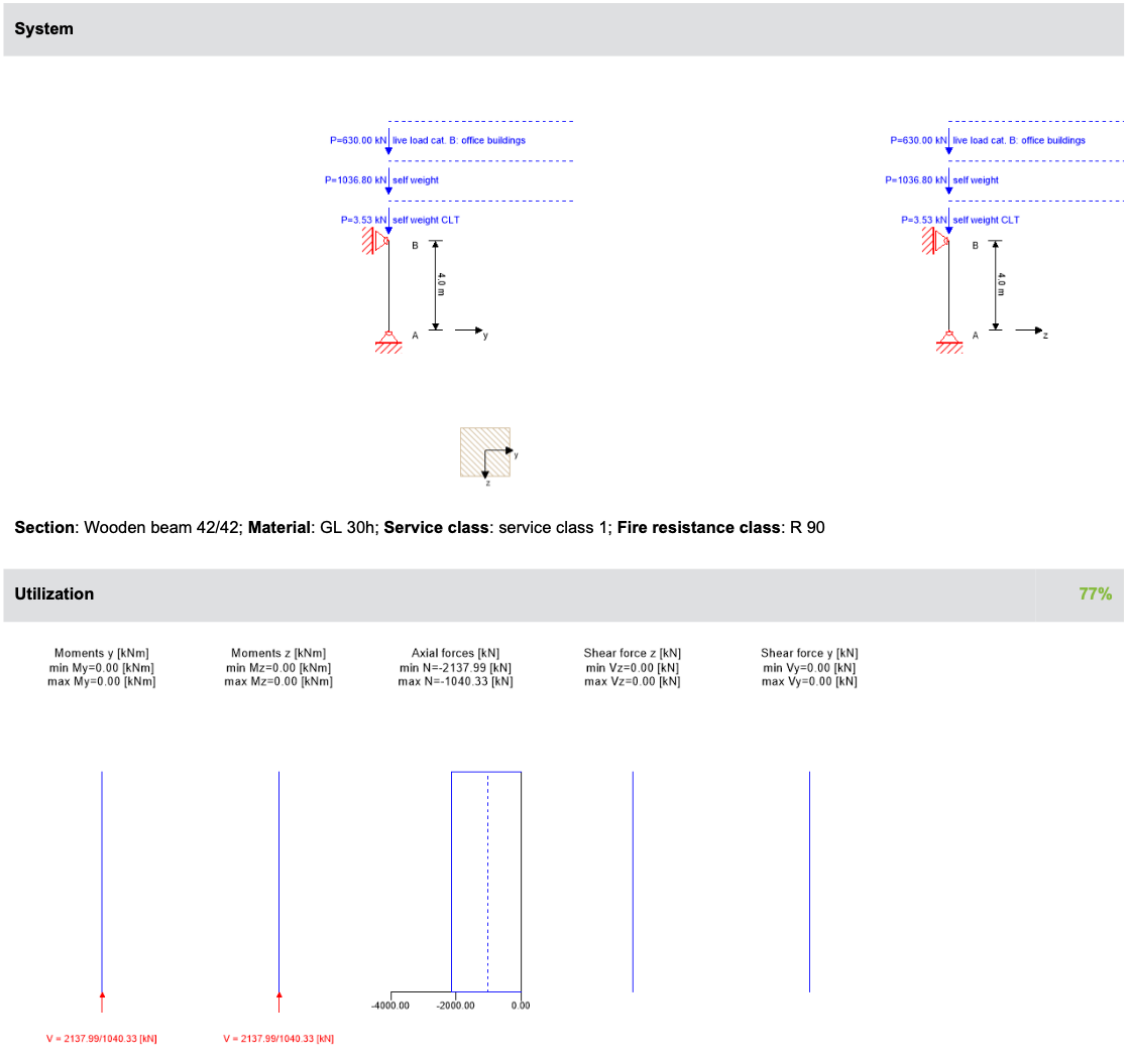

Figure A.5: Calculatis output for column sizing check (case 1).

Flexural stress analysis					63%
$M_{y,d}$ =	0.00	kNm	$f_{m,k}$ =	30.00	N/mm²
$M_{z,d}$ =	0.00	kNm	$f_{m,k,z}$ =	30.00	N/mm²
$N_{c,d}$ =	-2137.99	kN	$f_{c,0,k}$ =	30.00	N/mm²
$\sigma_{c,d}$ =	12.12	N/mm²	$f_{c,0,d}$ =	19.20	N/mm²
$\sigma_{m,y,d}$ =	0.00	N/mm²	$f_{m,y,d}$ =	19.90	N/mm²
$\sigma_{m,z,d}$ =	0.00	N/mm² <	$f_{m,z,d}$ =	19.90	N/mm² ✓
Shear stress analysis Y					**0%**
V_d =	0.00	kN	$f_{v,k}$ =	2.50	N/mm²
$\tau_{v,d}$ =	0.00	N/mm² <	$f_{v,d}$ =	1.60	N/mm² ✓
Shear stress analysis Z					**0%**
V_d =	0.00	kN	$f_{v,k}$ =	2.50	N/mm²
$\tau_{v,d}$ =	0.00	N/mm² <	$f_{v,d}$ =	1.60	N/mm² ✓
Shear stress analysis Combined					**0%**
$V_{y,d}$ =	0.00	kN	$V_{z,d}$ =	0.00	kN
$\tau_{v,y,d}$ =	0.00	N/mm²	$\tau_{v,z,d}$ =	0.00	N/mm²
			Ratio =	0%	✓

Lateral torsional buckling analysis					0%
$M_{y,d}$ =	0.00	kNm	$f_{m,k}$ =	0.00	N/mm²
$M_{z,d}$ =	0.00	kNm			
$N_{c,d}$ =	0.00	kN	$f_{c,0,k}$ =	0.00	N/mm²
$\sigma_{c,d}$ =	0.00	N/mm²	$f_{c,0,d}$ =	0.00	N/mm²
$\sigma_{m,y,d}$ =	0.00	N/mm²	$f_{m,y,d}$ =	0.00	N/mm²
$\sigma_{m,z,d}$ =	0.00	N/mm² <	$f_{m,z,d}$ =	0.00	N/mm² ✓
Buckling analysis					**71%**
$M_{y,d}$ =	0.00	kNm	$f_{m,k}$ =	30.00	N/mm²
$M_{z,d}$ =	0.00	kNm			
$N_{c,d}$ =	-2137.99	kN	$f_{c,0,k}$ =	30.00	N/mm²
$\sigma_{c,d}$ =	12.12	N/mm²	$f_{c,0,d}$ =	19.20	N/mm²
$\sigma_{m,y,d}$ =	0.00	N/mm²	$f_{m,y,d}$ =	19.90	N/mm²
$\sigma_{m,z,d}$ =	0.00	N/mm² <	$f_{m,z,d}$ =	19.90	N/mm² ✓

Figure A.6: Calculatis output for column sizing check (case 2).

Flexural stress analysis Fire						45%
$M_{y,d}$ =	0.00	kNm	$f_{m,k}$ =	30.00	N/mm²	
$M_{z,d}$ =	0.00	kNm	$f_{m,k,z}$ =	30.00	N/mm²	
$N_{c,d}$ =	-1229.33	kN	$f_{c,0,k}$ =	30.00	N/mm²	
$\sigma_{c,d}$ =	15.68	N/mm²	$f_{c,0,d}$ =	34.50	N/mm²	
$\sigma_{m,y,d}$ =	0.00	N/mm²	$f_{m,y,d}$ =	37.23	N/mm²	
$\sigma_{m,z,d}$ =	0.00	N/mm² <	$f_{m,z,d}$ =	37.23	N/mm²	✓
Shear stress analysis Y Fire						**0%**
V_d =	0.00	kN	$f_{v,k}$ =	2.50	N/mm²	
$\tau_{v,d}$ =	0.00	N/mm² <	$f_{v,d}$ =	2.88	N/mm²	✓
Shear stress analysis Z Fire						**0%**
V_d =	0.00	kN	$f_{v,k}$ =	2.50	N/mm²	
$\tau_{v,d}$ =	0.00	N/mm² <	$f_{v,d}$ =	2.88	N/mm²	✓
Shear stress analysis Combined Fire						**0%**
$V_{y,d}$ =	0.00	kN	$V_{z,d}$ =	0.00	kN	
$\tau_{v,y,d}$ =	0.00	N/mm²	$\tau_{v,z,d}$ =	0.00	N/mm²	
			Ratio =	0%		✓

Lateral torsional buckling analysis Fire						0%
$M_{y,d}$ =	0.00	kNm	$f_{m,k}$ =	0.00	N/mm²	
$M_{z,d}$ =	0.00	kNm				
$N_{c,d}$ =	0.00	kN	$f_{c,0,k}$ =	0.00	N/mm²	
$\sigma_{c,d}$ =	0.00	N/mm²	$f_{c,0,d}$ =	0.00	N/mm²	
$\sigma_{m,y,d}$ =	0.00	N/mm²	$f_{m,y,d}$ =	0.00	N/mm²	
$\sigma_{m,z,d}$ =	0.00	N/mm² <	$f_{m,z,d}$ =	0.00	N/mm²	✓
Buckling analysis Fire						**77%**
$M_{y,d}$ =	0.00	kNm	$f_{m,k}$ =	30.00	N/mm²	
$M_{z,d}$ =	0.00	kNm				
$N_{c,d}$ =	-1229.33	kN	$f_{c,0,k}$ =	30.00	N/mm²	
$\sigma_{c,d}$ =	15.68	N/mm²	$f_{c,0,d}$ =	34.50	N/mm²	
$\sigma_{m,y,d}$ =	0.00	N/mm²	$f_{m,y,d}$ =	37.23	N/mm²	
$\sigma_{m,z,d}$ =	0.00	N/mm² <	$f_{m,z,d}$ =	37.23	N/mm²	✓

Support reaction						
Load case category	k_{mod}	A_y	A_z	B_x	B_y	B_z
		[kN]	[kN]	[kN]	[kN]	[kN]
self weight CLT	0.6	0.00	0.00	3.53	0.00	0.00
	0.00	0.00	3.53	0.00	0.00	
self weight	0.6	0.00	0.00	1036.80	0.00	0.00
	0.00	0.00	1036.80	0.00	0.00	
live load cat. B: office buildings	0.8	0.00	0.00	0.00	0.00	0.00
	0.00	0.00	630.00	0.00	0.00	

Figure A.7: Calculatis output for column sizing check (case 3).

A.4 Beams

Figures A.8–A.10 present the Calculatis checks used to select the beam cross-sections, including bending, shear, and serviceability criteria used for preliminary sizing.

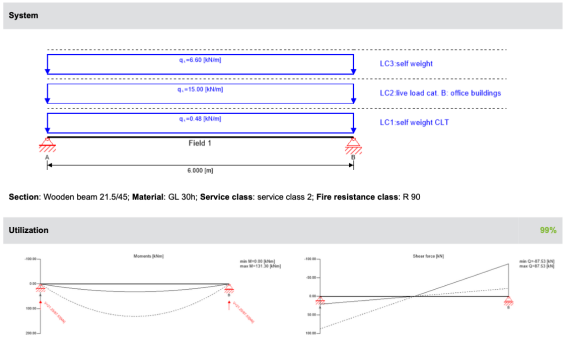

Figure A.8: Calculatis output for beam sizing check (case 1).

Flexural stress analysis						92%
$M_{y,d}$ =	131.30	kNm	$f_{m,k}$ =	30.00	N/mm²	
$M_{z,d}$ =	0.00	kNm	$f_{m,k,z}$ =	30.00	N/mm²	
$N_{t,d}$ =	0.00	kN	$f_{t,0,k}$ =	24.00	N/mm²	
$\sigma_{t,d}$ =	0.00	N/mm²	$f_{t,0,d}$ =	15.36	N/mm²	
$\sigma_{m,y,d}$ =	18.09	N/mm²	$f_{m,y,d}$ =	19.76	N/mm²	
$\sigma_{m,z,d}$ =	0.00	N/mm² <	$f_{m,z,d}$ =	21.12	N/mm²	✓
Shear stress analysis						**72%**
V_d =	74.40	kN	$f_{v,k}$ =	2.50	N/mm²	
$\tau_{v,d}$ =	1.15	N/mm² <	$f_{v,d}$ =	1.60	N/mm²	✓
Lateral torsional buckling analysis						**92%**
$M_{y,d}$ =	131.30	kNm	$f_{m,k}$ =	30.00	N/mm²	
$M_{z,d}$ =	0.00	kNm				
$N_{c,d}$ =	0.00	kN	$f_{c,0,k}$ =	30.00	N/mm²	
$\sigma_{c,d}$ =	0.00	N/mm²	$f_{c,0,d}$ =	19.20	N/mm²	
$\sigma_{m,y,d}$ =	18.09	N/mm²	$f_{m,y,d}$ =	19.76	N/mm²	
$\sigma_{m,z,d}$ =	0.00	N/mm² <	$f_{m,z,d}$ =	21.12	N/mm²	✓
Buckling analysis						**92%**
$M_{y,d}$ =	131.30	kNm	$f_{m,k}$ =	30.00	N/mm²	
$M_{z,d}$ =	0.00	kNm				
$N_{c,d}$ =	0.00	kN	$f_{c,0,k}$ =	30.00	N/mm²	
$\sigma_{c,d}$ =	0.00	N/mm²	$f_{c,0,d}$ =	19.20	N/mm²	
$\sigma_{m,y,d}$ =	18.09	N/mm²	$f_{m,y,d}$ =	19.76	N/mm²	
$\sigma_{m,z,d}$ =	0.00	N/mm² <	$f_{m,z,d}$ =	21.12	N/mm²	✓

w_{inst} = w[char]					✓
Field	**K_{def}**	**Limit**	**w_{limit}**	**$w_{calc.}$**	**Ratio**
		[-]	[mm]	[mm]	
1	0.8	L/300	20.0	16.8	84%
w_{fin} = w[char] + w[q.p.]*kdef					✓
Field	**K_{def}**	**Limit**	**w_{limit}**	**$w_{calc.}$**	**Ratio**
		[-]	[mm]	[mm]	
1	0.8	L/250	24.0	23.8	99%
$w_{net,fin}$ = w[q.p.] + w[q.p.]*kdef					✓
Field	**K_{def}**	**Limit**	**w_{limit}**	**$w_{calc.}$**	**Ratio**
		[-]	[mm]	[mm]	
1	0.8	L/300	20.0	15.8	79%

Figure A.9: Calculatis output for beam sizing check (case 2).

Flexural stress analysis Fire						80%
$M_{y,d}$ =	52.13	kNm	$f_{m,k}$ =	30.00	N/mm²	
$M_{z,d}$ =	0.00	kNm	$f_{m,k,z}$ =	30.00	N/mm²	
$N_{t,d}$ =	0.00	kN	$f_{t,0,k}$ =	24.00	N/mm²	
$\sigma_{t,d}$ =	0.00	N/mm²	$f_{t,0,d}$ =	27.60	N/mm²	
$\sigma_{m,y,d}$ =	28.88	N/mm²	$f_{m,y,d}$ =	36.11	N/mm²	
$\sigma_{m,z,d}$ =	0.00	N/mm² <	$f_{m,z,d}$ =	37.95	N/mm²	✓
Shear stress analysis Fire						**56%**
V_d =	30.35	kN	$f_{v,k}$ =	2.50	N/mm²	
$\tau_{v,d}$ =	1.60	N/mm² <	$f_{v,d}$ =	2.88	N/mm²	✓
Buckling analysis Fire						**80%**
$M_{y,d}$ =	52.13	kNm	$f_{m,k}$ =	30.00	N/mm²	
$M_{z,d}$ =	0.00	kNm				
$N_{c,d}$ =	0.00	kN	$f_{c,0,k}$ =	30.00	N/mm²	
$\sigma_{c,d}$ =	0.00	N/mm²	$f_{c,0,d}$ =	34.50	N/mm²	
$\sigma_{m,y,d}$ =	28.88	N/mm²	$f_{m,y,d}$ =	36.11	N/mm²	
$\sigma_{m,z,d}$ =	0.00	N/mm² <	$f_{m,z,d}$ =	37.95	N/mm²	✓
Lateral torsional buckling analysis Fire						**80%**
$M_{y,d}$ =	52.13	kNm	$f_{m,k}$ =	30.00	N/mm²	
$M_{z,d}$ =	0.00	kNm				
$N_{c,d}$ =	0.00	kN	$f_{c,0,k}$ =	30.00	N/mm²	
$\sigma_{c,d}$ =	0.00	N/mm²	$f_{c,0,d}$ =	34.50	N/mm²	
$\sigma_{m,y,d}$ =	28.88	N/mm²	$f_{m,y,d}$ =	36.11	N/mm²	
$\sigma_{m,z,d}$ =	0.00	N/mm² <	$f_{m,z,d}$ =	37.95	N/mm²	✓

Vibration analysis					59%
Criterion	Calc.	Cl. I	Cl. II	Cl. I	Cl. II
Frequency min	7.653	4.5	4.5	✓	✓
Frequency	7.653	8.0	6.0	-	✓
Acceleration	0.0	0.05	0.1	✓	✓
Stiffness	0.0	0.25	0.5	✓	✓

Figure A.10: Calculatis output for beam sizing check (case 3).

B

Appendix B

In this appendix, the Grasshopper–FEM-Design API workflow used in the study is documented. It describes how the parametric geometry and structural grid are converted into an analytical FEM-Design model, how materials, sections, elements, and loads are assigned through the API components, and how modal analysis results are extracted for post-processing.

B.1 Modelling using the FEM-Design API

After the base geometry and structural grid were defined, the FEM-Design API components were used to generate the analytical model. The API provides both modelling components for creating structural elements and database components for assigning materials and cross-sections.

B.1.1 Materials

Concrete and glulam materials (foundation, beams, and columns) were selected using the *Material.DataBase* component, which extracts available materials from the Swedish FEM-Design library (Figure B.1.1). While CLT materials for slabs and shear walls were defined using the *TimberPlate.Material* component, which requires additional input parameters (Figure B.2).

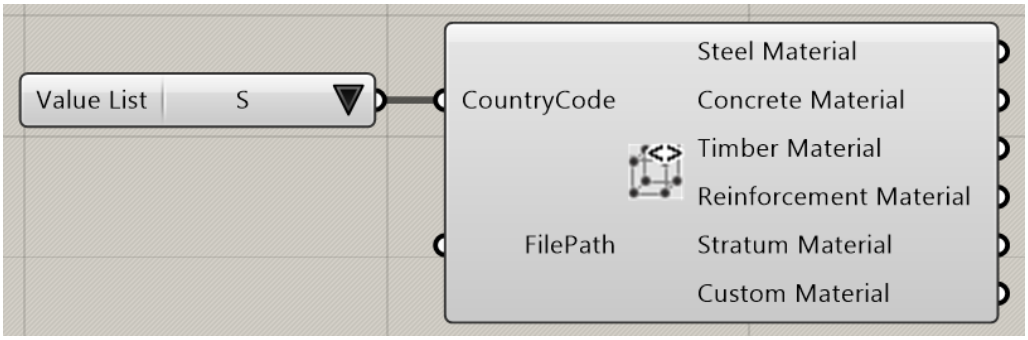

Figure B.1: Material.DataBase component connected to the Swedish material library in FEM-Design.

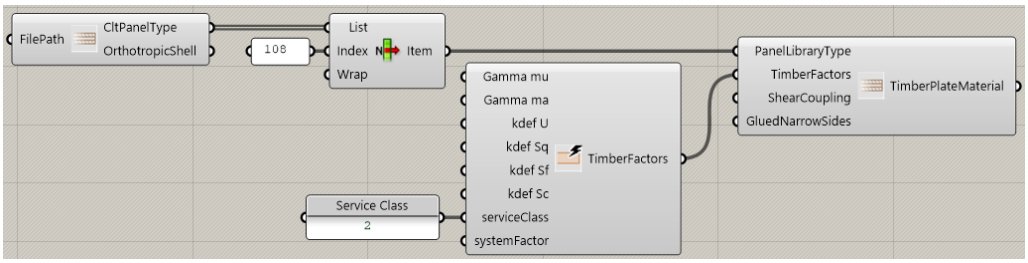

Figure B.2: The *TimberPlate.Material* component and its required input parameters.

B.1.2 Sections

Cross-sections for beams and columns were assigned using the *Section.Database* component (Figure B.3). This shows the selection of the beam cross-section.

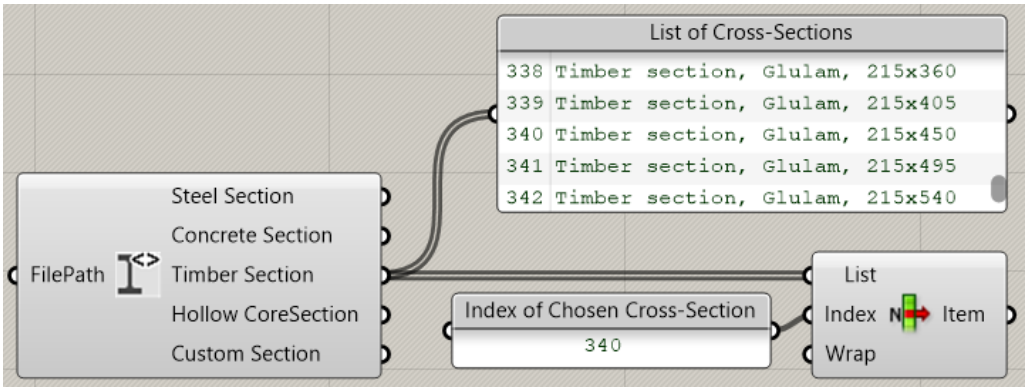

Figure B.3: The *Section.Database* component used to assign material-based cross-sections. Here it shows the chosen beam cross-section.

If a required section is not available, it can alternatively be defined using *Section.Define*. In this study, the columns section, 330×360 mm^2 was designed using the *Section.Define* component.

B.1.3 Structural Elements

After materials and sections were defined, the structural elements were created using FEM-Design API components:

- **Foundation**: The foundation of the building was modelled as a *Plate* component, using the plan outline, a thickness of 500 mm, the selected concrete material, and a rigid edge connection (Figure B.4).

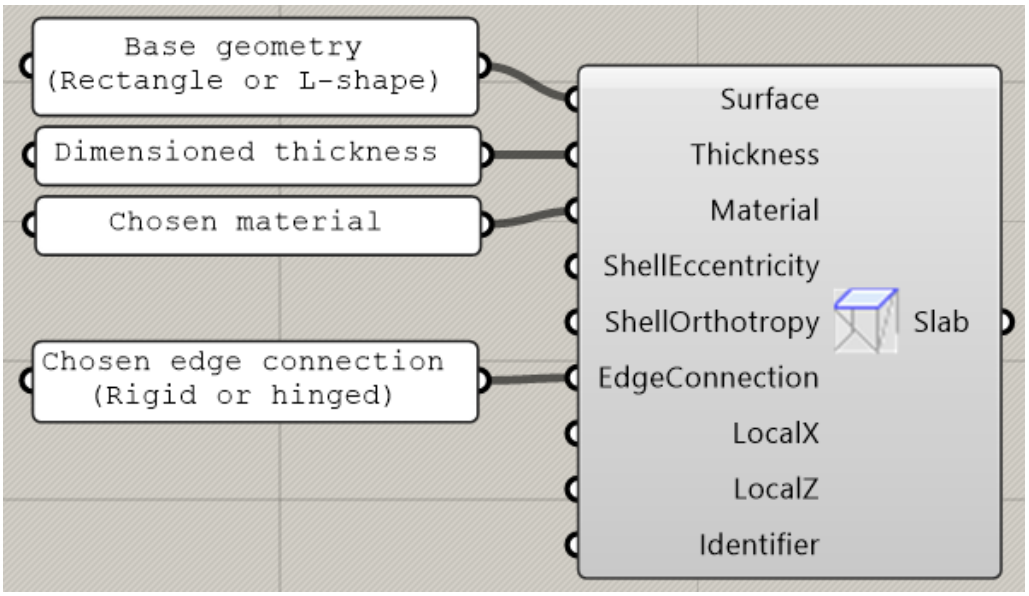

Figure B.4: Foundation modelled using the *Plate* component.

- **Slabs** and **Shear Walls**: The slabs and shear walls are modelled using *TimberPlate.Construct* with CLT material defined by *TimberPlate.Material*. For slabs, the plate span direction follows the short direction of each building part, while the shear walls, have a vertical span direction (global z-direction). The average mesh size is defined directly in the component (Figure B.5).

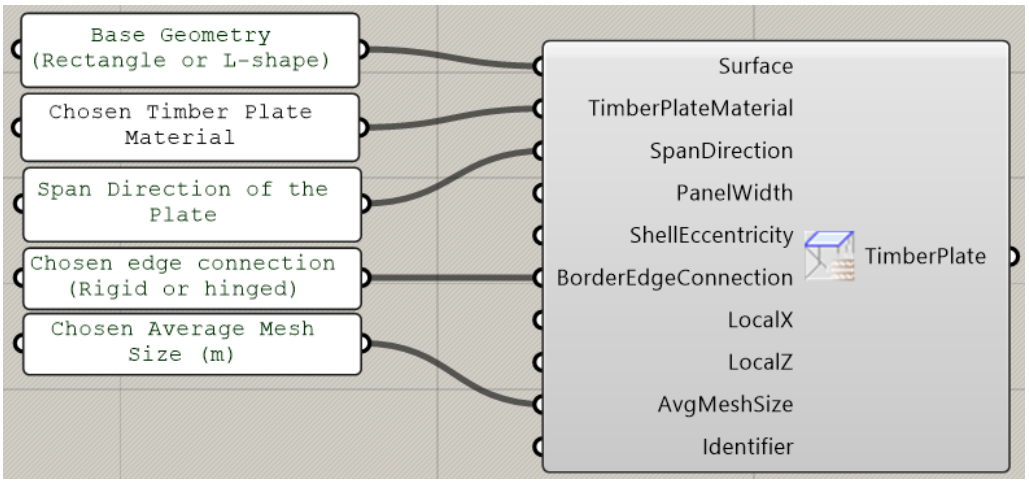

Figure B.5: CLT slabs and shear walls created using *TimberPlate.Construct*.

- **Columns**: Glulam columns were constructed using *Bars.Column*. Column center lines are defined by created lines between grid intersection points on successive floor levels, and the assigned section is taken from the section database (Figure B.3).

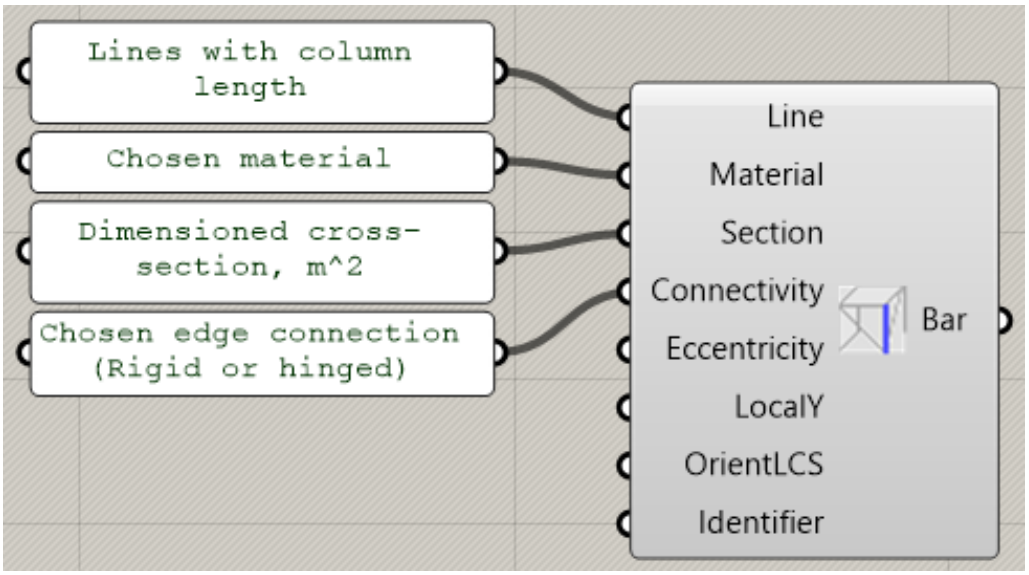

Figure B.6: Glulam columns created with the *Bars.Column* component.

- **Beams**:
  Glulam beams were generated using *Bars.Beam*. Beam centre lines are based on the 6 m grid lines and positioned at the corresponding floor level. Beams are oriented perpendicular to the slab span direction, arranged only along the long direction of the base geometry, as illustrated in Figure 3.2.

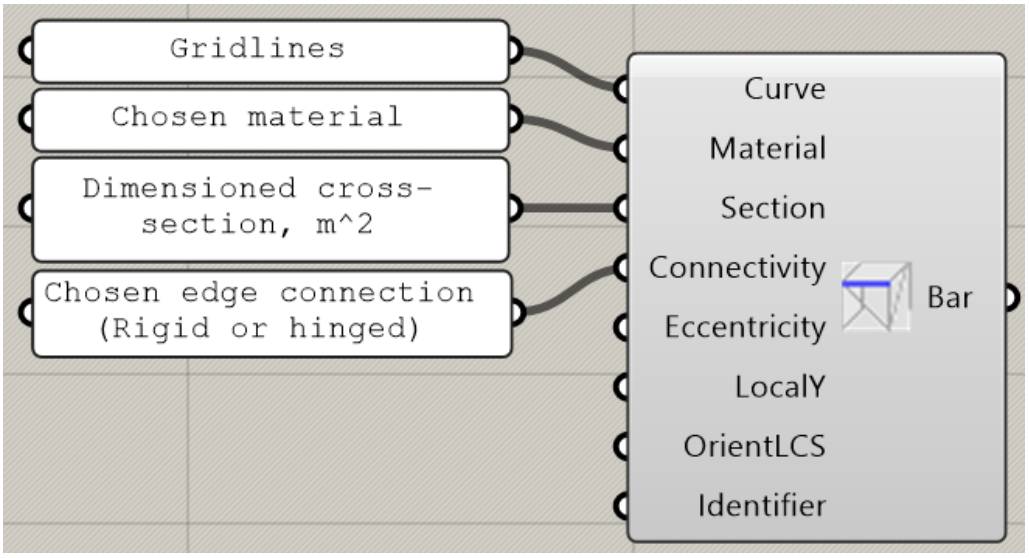

Figure B.7: Glulam beams are created using the *Bars.Beam* component.

To isolate the influence of the stabilizing layout on torsional behaviour, all shear walls were assigned the same thickness and material. This ensures that the stiffness

of each wall is comparable, allowing the study to focus on how the number and placement of stabilizing elements affect torsional response rather than variations in individual wall properties.

B.1.4 Loads

The loads applied in the FEM-Design model correspond to those listed in Table 3.1. In the FEM-Design API, self-weight is not added automatically. Therefore, the *MassDefine* component is used to compute the mass of each element, which is then applied as an equivalent gravity load to represent self-weight. The individual mass loads are summed to obtain the total self-weight of the structure (Figure B.8).

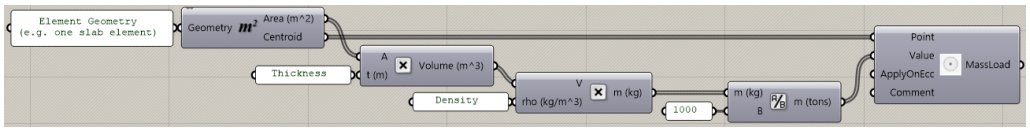

Figure B.8: Self-weight definition using the *MassDefine* component.

Additional loads, such as complementary permanent load, imposed load, and snow load, are applied as uniformly distributed surface loads using the *SurfaceLoad.Uniform* component. The loaded surface, load magnitude and direction, and the associated load case are specified as inputs (Figure B.9).

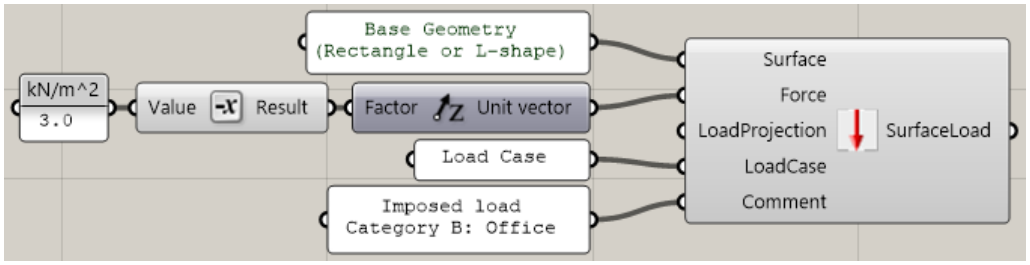

Figure B.9: Example of a uniformly distributed surface load defined using *SurfaceLoad.Uniform* (imposed load).

Finally, load cases are defined using *LoadCase.Construct*, and load combinations are assembled using *LoadCombination.Construct*, where load type, duration, and partial factors (γ) are specified. Figure B.10 illustrates the setup used for the permanent actions.

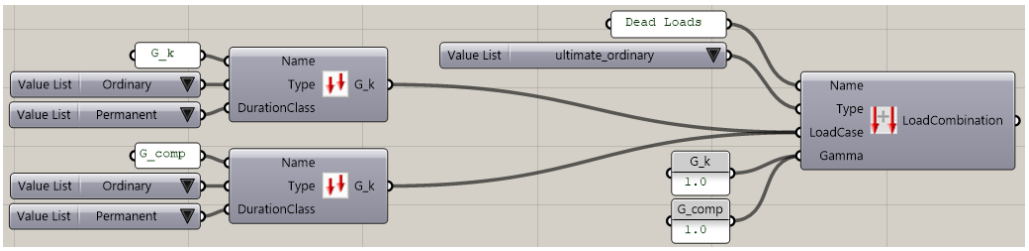

Figure B.10: Definition of load cases and load combinations for permanent actions in the model.

B.1.5 Connection to FEM-Design

After defining the structural elements and loads, the complete analytical model is assembled using the *Model.Construct* component, see Figure B.11.

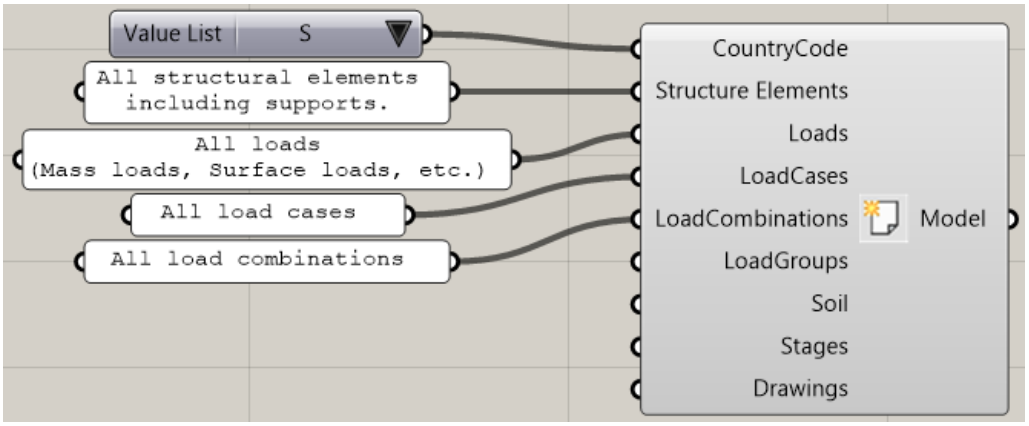

Figure B.11: Model assembly using *Model.Construct*.

The model is then linked to FEM-Design through the *FEM-Design.Connection*, opened using *FEM-Design.OpenModel*, and then analysed with *FEM-Design.RunAnalysis*, see Figure B.12. In this study, a modal analysis is performed by defining *Freq.Define* and connecting it to *Analysis.Define*.

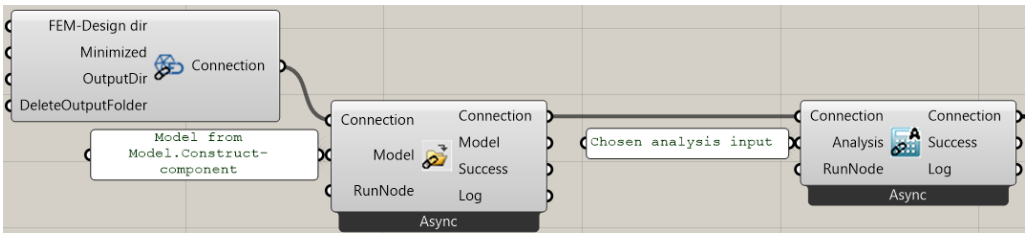

Figure B.12: How to connect the model to FEM-Design, open the model in the program, and run an analysis.

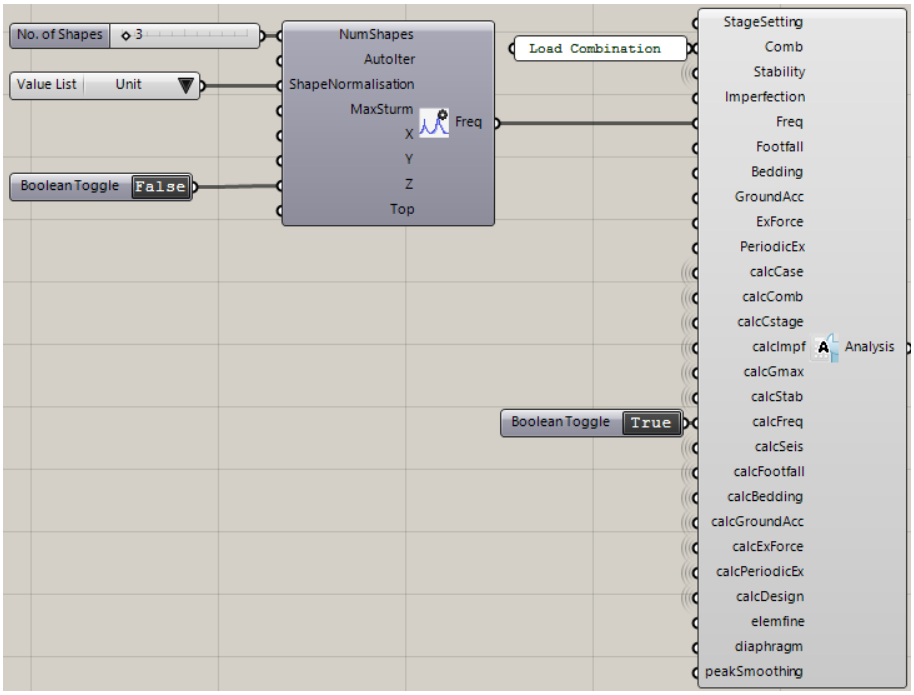

Figure B.13: Frequency analysis setup using *Freq.Define* and *Analysis.Define*.

Since the focus is on the lowest mode shapes, the number of extracted modes is limited to three. This reduces computation time and provides the mode shapes required for the torsional evaluation, even though the cumulative effective modal mass (EMM) does not reach the commonly used 90% criterion, see Section 1.3.2.3. Another decision was to set the vertical translational degrees of freedom to zero in the analysis setup, consistent with the assumption of negligible out-of-plane diaphragm motion.

When running the modal analysis using *Analysis.Define*, only the frequency analysis option (*calcFreq*) is enabled, while other analysis options are set to *False* (Figure B.13).

DEPARTMENT OF ARCHITECTURE AND CIVIL ENGINEERING
CHALMERS UNIVERSITY OF TECHNOLOGY
Gothenburg, Sweden
www.chalmers.se

CHALMERS
UNIVERSITY OF TECHNOLOGY